Biophysical applications of Lie groups and moving frames

by

Wilson B. Lough

A dissertation submitted in partial fulfillment of the requirements for the degree of

Doctor of Philosophy

(Physics)

at the

UNIVERSITY OF WISCONSIN-MADISON

2023

Date of final oral examination: 08/17/2013

The dissertation is approved by the following members of the Final Oral Committee:

Saverio E. Spagnolie, Professor, Mathematics

A. Baha Balantekin, Professor, Physics

Jean-Luc Thiffeault, Professor, Mathematics

Michael D. Graham, Professor, Chemical and Biological Engineering

To my wife, Karen.

ACKNOWLEDGMENTS

First, I would like to thank my advisor, Saverio Spagnolie for putting up with my constant diversions, and for disabusing me of the silly idea that fundamental physics can only be found at length scales near $\sqrt{\hbar G/c^3}$. I couldn't ask for a better mentor.

Words cannot express the depth of my gratitude to my wife, Karen, who has been a constant source of encouragement, love, and support.

Last but not least, I want to thank Alex Rivera for spreading the good word about my work with the HIGGINS.

CONTENTS

Contents iii

List of Figures v

Abstract viii

- 1 Introduction 1
- **2** Lie theory 7
 - 2.1 Introduction 7
 - 2.2 Geometry 7
 - 2.3 Euclidean submanifolds 14
 - 2.4 Groups 15
 - 2.5 Representations 23
- 3 Mechanics 31
 - 3.1 Introduction 31
 - 3.2 Rigid bodies 31
 - 3.3 Moving frames and Cosserat rods 45
 - 3.4 Cosserat media 53
- 4 Swimming microorganisms 56
 - 4.1 Introduction 56
 - 4.2 Active Kirchhoff rod model 61
 - 4.3 Body configurations and dynamics 70
- 5 Surface-bound biopolymers 82
 - 5.1 Introduction 82
 - 5.2 Filament kinematics and surface geometry 83
 - 5.3 Stress balance 89
 - 5.4 Shape equations 91
 - 5.5 Applications 93

- 6 Concluding remarks 99
- A Appendix: The Orthogonal group 103
 - A.1 The exponential map 108
 - A.2 Euler angles 110
 - A.3 Diagonalization113
- **B** Appendix: The Euclidean Group115
- C Appendix: Swimming microorganisms121
 - C.1 Integral equation for tension 121
 - C.2 Estimate of critical dimensional bending stiffness 123
 - C.3 Evolution equations in an inertial frame 123
 - C.4 Symmetries 125
- **D** Appendix: Surface-bound biopolymers138
 - D.1 Surface geometry and constraints 140
 - D.2 The mobility tensor142
 - D.3 Shape equations 145
 - D.4 Boundary conditions 146
 - D.5 Numerics149
 - D.6 Yukawa potential 154

Bibliography 156

LIST OF FIGURES

3.1	Illustration of a framed curve highlighting its centerline (green), cross-sections (orange), and adapted frame (red)	48
3.2	The modes of deformation of a Cosserat rod include (a) twisting,	10
J.Z	(b) bending, (c) shearing, (d) and stretching	50
4.1	(a-d) Swarmer P. mirabilis cells bend, rotate, and twist under their	
	own flagellar activity. Solid arrows indicate the direction of motion.	
	(e) Flagellar stresses are modeled as a continuous force density	
	f(s,t) and proportional moment density $m(s,t)$ which drives and	
	rotates the body through the fluid. (f) An active swimming Kirch-	
	hoff rod reproduces U-shaped swimming, S-shaped rotation, and	
	twisted, rotating swimming states found in experiments. Dashed	
	arrows indicate the direction of the local flagellar force and mo-	
	ment densities. (g) Phase diagram illustrating periodic symmetric	
	dynamics in the absence of an active moment $m(s,t)=0$. The	
	centerline curvature $\kappa(s,t) = \sum_{k=0}^{\infty} a_k(t) \phi_k(s)$ is projected onto the	
	first two even biharmonic modes $(a_0(t), a_2(t))$ and trajectories in	
	a_0 - a_2 space are plotted against $\beta_{\perp}^{-1/3}$ where $\beta_{\perp}=B_{\perp}/(f^*L^3)$ is a	
	dimensionless bending stiffness, with B_{\perp} the bending modulus,	
	f^* a characteristic active force density, and L the body length. Bi-	
	furcations from straight filaments to swimming-U shapes, then	
	to periodic waving-U dynamics, then to periodic flapping-W dy-	
	namics are observed as the bending stiffness is reduced. (h) A	
	cross-section of the phase diagram in (g) with $\beta_{\perp}=1.3\times 10^{-4}$	
	(waving-U dynamics). (i) A cross-section of the phase diagram in	
	(g) with $\beta_{\perp} = 7.6 \times 10^{-5}$ (flapping-W dynamics)	58
4.2	(a) Dominant eigenvalues μ_n of the linearized curvature dynamics	
	with no active moment and a piecewise constant force density	
	show the emergence of multiple unstable modes at critical bending	
	stiffnesses; the first at $\beta_{\perp} \approx 1.0 \times 10^{-2}$, or $\beta_{\perp}^{-1/3} \approx 4.6.$	73

4.3	(a-d) New attractors emerge upon the addition of an active mo-	
	ment (with body symmetry assumed). Top - snapshots of body	
	configurations over a half-period, bottom - trajectories of the first	
	two bending (a_0, a_1) and the first twisting (b_0) mode coefficients	
	suggests convergence to a fixed shape. (a) $(\beta_{\parallel}, \beta_{\perp}, M) = (1 \times 1)$	
	$10^{-4}, 2.5 \times 10^{-4}, 6 \times 10^{-3}$): a U-shaped swimmer with a twist.	
	(b) $(\beta_{\parallel}, \beta_{\perp}, M) = (1 \times 10^{-5}, 8 \times 10^{-5}, 1.35 \times 10^{-2})$: reduced stiff-	
	ness and increased active moment introduces a limit cycle cor-	
	responding to waving while twisting. (c) $(eta_\parallel,eta_\perp,M)=(1 imes$	
	$10^{-3}, 5.45 \times 10^{-5}, 1 \times 10^{-2})$: convergence to a new twisted-S shape.	
	(d) $(\beta_\parallel, \beta_\perp, M) = (1 \times 10^{-3}, 1.25 \times 10^{-4}, 2 \times 10^{-2})$: periodic flap-	
	ping appears with further increases in $M.$ (e) Swimming speed	
	across a range of active moments for $\beta_{\parallel}=2.5\times 10^{-4}$, for a stiffer	
	$(\beta_{\perp} = 5 \times 10^{-4}, \text{ squares}) \text{ and softer } (\beta_{\perp} = 5 \times 10^{-5}, \text{ circles})$	
	body. (f) Swimming speed across a range of bending stiffness for	
	$eta_{\parallel}=2.5 imes10^{-4}$ and active moments $M=0$ (circles), $M=0.002$	
	(squares), and $M=0.01$ (triangles)	74
5.1	Equilibrated molecular dynamics simulation of an ESCRT filament	
	illustrating spontaneous curvature and twist reproduced from [1].	
	(a) Top view and (b) side view show preferred curvatures. (c)	
	Close-up view illustrates intrinsic twist	94
5.2	Growth of a biofilament on the surface of a lipid bilayer. (a) When	
	proteins are not bound to the membrane, both the membrane and	
	proteins attain their preferred curvatures and store no elastic energy.	
	(b-c) The energy required to bind each subunit of the filament to	
	the membrane includes elastic contributions from both the filament	
	and the membrane. (d) A biofilament composed of sufficiently stiff	
	proteins forms a scaffold which is able to support larger and larger	
	membrane deformations as the filament continues to grow	95

5.3	With time increasing from left to right, a membrane-bound fil-	
	ament (colored by total energy density) grows from its nucle-	
	ation site (white circle) around the intercellular bridge connect-	
	ing two daughter cells. As it reaches the critical length required	
	for buckling, the localization of twist $\mathcal{E}_1 = \frac{1}{2}B_1\Omega_1^2$ and curvature	
	$(\mathcal{E}_2, \mathcal{E}_3) = (\frac{1}{2}B_2\Omega_2^2, \frac{1}{2}B_3\Omega_3^2)$ energy results in large stresses being	
	applied to the membrane.	96
5.4	Curvature sensing proteins, colored by elastic energy density, with	
	positive preferred curvature $\sigma_2 > 0$ begin to congregate near re-	
	gions of positive Gaussian curvature. Chiral proteins (bottom)	
	quickly reach equilibria, while achiral proteins (top) approach	
	equilibria much more slowly.	98
5.5	Curvature sensing proteins, colored by elastic energy density, with	
	negative preferred curvature $\sigma_2 < 0$ congregate near regions of	
	negative Gaussian curvature	98

Living matter is often composed of microstructures which possess rotational degrees of freedom, in addition to the translational degrees of freedom which describe the point-like material particles of classical continuum mechanics. Lie theory and Cartan's method of moving frames provides a natural framework in which both translational and rotational aspects of microstructured materials can be treated in a unified manner. In this framework, the state of the material is described by a collection of fields which take values in the special Euclidean group and its Lie algebra. These fields are governed by Euler-Poincaré equations which enforce the local balance of linear and angular momentum. In this dissertation, we develop theoretical and computational tools for modeling these generalized continua. We then apply these methods to a number of biophysical systems.

The twisting and writhing of a cell body and associated mechanical stresses is an underappreciated constraint on microbial self-propulsion. Multi-flagellated bacteria can even buckle and writhe under their own activity as they swim through a viscous fluid. Modeling the cell body as a semi-flexible Kirchhoff rod and coupling the mechanics to a dynamically evolving flagellar orientation field, we derive reduced Euler-Poincaré equations governing dynamics of the system, and rationalize experimental observations of buckling and writhing of elongated swarmer cells of the bacterium *Proteus mirabilis*. Our analysis reveals a minimal stiffness required of a cell, below which its motility is severely hampered.

Remodeling of biological membranes often involves interactions with biofilaments which polymerize on the membrane surface. Using a combination of moving frame and level-set methods to describe membrane geometry, we derive constrained Euler-Poincaré equations governing a surface-bound flexible filament. We find that a membrane-bound filament can undergo growth-induced buckling which results in highly localized forces and moments being applied to the membrane. Our simulations also suggest that chirality may play a role in a protein's ability to sense membrane curvature.

1 INTRODUCTION

Lie theory is the language of symmetry and invariance. Its mathematical foundations were laid down by Sophus Lie in his study of the symmetries of differential equations [2]. In its original incarnation, a Lie group was a group which was parameterized by a set of continuous variables, and each element of the group was considered a transformation which mapped one solution of the system of differential equations to another solution [3]. Lie's fundamental insight was that continuous groups can be generated by a much simpler set of linear transformations, even when the groups themselves are highly nonlinear. The space of such linear transformations is now called a *Lie algebra*.

Following Lie's initial work with symmetry groups of differential equations, numerous applications of Lie groups quickly emerged. Chief among these is the result of Emmy Noether that there is a one-to-one correspondence between continuous symmetries of the an action functional and conserved quantities of the associated Euler-Lagrange equations [4, 5]. The theories of relativity and quantum mechanics, which form the bedrock of our current understanding of physics, are likewise deeply intertwined with Lie theory. The discovery that the equations of classical electrodynamics were invariant under the action of the Lorentz group served as an impetus for development of special relativity [6–8], and work initiated by Eugene Wigner and Hermann

Weyl revealed a deep connection between the description of quantum mechanical phenomena and the representation theory of Lie groups and Lie algebras [9–12]. Closely related to these quantum mechanical applications, are the myriad of special functions which emerge as characters and matrix elements of Lie group representations [13]. This thread continues to this day with Lie groups appearing as gauge groups of standard model of particle physics [14]. Outside of physics, the tools of Lie theory can be be found in robotics and control theory [15, 16], computer vision [17], probability and statistics [18], information theory [19], and a wide range of other fields [20].

In the modern conception of Lie theory, pioneered by Wilhelm Killing and Élie Cartan, continuous group parameters are viewed as local coordinates in smooth manifold and the Lie algebra is interpreted as the tangent space at the identity element of the group [21]. This geometrization of Lie theory paved the way for many of the powerful, geometric techniques which permeate much of modern mathematical physics [22–25]. Cartan's *method of moving frames* [26, 27], in particular, will be used extensively throughout this work. The method of moving frames is a technique which can be used to analyze geometric properties of a manifold by studying transformation groups which act upon it [28]. This provides a natural framework in which to model a physical system whose state evolves under the action of a Lie group.

Euler-Lagrange equations for a system evolving under the action of a Lie group, G, with Lie algebra, \mathfrak{g} , are equivalent to a set of differential equations governing the G-valued evolution operator and an associated *quasi-velocity*, or \mathfrak{g} -valued infinitesimal generator [29]. We call these equations the *Euler-Poincaré equations* [30]. This formalism can be particularly useful when the Lagrangian of the system satisfies certain symmetry requirements. Through a process known as *Euler-Poincaré reduction*, the equations of motion can be replaced by a reduced order system depending only on the \mathfrak{g} -valued infinitesimal generator [31]. Solutions to the original variational problem can then be recovered by integration of the generator. Euler-Poincaré reduction and its Hamiltonian analogue, *Lie-Poisson reduction*, are now a classical tools of geometric mechanics [32, 33].

The prototypical example of a system which can be described using a Lie group-valued evolution operator is the rigid body [34]. Each configuration of the body is associated with the Euclidean transformation which maps a chosen reference frame onto the body's material frame. In this way, the configuration space of the body can be identified with the special Euclidean group, SE(3), and dynamics of the body can be described by Euler-Poincaré equations. The Lie theoretic approach was beautifully demonstrated in the context of fluid mechanics by Vladimir Arnold, who showed that the Euler equations for a

perfect fluid are equivalent to the reduced Euler-Poincaré equations on the infinite-dimensional group of volume preserving diffeomorphisms of the region occupied by the fluid [35]. Arnold's approach has since been extended and applied to complex fluids, plasmas, and many other continua [36–40].

The Euler-Poincaré and Lie-Poisson formalisms have more recently been extended to a field-theoretic context [41–44]. The time evolution operator of the classical Euler-Poincaré system is replaced by a *G*-valued configuration field over a base space parameterized by material coordinates and time. This configuration field is related to a g-valued differential one-form, or gauge potential, whose components are the infinitesimal generators associated with coordinate translations in the base space [45]. The Euler-Poincaré equations for these systems can be recast as covariant field equations satisfied by the gauge potential. In contrast with the classical case, these generalized Euler-Poincaré equations are insufficient to reconstruct solutions of the original variational problem, and must be augmented with a set of integrability conditions. In mathematical terms, a solution to the Euler-Poincaré field equations defines a connection on a principal bundle with structure group G. The integrability conditions, often referred to as structure equations and Maurer-Cartan equations, state that the curvature of this principal connection must be identically zero [25]. When the base space is taken to be \mathbb{R} and interpreted as time, the zero-curvature

condition is trivially satisfied and the field equations reduce to the classical Euler-Poincaré equations on the structure group of the bundle [41].

Here we are interested in applying this extended Euler-Poincaré framework to model microstructured continua. The simplest continuum theories treat matter as if it consists of identical point-like material particles. In reality, a material may exhibit varying degrees of structure depending on the scale at which the it is examined [46]. When the minimum length scale set by microstructure is comparable to the length scale associated with applied stresses or to the overall size of the medium, predictions of classical theories begin to fail and it becomes necessary to consider the mechanical response of the individual microstructures [47, 48].

Microstructured materials are often composed of subunits which are effectively indivisible at the energy scales under consideration. These microstructures may have internal degrees, in addition to the three translational degrees of freedom which describe classical point-like material particles. A material composed of rigid microstructures which are fully characterized by a position and orientation is called a *Cosserat medium* [49]. The state of a Cosserat medium is given by assigning a Euclidean transformation to each microstructure, making it the field-theoretic analogue of the rigid body. The gauge potential associated with this field of Euclidean transformations contains in-

formation about the medium's local deformation and velocity. Cosserat media encompass a large class of models for structured and oriented materials which include rods [50, 51], plates and shells [52], flexible polymers [53], carbon nano-tubes and graphene [54], lipid membranes [55], bone [56], liquid crystals [57], granular media [58], continuum spin systems [59–62], and certain nonlinear sigma models [63–65].

The remainder of this dissertation will be spent developing the theory of Cosserat media within the Euler-Poincaré framework and investigating various applications. A proper discussion of the ideas outlined above requires a variety of techniques rooted in differential geometry and group theory which will covered in chapter 2. We will examine Cosserat media through the lens of Euler-Poincaré theory in chapter 3, beginning with the case of a single rigid body. Chapter 4 presents a model for an active flexible body at low Reynolds number with applications to the biolocomotion of multi-flagellated microorganisms. In chapter 5 we investigate the constrained dynamics of flexible filaments, motivated primarily by biopolymers and their interactions with cell membranes. We conclude with a discussion of possible future research directions.

2.1 Introduction

In this chapter, we will introduce basic notation and terminology for discussing Lie groups and Lie algebras. We begin by recalling some facts about manifolds and differential forms, then we review the geometry and representation theory of Lie groups and their Lie algebras. For a more thorough treatment of the mathematical methods discussed in this chapter, we direct the reader to [21, 66–69].

2.2 Geometry

Consider a smooth manifold M. The space of smooth functions on M will be denoted $C^{\infty}(M)$, and the space real-valued functions which are smooth at the point $x \in M$ by $C^{\infty}(x)$. There are a number of equivalent intrinsic definitions of the tangent space T_xM at a point $x \in M$, and the utility of these definitions can vary greatly depending on the context. We will adopt the view that elements of T_xM are either derivations on $C^{\infty}(x)$, or germs of smooth curves through the point x. A derivation on $C^{\infty}(x)$ is linear map

 $a(x): C^{\infty}(x) \to \mathbb{R}$ which satisfies the product rule,

$$\mathbf{a}(x)(fg) = (\mathbf{a}(x)f)g(x) + f(x)(\mathbf{a}(x)g), \tag{2.1}$$

for any $f,g\in C^\infty(x)$. A germ is an equivalence class of smooth curves through x where curves are taken to be equivalent if there is some neighborhood of x on which they agree. To simplify notation, we may drop the 'x' in (2.1) when it can be understood from context. The set of partial derivative operators $e_i=\partial_i$ with respect to any set of local coordinates x^i , or the corresponding germs, provides a basis for T_xM . Unless otherwise stated, we will take repeated indices to imply summation:

$$a^i \mathbf{e}_i := \sum_i a^i \mathbf{e}_i. \tag{2.2}$$

The cotangent space, T_x^*M , is defined to be the dual space of T_xM . An element of T_x^*M , called a covector, is a linear functional, $\tilde{\boldsymbol{a}}:T_xM\to\mathbb{R}$, which maps each vector $\boldsymbol{v}\in T_xM$ to a real number, which we will denote by $\langle \tilde{\boldsymbol{a}}|\boldsymbol{v}\rangle$ or $\tilde{\boldsymbol{a}}(\boldsymbol{v})$. The differential $\mathrm{d}f$ of a real-valued function f can be interpreted as an element of T^*M by defining

$$\langle df | \boldsymbol{v} \rangle = \boldsymbol{v}(f) = v^i \frac{\partial f}{\partial x^i}.$$
 (2.3)

Applying this definition to differentials of the coordinate functions results in a basis, $\tilde{e}^i = \mathrm{d} x^i$, for the cotangent space which satisfies,

$$\left\langle dx^{i} \middle| \partial_{j} \right\rangle = \frac{\partial x^{i}}{\partial x^{j}} = \delta^{i}_{j} = \begin{cases} 1 & \text{if } i = j \\ 0 & \text{if } i \neq j \end{cases}$$
 (2.4)

We define the tangent bundle $TM = \bigcup_{x \in M} T_x M$ and cotangent bundle $T^*M = \bigcup_{x \in M} T_x^*M$ to be the collection all tangent and cotangent spaces, respectively.

Higher order tensor fields can be constructed by taking tensor products of collections of vector and covector fields. We will be particularly interested in covariant tensors. A p^{th} order covariant tensor on M is a real-valued multilinear map $F: \bigotimes^p T_x M \to \mathbb{R}$ defined on p copies of $T_x M$. If F is a p^{th} order covariant tensor field on M, its symmetric and antisymmetric parts, denoted $\mathcal{S}(F)$ and \mathcal{A} , respectively, can be defined by their action on p vectors (u_1, \ldots, u_p) :

$$S(F)(u_1, \dots, u_p) = \frac{1}{p!} \sum_{\pi \in S_p} F(u_{\pi(1)}, \dots, u_{\pi(p)}),$$
(2.5)

$$\mathcal{A}(F)(\boldsymbol{u}_1,\ldots,\boldsymbol{u}_p) = \frac{1}{p!} \sum_{\pi \in S_p} \operatorname{sgn}(\pi) F(\boldsymbol{u}_{\pi(1)},\ldots,\boldsymbol{u}_{\pi(p)}), \tag{2.6}$$

where S_p is the permutation group on $\{1,\ldots,p\}$. If F satisfies $\mathcal{A}(F)=F$ we say that it is totally antisymmetric. Fields of these totally antisymmetric

covariant tensors are known as differential forms. We will denote the space rank p differential forms (p-forms) defined on M, by $\Lambda^p M$. A one-form is simply a covector field, and can be expressed in terms of the coordinate differentials, $\tilde{a} = a_i \, \mathrm{d} x^i$. Higher order differential forms can be constructed using a bilinear, associative operation called the wedge product. If \tilde{a} is a p-form and \tilde{b} is a q-form, then their wedge product is the (p+q)-form defined by

$$\tilde{\boldsymbol{a}} \wedge \tilde{\boldsymbol{b}} = \frac{(p+q)!}{p!q!} \mathcal{A}(\tilde{\boldsymbol{a}} \otimes \tilde{\boldsymbol{b}}).$$
 (2.7)

For example, the wedge product of a pair of one forms, \tilde{a} and \tilde{b} , is defined to be twice the antisymmetric part of their tensor product,

$$\tilde{a} \wedge \tilde{b} = \tilde{a} \otimes \tilde{b} - \tilde{b} \otimes \tilde{a},$$
 (2.8)

and the three-fold wedge product of one forms, \tilde{a}, \tilde{b} , and \tilde{c} , is

$$\tilde{a} \wedge \tilde{b} \wedge \tilde{c} = \tilde{a} \otimes \tilde{b} \otimes \tilde{c} + \tilde{b} \otimes \tilde{c} \otimes \tilde{a} + \tilde{c} \otimes \tilde{a} \otimes \tilde{b}$$

$$- \tilde{a} \otimes \tilde{c} \otimes \tilde{b} - \tilde{c} \otimes \tilde{b} \otimes \tilde{a} - \tilde{b} \otimes \tilde{a} \otimes \tilde{c}.$$
(2.9)

A basis for $\Lambda^p M$ can be constructed by taking wedge products of coordinate

differentials,

$$\mathcal{B}_p(M) = \left\{ dx^{i_1} \wedge \ldots \wedge dx^{i_p} \middle| 1 \le i_1 < \ldots < i_p \le \dim(M) \right\}, \tag{2.10}$$

and we can write a *p*-form as

$$\tilde{\boldsymbol{a}} = a_{i_1 \dots i_p} \, \mathrm{d} x^{i_1} \, \otimes \dots \otimes \mathrm{d} x^{i_p} \tag{2.11}$$

$$= \sum_{i_1 < \dots < i_p} a_{i_1 \dots i_p} \, \mathrm{d}x^{i_1} \wedge \dots \wedge \mathrm{d}x^{i_p}$$
 (2.12)

$$= \frac{1}{p!} a_{i_1 \dots i_p} dx^{i_1} \wedge \dots \wedge dx^{i_p}$$
(2.13)

Having dealt with their algebraic properties, we now turn to the exterior calculus of differential forms. The central object of exterior calculus is exterior derivative, denoted d, which acts on p-forms to produce (p+1)-forms. Given a p-form, $\tilde{\pmb{a}} = \sum_{i < \dots < j} a_{i \dots j} \mathrm{d} x^i \wedge \dots \wedge \mathrm{d} x^j$, its exterior derivative is,

$$d\tilde{\boldsymbol{a}} = \sum_{i < \dots < j} \partial_k a_{i \dots j} dx^k \wedge dx^i \wedge \dots \wedge dx^j.$$
 (2.14)

Given a map $F:A\to B$ from a manifold A into a manifold B, the pullback F^* and pushforward 1F_* can be used to 'pull' certain quantities from $F(A)\subset B$ back to A and 'push' certain quantities from A forward to $F(A)\subset B$. In 1-sometimes called the differential/derivative

general, objects which are expressed in terms of vector fields can be pushed forward, while real-valued functions and differential forms can be pulled back. Given a function f in $C^{\infty}(B)$, a vector \mathbf{a} in TA, and a covector $\tilde{\mathbf{b}}$ in T^*B we define a new function F^*f , vector $F_*\mathbf{a}$, and covector $F^*\tilde{\mathbf{b}}$, in $C^{\infty}(A)$, TB, and T^*A , respectively, by

$$F^*f := f \circ F, \tag{2.15}$$

$$(F_*\boldsymbol{a})f := \boldsymbol{a}(F^*f), \tag{2.16}$$

$$\left\langle F^* \tilde{\boldsymbol{b}} \middle| \boldsymbol{a} \right\rangle := \left\langle \tilde{\boldsymbol{b}} \middle| F_* \boldsymbol{a} \right\rangle.$$
 (2.17)

In the case that F=y(x) and its inverse $F^{-1}=x(y)$ represent a transition map between local coordinate charts in a manifold, the pushforward and pullback just describe the classical transformation properties of covariant and contravariant vectors,

$$F_* \frac{\partial}{\partial x^j} = \frac{\partial y^j}{\partial x^i} \frac{\partial}{\partial y^j}$$
 (2.18)

$$(F^{-1})^* dx^i = \frac{\partial x^i}{\partial y^j} dy^j.$$
 (2.19)

The '*' notation can be quite cumbersome, so, we will often simply write expression like (2.18) and (2.19) as $\frac{\partial}{\partial x^j} = \frac{\partial y^j}{\partial x^i} \frac{\partial}{\partial y^j}$ and $\mathrm{d} x^i = \frac{\partial x^i}{\partial y^j} \mathrm{d} y^j$ when it

will not result in ambiguity.

The Lie derivative with respect to a vector field u, denoted \mathcal{L}_u , is a generalization of the directional derivative along the vector field. When applied to a function f, it is equivalent to the standard directional derivative of f with respect to u,

$$\mathcal{L}_{\boldsymbol{u}}f = u^i \frac{\partial f}{\partial x^i}.$$
 (2.20)

Its action on a vector field v, is given by the commutator of the differential operators u and v,

$$\mathcal{L}_{\boldsymbol{u}}\boldsymbol{v} = [\boldsymbol{u}, \boldsymbol{v}] = \left(u^{i} \frac{\partial v^{j}}{\partial x^{i}} - v^{i} \frac{\partial u^{j}}{\partial x^{i}}\right) \partial_{j}. \tag{2.21}$$

This is essentially a local measure of the coherence or independence the two vector fields. Further discussion of the Lie derivative in the context of Lie groups and algebras can be found in sections 2.4- 2.5.

2.3 Euclidean submanifolds

It is often the case that we are interested in the embedding,

$$r: M \to \mathbb{R}^n \tag{2.22}$$

of an m-dimensional manifold M into \mathbb{R}^n . The prototypical examples are, of course, embeddings of curves and surfaces in \mathbb{R}^3 . Another important case which we will encounter in section 2.5 involves the embedding of a Lie group into the vector space of n-by-n matrices which can be identified with \mathbb{R}^{n^2} . At each point $\mathbf{r}(x) \in \mathbb{R}^n$, the ambient tangent space $T_{\mathbf{r}(x)}\mathbb{R}^n \simeq \mathbb{R}^n$ splits into an orthogonal direct sum of vectors tangent and normal to the embedded manifold $S := \mathbf{r}(M)$. We denote these vector spaces by $T_{\mathbf{r}(x)}S$ and $N_{\mathbf{r}(x)}S$, and define the tangent and normal bundles to be $TS := \bigcup_{x \in M} T_{\mathbf{r}(x)}S$ and $NS := \bigcup_{x \in M} N_{\mathbf{r}(x)}S$, respectively.

Suppose the vector fields $b_i = b_i^{\nu} \partial_{\nu}$, for $1 \leq i \leq m$, form a basis for each $T_x M$. The pushforward of this basis by r,

$$e_i := b_i^{\nu} \frac{\partial \mathbf{r}}{\partial x^{\nu}},\tag{2.23}$$

can always be extended to a basis for all of \mathbb{R}^n ,

$$(e_1,\ldots,e_m,e_{m+1}\ldots e_n). (2.24)$$

Basis fields of the form 2.24 are said to be *adapted* to M. We will continue with adapted frames in section 3.3, after our discussion of group theory and the rigid body.

2.4 Groups

A Lie group G is a space that is simultaneously a manifold and group with smooth composition $(g,h)\mapsto gh$ and smooth inversion $g\mapsto g^{-1}$ operations. By this we mean that for any $g,h\in G$, there is a local coordinate chart containing g,h,gh, and g^{-1} , in which the coordinates of gh are smooth functions of the coordinates of g and h, and similarly, the coordinates of g^{-1} are smooth functions of the coordinates of g. More explicitly, if we write g(x) for the group element with coordinates $x\in\mathbb{R}^n$, then group composition can be expressed in local coordinates by a smooth map $m:\mathbb{R}^n\times\mathbb{R}^n\to\mathbb{R}^n$ which satisfies g(m(x,y))=g(x)g(y), and group inversion is described by a smooth map $f:\mathbb{R}^n\to\mathbb{R}^n$ which satisfies $g(f(x))=g(x)^{-1}$. Demanding that the group operations are smooth tightly constrains the local geometric structure

of the group. We can answer many questions about the group as a whole by examining a neighborhood of the identity $1 \in G$, and then mapping the results to other regions by left translation, $L_g(h) = gh$.

The Lie algebra $\mathfrak{g}=T_1G$ of the group G, defined as the tangent space at the identity $1\in G$, and its dual space $\mathfrak{g}^*=T_1^*G$ contain basic information about the structure of G, and will play a fundamental roll in what follows. We can associate with each $\alpha\in\mathfrak{g}$, a vector field,

$$a(g) = L_{g*}\alpha, \tag{2.25}$$

defined as the pushforward of α by the left translation map. Similarly, we can associate with each $\beta \in \mathfrak{g}^*$, a one-form,

$$b(g) = L_{q-1}^* \beta. (2.26)$$

defined as the pullback of β by the inverse left translation map. The fields a and b are invariant under pushforward/pullback by the left translation operator:

$$\boldsymbol{a}(gh) = (L_{g*}\boldsymbol{a})(h), \tag{2.27}$$

$$\boldsymbol{b}(g) = (L_h^* \boldsymbol{b}) (hg). \tag{2.28}$$

Objects which satisfy this condition are called *left-invariant*. Left-invariant vector fields form a Lie subalgebra of the space of all vector fields on G. That is, the space of left-invariant vector fields is closed under the standard vector space operations, as well as the Lie derivative, $\mathcal{L}_a b = [a, b]$, defined in section 2.2. Then, given any two left-invariant vector fields a and b, we can produce a third left-invariant vector field,

$$L_{q*}\left[\boldsymbol{a},\boldsymbol{b}\right](h) = \left[\boldsymbol{a},\boldsymbol{b}\right](gh). \tag{2.29}$$

The fact that left invariant vector fields are uniquely determined by their values at the identity allows us to define the Lie bracket of $\alpha, \beta \in \mathfrak{g}$ as,

$$[\alpha, \beta] := L_{q^{-1}*}[L_{q*}\alpha, L_{q*}\beta].$$
 (2.30)

The tangent space at the identity, $\mathfrak{g}=T_1G$, together with the bracket (2.30) is called the Lie algebra of the Lie group G. We note that some authors [21] define the Lie algebra of a Lie group to be the space of left-invariant invariant vector fields. These two definitions are equivalent by the isomorphism given in equation (2.25).

By choosing bases, β_i and β^i , for \mathfrak{g} and \mathfrak{g}^* , respectively, we can construct

left invariant frame fields,

$$\boldsymbol{b}_i := L_{q*} \boldsymbol{\beta}_i, \tag{2.31}$$

which provide a basis for each T_gG , and left-invariant coframe fields,

$$b^i := L_{g^{-1}}^* \beta^i, \tag{2.32}$$

which provide a basis for each T_g^*G . Basic information about the structure of G is contained in the *structure constants*, c_{jk}^i , which are related to the (co)frame fields by

$$\mathrm{d}\boldsymbol{b}^i = -\frac{1}{2}c^i_{jk}\boldsymbol{b}^j \wedge \boldsymbol{b}^k, \tag{2.33}$$

$$[\boldsymbol{\beta}_i, \boldsymbol{\beta}_j] = c_{ij}^k \boldsymbol{\beta}_k. \tag{2.34}$$

Many aspects of Lie theory can be essentially be reduced to the study of these structure constants.

The Maurer-Cartan form is a left-invariant $\mathfrak g$ -valued one-form on G which is central to the dynamics problems we will consider in later chapters. It is a

map which associates a g-valued field,

$$\Psi(\boldsymbol{a}) = L_{q^{-1}*}\boldsymbol{a},\tag{2.35}$$

with each vector field a on G. In terms of the left-invariant frame (2.31) and coframe fields (2.32), we can express the Maurer-Cartan form as,

$$\Psi = \beta_i \otimes b^i = \left(L_{g^{-1}} * b_i\right) \otimes b^i \tag{2.36}$$

Then, by (2.33), the Maurer-Cartan form satisfies,

$$d\Psi = -\frac{1}{2}c_{jk}^{i}\boldsymbol{\beta}_{i}\otimes\boldsymbol{b}^{j}\wedge\boldsymbol{b}^{k} = -\frac{1}{2}\left[\boldsymbol{\beta}_{j},\boldsymbol{\beta}_{j}\right]\otimes\boldsymbol{b}^{j}\wedge\boldsymbol{b}^{k}$$
(2.37)

Equation (2.37) is commonly written in the coordinate-free form,

$$d\Psi + \frac{1}{2} \left[\Psi \wedge \Psi \right] = 0 \tag{2.38}$$

by defining the bracket,

$$[\Theta \wedge \Phi](\boldsymbol{u}, \boldsymbol{v}) = [\Theta(\boldsymbol{u}), \Phi(\boldsymbol{v})]_{\mathfrak{g}} - [\Theta(\boldsymbol{v}), \Phi(\boldsymbol{u})]_{\mathfrak{g}}$$
(2.39)

for Lie algebra-valued one-forms, Θ and Φ , where u and v are vector fields. The

coordinate-free definition of the bracket can be extended to Lie algebra-valued forms of higher degree, but this will be sufficient for our purposes.

Left/right-invariant vector fields and their integral curves are often encountered in the study of physical systems. Given an element $\alpha \in \mathfrak{g}$ we can define a curve, $g: \mathbb{R} \to G$, as the solution to the initial value problem,

$$\dot{g} = L_{g*}\alpha, \quad g(0) = 1.$$
 (2.40)

This curve is the integral curve of the left-invariant vector field, $a=L_{g*}\alpha$ which passes through the identity. The solution to (2.40) is called the one-parameter subgroup of G generated by α and will be written as,

$$g(t) = e^{t\alpha}. (2.41)$$

In the case that G is a linear group, this notation is consistent with the standard exponential of a linear operator.

One-parameter subgroups can provide us with a simple, intuitive view of many of concepts encountered in the study of Lie theory. The Lie bracket of elements of the Lie algebra is one such example. In section 2.2, we introduced the interpretation of a tangent vector as an equivalence class of curves. Under this interpretation, a parameterized curve, g(t), can be viewed as a differential

operator with its action on a real-valued function defined by,

$$g \cdot f := \frac{\mathrm{d}}{\mathrm{d}t} f(g(t)) \tag{2.42}$$

We can similarly define the action of a G-valued function, g(s,t), which depends on multiple parameters by

$$g \cdot f := \frac{\partial^2}{\partial s \partial t} f(g(s, t)) = \frac{\partial^2}{\partial t \partial s} f(g(s, t))$$
 (2.43)

The product of one-parameter subgroups, $e^{s\alpha}e^{t\beta}e^{-s\alpha}e^{-t\beta}$, viewed as a differential operator, can then be expanded in powers of s and t,

$$e^{s\alpha}e^{t\beta}e^{-s\alpha}e^{-t\beta} = 1 + st\left[\alpha,\beta\right] + O(s^2) + O(t^2). \tag{2.44}$$

From this result, it is apparent that the Lie bracket encodes information about non-commutativity of the group composition law.

The dynamics problems treated in this work will often require us to consider integral curves generated by vector fields which lack the invariance properties discussed above. When a vector field is not left-invariant, $a(gh) \neq L_{g*}a(h)$, it can no longer be expressed in terms of a constant element of \mathfrak{g} , but

can still be associated with a g-valued field,

$$\alpha(g) := \left(L_{g^{-1}} * \boldsymbol{a}\right)(g). \tag{2.45}$$

The integral curve through $1 \in G$, generated by (2.45) is no longer simply given by the exponential, but rather by the *path-ordered exponential*, or product integral,

$$g(t) = \mathcal{P}\exp \int_0^t \alpha(\xi) \,\mathrm{d}\xi\,,\tag{2.46}$$

which is the formal solution to the nonhomogeneous differential equation,

$$\dot{g}(t) = L_{g(t)*} \alpha(t), \quad g(0) = 1.$$
 (2.47)

The path-ordered exponential can be computed as the limit of an ordered product of one-parameter subgroups,

$$\mathcal{P}\exp \int_{a}^{b} \boldsymbol{\alpha}(\xi) \,\mathrm{d}\xi = \prod_{a}^{b} e^{\boldsymbol{\alpha}(\xi) \,\mathrm{d}\xi} = \lim_{n \to \infty} e^{\boldsymbol{\alpha}(\xi_{0}) \Delta \xi} e^{\boldsymbol{\alpha}(\xi_{1}) \Delta \xi} \dots e^{\boldsymbol{\alpha}(\xi_{n}) \Delta \xi}, \quad (2.48)$$

where $\Delta \xi = (b - a)/n$ and $\xi_k = a + k\Delta \xi$.

2.5 Representations

Many Lie groups and algebras of physical interest can be represented by linear transformations. The class of functions which associate elements of Lie groups and their Lie algebras with linear transformations in a way that preserves their algebraic structure are called representations. We begin this section by constructing the prototypical examples of Lie group and Lie algebra representations: the adjoint representations, Ad and ad. This is followed by a general discussion of linear representations, and the geometry of linear groups.

Given a one-parameter subgroup, $e^{t\alpha}$, and a group element, $g\in G$, we can construct a new one-parameter subgroup,

$$L_g R_{q^{-1}} e^{t\alpha} = g e^{t\alpha} g^{-1}, \tag{2.49}$$

where L_g and $R_{g^{-1}}$ are left and right translation operators by g and g^{-1} , respectively. We denote the generator of this new one-parameter subgroup by

$$\operatorname{Ad}_{g}\boldsymbol{\alpha} := \frac{\mathrm{d}}{\mathrm{d}t} L_{g} R_{g^{-1}} e^{t\boldsymbol{\alpha}} \bigg|_{t=0} = L_{g*} R_{g^{-1}*} \boldsymbol{\alpha}, \tag{2.50}$$

and denote the derivative of $g \mapsto \operatorname{Ad}_g$ at g = 1 by

$$\operatorname{ad}_{\alpha} \beta := \frac{\mathrm{d}}{\mathrm{d}s} \operatorname{Ad}_{e^{s\alpha}} \beta|_{s=0} = (\operatorname{Ad}_{1*} \alpha) \beta. \tag{2.51}$$

The maps, $g \mapsto \operatorname{Ad}_g$ and $\alpha \mapsto \operatorname{ad}_{\alpha}$, are known as the adjoint representations of G and \mathfrak{g} , respectively. Expanding the expression,

$$e^{s\alpha}e^{t\beta}e^{-t\alpha} = 1 + t\beta + st\left[\alpha, \beta\right] + O(s^2) + O(t^2)$$
(2.52)

to second order in s and t, and using the fact

$$\frac{\mathrm{d}}{\mathrm{d}s} \operatorname{Ad}_{e^{s\alpha}} \boldsymbol{\beta}|_{s=0} = \left. \frac{\partial^2}{\partial s \partial t} \left(e^{s\alpha} e^{t\beta} e^{-s\alpha} \right) \right|_{s,t=0}, \tag{2.53}$$

we find that the action of ad_{α} is equivalent the Lie bracket,

$$\mathrm{ad}_{\alpha}\beta = [\alpha, \beta]. \tag{2.54}$$

In general, we define a representation 2 of a Lie group G to be a smooth homomorphism, $\Pi:G\to \operatorname{GL}(V)$, from G onto a subgroup of $\operatorname{GL}(V)$, the group of invertible linear operators acting on a vector space V. In the case of $\overline{\ }^2$ It is also common to refer to the vector space V as the representation, rather than the map Π .

the adjoint representation defined above the vector space is the Lie algebra, $V=\mathfrak{g}$, of the group. The general linear group, and any subgroup of the general linear group, can be viewed as a submanifold of the set of all linear operators on V. Since this space is itself a vector space, we may apply the methods of 2.3, with the representation Π playing the role of the position vector. As the tangent space of any vector space is naturally isomorphic to the space itself, it is customary to simply define the Lie algebra $\mathfrak{gl}(V)$ of the general linear group to be the vector space of all linear transformations on V. The derivative of the group representation at the identity, $\pi:=\Pi_{1*}:\mathfrak{g}\to\mathfrak{gl}(V)$, defines a Lie algebra representation which maps the Lie bracket in \mathfrak{g} to the commutator in $\mathfrak{gl}(V)$,

$$\pi \left[\boldsymbol{\mu}, \boldsymbol{\nu} \right]_{\mathfrak{g}} = \left[\pi \boldsymbol{\mu}, \pi \boldsymbol{\nu} \right]_{\mathfrak{gl}(V)}. \tag{2.55}$$

We call π the Lie algebra representation induced by Π .

The general group $\mathrm{GL}(V)$ on an n-dimensional vector space V is an n^2 -dimensional submanifold of the n^2 -dimensional vector space $\mathfrak{gl}(V)$. Choosing a basis, e_i , for V and dual basis, e^j , for V^* defines a basis, $e_ie^j:=e_i\otimes e^j$, for

 $\mathfrak{gl}(V)$, and induces a coordinate system on $\mathrm{GL}(V)$,

$$x_j^i(g) = \left\langle e^i \middle| g e_j \right\rangle, \tag{2.56}$$

with the property that,

$$x_i^i(gh) = x_k^i(g)x_i^k(h),$$
 (2.57)

holds for all $g,h\in \mathrm{GL}(V)$. If f is a real-valued function on $\mathrm{GL}(V)$, then, writing $\frac{\partial}{\partial x^i_j(g)}:=\left.\frac{\partial}{\partial x^i_j}\right|_g$, the pushforward of the coordinate basis by L_g satisfies

$$L_{g*} \frac{\partial}{\partial x_{j}^{i}(h)} f(h) = \frac{\partial}{\partial x_{j}^{i}(h)} f(gh)$$

$$= \frac{\partial x_{\ell}^{k}(gh)}{\partial x_{j}^{i}(h)} \frac{\partial}{\partial x_{\ell}^{k}(gh)} f(gh)$$

$$= x_{i}^{k}(g) \frac{\partial}{\partial x_{j}^{k}(gh)} f(gh).$$
(2.58)

Suppressing explicit dependence on g and h, and writing $g_i^k = x_i^k(g)$, we have

$$L_{g*} \frac{\partial}{\partial x_j^i} = g_i^k \frac{\partial}{\partial x_j^k}.$$
 (2.59)

By a similar argument, R_g satisfies

$$R_{g*} \frac{\partial}{\partial x_j^i} = g_k^j \frac{\partial}{\partial x_k^i}.$$
 (2.60)

It follows that the adjoint action of $g \in G$ on $\mu = \mu_j^i \left. \frac{\partial}{\partial x_j^i} \right|_{x=1}$ is given by

$$\operatorname{Ad}_{g} \boldsymbol{\mu} = L_{g*} R_{g^{-1}*} \left(\mu_{j}^{i} \frac{\partial}{\partial x_{j}^{i}} \right)$$

$$= L_{g*} \left(\mu_{j}^{i} \left[g^{-1} \right]_{\ell}^{j} \frac{\partial}{\partial x_{\ell}^{i}} \right)$$

$$= g_{i}^{k} \mu_{j}^{i} \left[g^{-1} \right]_{\ell}^{j} \frac{\partial}{\partial x_{\ell}^{k}}$$

$$(2.61)$$

where we have written $\left[g^{-1}\right]^i_j:=x^i_j(g^{-1}).$ The left invariant vector field associated with $\pmb{\mu}$ must be of the form

$$L_{x*}\boldsymbol{\mu} = x_k^i \mu_j^k \frac{\partial}{\partial x_j^i},\tag{2.62}$$

so, the adjoint action of μ on $\nu=\nu_j^i\left.\frac{\partial}{\partial x_j^i}\right|_{x=1}$ is given by

$$\operatorname{ad}_{\mu}\nu = [\mu, \nu]$$

$$= L_{x*}^{-1} [L_{x*}\mu, L_{x*}\nu]$$

$$= L_{x*}^{-1} \left(x_k^i \mu_j^k \nu_m^n \frac{\partial x_n^\ell}{\partial x_j^i} \frac{\partial}{\partial x_m^\ell} - x_n^\ell \nu_m^n \mu_j^k \frac{\partial x_k^i}{\partial x_m^\ell} \frac{\partial}{\partial x_j^i} \right)$$

$$= L_{x*}^{-1} \left(x_m^i \mu_n^m \nu_j^n - x_m^i \nu_n^m \mu_j^n \right) \frac{\partial}{\partial x_j^i}$$

$$= \left(\mu_n^i \nu_j^n - \nu_n^i \mu_j^n \right) \frac{\partial}{\partial x_j^i}.$$
(2.63)

We can take the embedding, $g=x_j^ie_ie^j$, of GL(V) into $\mathfrak{gl}(V)$ to be the operator-valued analogue of the position vector in Euclidean space. As discussed in section 2.3, we can then identify each tangent vector, $\boldsymbol{u}=u_j^i\frac{\partial}{\partial x_j^i}$, with

$$dg(\mathbf{u}) = u_j^i \frac{\partial g}{\partial x_j^i} = u_j^i \mathbf{e}_i \mathbf{e}^j.$$
 (2.64)

This identification allows us to make sense of expressions like $g\mu$ or $\mu\nu$ as a product of matrices, or more generally, as composition of linear operators acting on the same vector space, and facilitates the numerical computation of many abstract geometric operations introduced in section 2.4. For example,

the pushforward by L_g is simply given by,

$$L_{g*}\boldsymbol{w} = g\boldsymbol{w},\tag{2.65}$$

and the adjoint representations are given by,

$$\mathrm{ad}_{\mu}\nu = \mu\nu - \nu\mu,\tag{2.66}$$

$$\mathrm{Ad}_g \boldsymbol{\mu} = g \boldsymbol{\mu} g^{-1}. \tag{2.67}$$

Any representation Π of a Lie group G can similarly be viewed as an embedding of the group into $\mathfrak{gl}(V)$. In this context, a Lie algebra-valued form is viewed as a matrix, $\Theta=\Theta^i_je_ie^j$, of ordinary differential forms on G. For example, the Maurer-Cartan form can be expressed in terms of the representation as,

$$\Psi = \Pi^{-1} \mathrm{d}\Pi \,, \tag{2.68}$$

where Π^{-1} denotes the matrix inverse of the representation. We can now write the product of $\mathfrak{gl}(V)$ -valued forms in terms matrix multiplication by taking

wedge products of matrix elements,

$$\Theta \wedge \Phi = \Theta_k^i \wedge \Phi_j^k e_i e^j. \tag{2.69}$$

The bracket of Lie algebra-valued forms, defined by equation (2.39), reduces to

$$\begin{aligned} [\Theta \wedge \Phi] &= \Theta_j^i \wedge \Phi_\ell^k \left[e_i e^j, e_k e^\ell \right] \\ &= \Theta \wedge \Phi - (-1)^{p+q} \Phi \wedge \Theta, \end{aligned} \tag{2.70}$$

where p and q are of degrees of Θ and Φ , respectively. In particular, for a Lie algebra-valued one-form, like the Maurer-Cartan form, we have

$$[\Psi \wedge \Psi] = 2\Psi \wedge \Psi. \tag{2.71}$$

It follows that the Maurer-Cartan equation 2.38 for a matrix group can be reduced to

$$d\Psi + \Psi \wedge \Psi = 0. \tag{2.72}$$

3.1 Introduction

Motivated by the results of Castrillón López, Gay-Balmaz, Boyer, Ellis, and others [41–43, 52, 59], we develop the theory of Cosserat media within the Euler-Poincaré framework. The structure of this chapter is as follows. We first examine in some detail the group of rotations SO(3) and the group of rigid transformation SE(3) as applied to rigid body dynamics. Our examination of the rigid body motivates a discussion of variational principles on Lie groups and the method of moving frames. The culmination of this chapter is the derivation of generalized Euler-Poincaré equations governing the dynamics of an (n+1)-dimensional Cosserat medium. Detailed discussion of the background required for this chapter may be found in [32–34, 70, 71].

3.2 Rigid bodies

We begin our discussion of mechanics by considering the case of a single rigid body, the equivalent of a zero-dimensional Cosserat medium. The majority of concepts which are required for the study of higher dimensional Cosserat media will appear in the derivation of Euler-Poincaré equations for the rigid body. First, suppose the rigid body has a fixed point p. By choosing an

orthonormal frame, $b_i = b_i(t)$, affixed to the body at p, we can associate it's configuration with the orthogonal transformation, $R = b_i(t)e^i$, which maps an inertial orthonormal frame, e_i , to the body frame at the current time t. If we identify the inertial frame vectors, e_i , with the canonical basis for \mathbb{R}^3 , and the coframe vectors with $e^i = e_i^T$, we can view R as the transformation which maps a coordinate vector measured in the body frame, $v^{(B)}$, to the coordinate vector measured in the inertial frame $v^{(I)} = Rv^{(B)}$. After fixing $b_i(0)$, the configuration space of the rigid body can be identified with the orthogonal group on \mathbb{R}^3 ,

$$O(3) = \left\{ R \in \mathbb{R}^{3 \times 3} \middle| R^T R = 1 \right\}. \tag{3.1}$$

This group consists of two disconnected components, the special orthogonal group,

$$SO(3) = \left\{ R \in \mathbb{R}^{3 \times 3} \middle| R^T R = 1, \quad \det(R) = +1 \right\},$$
 (3.2)

and its complement of orientation-reversing transformations. As we can always choose the initial body frame, $b_i(0)$, such that det(R) = +1, we will restrict ourselves the special orthogonal group.

A common way of approaching the problem is to introduce a local coordi-

nate system

$$x: U \to \mathbb{R}^3 \tag{3.3}$$

which identifies some neighborhood $U \subset SO(3)$ of the initial configuration $R(0) \in U$ with a region $x(U) \subset \mathbb{R}^3$. A drawback of this method is that the system may approach a state $R(t) \approx Q \notin U$ outside of the region in which x is invertible. In this region of configuration space, small changes in the coordinates can correspond to very large changes in the actual state of the system, or vice versa, resulting in numerical difficulties. This is what occurs, for example, during gimble lock (see Appendix A.2) when rotations are described using Euler angles. This can be overcome, in part, by choosing a another local coordinate system,

$$y: V \to \mathbb{R}^3, \tag{3.4}$$

which is better behaved in a neighborhood V of the current configuration R(t). This approach requires the computation of transition functions, $y\circ x^{-1}$, which are often quite complicated, and highly nonlinear.

We will adopt an alternative approach which dispenses with local coordinates entirely, and describe the evolution of the body using the framework which we developed in section 2.4 and 2.5. Consider a trajectory R(t) which passes through the identity element, R(0) = 1, with velocity, $\dot{R}(0)$, at t = 0. By differentiating the constraint $R^T(t)R(t) = 1$,

$$0 = \frac{\mathrm{d}}{\mathrm{d}t} \left(R^T R \right) \Big|_{t=0} = \dot{R}^T R + R^T \dot{R} \Big|_{t=0} = \dot{R}^T (0) + \dot{R}(0), \tag{3.5}$$

we find that the Lie algebra $\mathfrak{so}(3) = T_1 \mathrm{SO}(3)$ consists of antisymmetric matrices:

$$\mathfrak{so}(3) = \left\{ \hat{\boldsymbol{\omega}} \in \mathbb{R}^{3 \times 3} \middle| \hat{\boldsymbol{\omega}}^T = -\hat{\boldsymbol{\omega}} \right\}.$$
 (3.6)

We define the canonical basis for $\mathfrak{so}(3)$ to be

$$\hat{\boldsymbol{e}}_{1}, \hat{\boldsymbol{e}}_{2}, \hat{\boldsymbol{e}}_{3} = \begin{pmatrix} 0 & 0 & 0 \\ 0 & 0 & -1 \\ 0 & 1 & 0 \end{pmatrix}, \begin{pmatrix} 0 & 0 & 1 \\ 0 & 0 & 0 \\ -1 & 0 & 0 \end{pmatrix}, \begin{pmatrix} 0 & -1 & 0 \\ 1 & 0 & 0 \\ 0 & 0 & 0 \end{pmatrix}. \tag{3.7}$$

With respect to this basis, the structure constants are given by the permutation

symbol,

$$[\hat{\boldsymbol{e}}_{i}, \hat{\boldsymbol{e}}_{j}] = c_{ij}^{k} \hat{\boldsymbol{e}}_{k},$$

$$c_{ij}^{k} = \varepsilon_{ijk} = \begin{cases} +1, & \text{if } (i, j, k) = (1, 2, 3), (2, 3, 1), (3, 1, 2) \\ -1, & \text{if } (i, j, k) = (2, 1, 3), (3, 2, 1), (1, 3, 2) \\ 0. & \text{otherwise} \end{cases}$$

$$(3.8)$$

We note the similarity between the commutation relations 3.8 and the cross products of the canonical basis vectors in \mathbb{R}^3 ,

$$\mathbf{e}_i \times \mathbf{e}_j = \varepsilon_{ijk} \mathbf{e}_k. \tag{3.9}$$

In fact, the hat map,

$$\hat{\cdot}: \mathbb{R}^3 \to \mathfrak{so}(3) \tag{3.10}$$

$$e_i \mapsto \hat{e}_i,$$
 (3.11)

defines a Lie algebra isomorphism between $\mathfrak{so}(3)$ and \mathbb{R}^3 with the cross product as its Lie bracket,

$$[\mathbf{e}_i, \mathbf{e}_j]_{\mathbb{R}^3} := \mathbf{e}_i \times \mathbf{e}_j. \tag{3.12}$$

Furthermore, the hat map relates the adjoint representation of SO(3),

$$Ad_R \hat{\boldsymbol{\omega}} = R \hat{\boldsymbol{\omega}} R^T, \tag{3.13}$$

to the standard action of SO(3) on \mathbb{R}^3 ,

$$Ad_R \hat{\boldsymbol{\omega}} = \widehat{R\boldsymbol{\omega}}.$$
 (3.14)

This can be shown by noting that for any vectors a and b,

$$\hat{a}b = a \times b, \tag{3.15}$$

and using elementary properties of the cross product,

$$\widehat{Re_i}e_j = (Re_i) \times e_j = R\left(e_i \times \left(R^T e_j\right)\right) = R\hat{e}_i R^T e_j.$$
 (3.16)

If we define,

$$\langle \hat{\boldsymbol{\alpha}}, \hat{\boldsymbol{\omega}} \rangle_{\mathfrak{so}(3)} := \frac{1}{2} \operatorname{tr}(\hat{\boldsymbol{\alpha}}^T \hat{\boldsymbol{\omega}}),$$
 (3.17)

then $\mathfrak{so}(3)$ is also isomorphic to \mathbb{R}^3 as an inner product space,

$$\langle \hat{\alpha}, \hat{\omega} \rangle_{\mathfrak{so}(3)} = \langle \alpha, \omega \rangle_{\mathbb{R}^3} = \alpha \cdot \omega.$$
 (3.18)

By differentiating the identities, $R^TR=1$ and $RR^T=1$, an arbitrary trajectory, R(t), with instantaneous velocity $\dot{R}(t)=\partial_t R(t)$, can be naturally associated with two $\mathfrak{so}(3)$ -valued matrices,

$$\hat{\boldsymbol{\omega}} = R^T \dot{R}, \quad \hat{\boldsymbol{\omega}}' = \dot{R}R^T \tag{3.19}$$

which are related by the adjoint action of SO(3),

$$\hat{\omega}' = \mathrm{Ad}_R \hat{\omega} = R \hat{\omega} R^T, \tag{3.20}$$

and lead to two separate characterizations of the tangent space,

$$T_RSO(3) = \{ R\hat{\boldsymbol{\omega}} | \hat{\boldsymbol{\omega}} \in \mathfrak{so}(3) \} = \{ \hat{\boldsymbol{\omega}}'R | \hat{\boldsymbol{\omega}}' \in \mathfrak{so}(3) \}.$$
 (3.21)

This fact is more than just a mathematical curiosity, and has a concrete physical interpretation related to the frame of reference in which velocities are measured. For simplicity, we will choose the body frame, b_i , to satisfy $b_i(0) = e_i$, so that R(0) = 1. Consider the trajectory of a material point with coordinates $x_i^{(I)}(t)$

and $x_i^{(B)}$ measured in the inertial and body frame, respectively, relative to the center of rotation. The corresponding coordinate vectors, $r^{(I)}=x_i^{(I)}(t)e_i$ and $r^{(B)}=x_i^{(B)}e_i$, must be related by

$$\boldsymbol{r}^{(I)} = R\boldsymbol{r}^{(B)}.\tag{3.22}$$

Similarly, the linear and angular velocities in the two frames are related by

$$\boldsymbol{u}^{(I)} = R\boldsymbol{u}^{(B)}, \quad \boldsymbol{\omega}^{(I)} = R\boldsymbol{\omega}^{(B)}. \tag{3.23}$$

Taking a time derivative of the position vector,

$$\boldsymbol{u}^{(I)} = (\dot{R}R^T)\boldsymbol{r}^{(I)} = R(R^T\dot{R})\boldsymbol{r}^{(B)} = R\boldsymbol{u}^{(B)}, \tag{3.24}$$

and comparing to the kinematic relations,

$$\boldsymbol{u}^{(I)} = \boldsymbol{\omega}^{(I)} \times \boldsymbol{r}^{(I)}, \quad \boldsymbol{u}^{(B)} = \boldsymbol{\omega}^{(B)} \times \boldsymbol{r}^{(B)},$$
 (3.25)

we find that

$$\hat{\boldsymbol{\omega}}^{(I)} = \dot{R}R^T, \quad \hat{\boldsymbol{\omega}}^{(B)} = R^T \dot{R}. \tag{3.26}$$

We now consider a body which is free to translate, as well as rotate, and must therefore expand our notion of a frame to include the point, $o \in \mathbb{E}^3$, at which the orthonormal triad, (e_1, e_2, e_3) , is located in Euclidean space. We choose $f = (o, e_i)$ to be a frame located at the origin o, and identify the vectors, e_i , with the canonical basis for \mathbb{R}^3 . The affine space \mathbb{E}^3 is distinguished from the vector space \mathbb{R}^3 in that it has neither a preferred origin, or a canonical set of coordinate axes. Had we chosen a coordinate system induced by another frame, $f' = (o', e_{i'}) = (o + r, Re_i)$, then coordinate vectors, z and z', of a point $p \in \mathbb{E}^3$ relative to the frames f and f', respectively, would be related by

$$z = Rz' + r. \tag{3.27}$$

By fixing a reference frame, f, any other frame with similar orientation can be defined relative to f by the pair, (R, r), with $R \in SO(3)$. These transformations form a group, SE(3), called the special Euclidean group, with a composition law given by (R, r)(R', r') = (RR', Rr' + r), and inverses by $(R, r)^{-1} = (R^{-1}, -R^{-1}r)$.

While the transformation (3.27) is affine rather than linear, SE(3) does in fact have a faithful representation as a subgroup of GL(4). We choose to

identify the special Euclidean group with this 4-by-4 matrix representation,

$$SE(3) = \left\{ \begin{pmatrix} R & r \\ 0 & 1 \end{pmatrix} \middle| R \in SO(3), r \in \mathbb{R}^3 \right\}.$$
 (3.28)

We can represent the transformation (3.27) by identifying \mathbb{E}^3 with an affine subspace of \mathbb{R}^4 ,

$$\begin{pmatrix} z \\ 1 \end{pmatrix} = \begin{pmatrix} R & r \\ 0 & 1 \end{pmatrix} \begin{pmatrix} z' \\ 1 \end{pmatrix}.$$
 (3.29)

The Lie algebra representation induced by (3.28),

$$\mathfrak{se}(3) = \left\{ \begin{pmatrix} \hat{\boldsymbol{\omega}} & \boldsymbol{\mu} \\ 0 & 0 \end{pmatrix} \middle| \hat{\boldsymbol{\omega}} \in \mathfrak{so}(3), \boldsymbol{\mu} \in \mathbb{R}^3 \right\}, \tag{3.30}$$

is spanned by the six generators,

$$\begin{pmatrix}
\hat{e}_1 & 0 \\
0 & 0
\end{pmatrix}, \begin{pmatrix}
\hat{e}_2 & 0 \\
0 & 0
\end{pmatrix}, \begin{pmatrix}
\hat{e}_3 & 0 \\
0 & 0
\end{pmatrix}$$

$$\begin{pmatrix}
0 & e_1 \\
0 & 0
\end{pmatrix}, \begin{pmatrix}
0 & e_2 \\
0 & 0
\end{pmatrix}, \begin{pmatrix}
0 & e_3 \\
0 & 0
\end{pmatrix}, (3.31)$$

By a slight abuse of notation, we will often simply write the 4-by-4 matrices in Eq. (3.31) as \hat{e}_i and e_i when it is clear that we are discussing elements of $\mathfrak{se}(3)$ rather than elements of $\mathfrak{so}(3)$ or \mathbb{R}^3 . The structure constants for $\mathfrak{se}(3)$ are given by the following commutation relations,

$$[\hat{\boldsymbol{e}}_a, \hat{\boldsymbol{e}}_b] = \varepsilon_{abc} \hat{\boldsymbol{e}}_c, \quad [\boldsymbol{e}_a, \boldsymbol{e}_b] = 0$$

$$[\hat{\boldsymbol{e}}_a, \boldsymbol{e}_b] = [\boldsymbol{e}_a, \hat{\boldsymbol{e}}_b] = \varepsilon_{abc} \boldsymbol{e}_c$$
(3.32)

The velocity, $\dot{S} = \partial_t S$, tangent to any trajectory, S, through SE(3), is associated with an $\mathfrak{se}(3)$ -valued field by left translation,

$$A_t = \hat{\omega}_t + \mu_t, \quad \dot{S} = SA_t, \tag{3.33}$$

where $\hat{\omega}_t = \mathsf{R}^{-1}\dot{\mathsf{R}}$ and $\mu_t = \mathsf{R}^{-1}\dot{r}$, are the linear and angular velocities measured in the body frame. We can endow $\mathrm{SE}(3)$ with a left-invariant Riemannian metric by defining the inner product of tangent vectors, $\dot{\mathsf{S}} = \mathsf{SA}_t$ and $\dot{\mathsf{S}}' = \mathsf{S}'\mathsf{A}_t'$ to be the sum of inner products of their linear and angular components,

$$\left\langle \dot{\mathsf{S}}, \dot{\mathsf{S}}' \right\rangle_{\mathrm{SE}(3)} = \frac{1}{2} \mathrm{tr}(\dot{\mathsf{R}}^T \dot{\mathsf{R}}') + \dot{\boldsymbol{r}}^T \dot{\boldsymbol{r}}' = \boldsymbol{\omega}_t \cdot \boldsymbol{\omega}_t' + \boldsymbol{\mu}_t \cdot \boldsymbol{\mu}_t'$$
 (3.34)

The basis 3.31 is orthonormal with respect to this metric.

Having dealt with kinematics, we now turn to dynamics of the rigid body and seek solutions of the constrained variational problem,

$$\delta \int \mathcal{L}(S, A_t) dt = 0, \quad \partial_t S = SA_t.$$
 (3.35)

We introduce a real parameter, ξ , and write variations, $\delta S = \partial_{\xi} \tilde{S} \Big|_{\xi=0}$ and $\delta A_t = \partial_{\xi} \tilde{A}_t \Big|_{\xi=0'}$ in terms of the fields satisfying, $\tilde{S} \Big|_{\xi=0} = S$ and $\tilde{A}_t \Big|_{\xi=0} = A_t$. The vector $\partial_{\xi} \tilde{S}$ is tangent to SE(3) at the point \tilde{S} , so, it is the left translate of an $\mathfrak{se}(3)$ -valued field, $\partial_{\xi} \tilde{S} = \tilde{S} \tilde{A}_{\xi}$. Smoothness of \tilde{S} requires $\partial_t \partial_{\xi} \tilde{S} - \partial_{\xi} \partial_t \tilde{S} \Big|_{\xi=0} = 0$, which places constraints on δA_t and $A_{\xi} := \tilde{A}_{\xi} \Big|_{\xi=0}$. A straightforward exercise in linear algebra shows these constraints are given in terms of the adjoint representation by,

$$\operatorname{ad}_{\mathsf{A}_t} \mathsf{A}_{\xi} = [\mathsf{A}_t, \mathsf{A}_{\xi}] = \widehat{\omega_t \times \omega_{\xi}} + \omega_t \times \mu_{\xi} - \omega_{\xi} \times \mu_t, \tag{3.36}$$

$$\delta A_t = \partial_t A_\xi + \operatorname{ad}_{A_t} A_\xi, \tag{3.37}$$

where $\hat{\omega}_{\xi}$ and μ_{ξ} are the angular and linear parts of $A_{\xi} = \hat{\omega}_{\xi} + \mu_{\xi}$, respectively. We note that this commutation relation is simply the pullback of Maurer-Cartan equation, Eq. (2.38), by \tilde{S} . This fact will be useful as we continue our discussion of higher dimensional Cosserat media.

With expressions for the constrained field variations in hand, we find that

the first variation of the action, $\mathcal{A}=\int_{t_1}^{t_2}\mathscr{L}\mathrm{d}t$, is given by

$$\delta \mathcal{A} = \int_{t_1}^{t_2} \left\langle \frac{\delta \mathcal{L}}{\delta \mathsf{A}_t} \middle| \delta \mathsf{A}_t \right\rangle + \left\langle \frac{\delta \mathcal{L}}{\delta \mathsf{S}} \middle| \delta \mathsf{S} \right\rangle dt
= \int_{t_1}^{t_2} \left\langle \frac{\delta \mathcal{L}}{\delta \mathsf{A}_t} \middle| \partial_t \mathsf{A}_\xi + \operatorname{ad}_{\mathsf{A}_t} \mathsf{A}_\xi \right\rangle + \left\langle \frac{\delta \mathcal{L}}{\delta \mathsf{S}} \middle| \mathsf{S} \mathsf{A}_\xi \right\rangle dt
= \int_{t_1}^{t_2} \left\langle -\partial_t \frac{\delta \mathcal{L}}{\delta \mathsf{A}_t} + \operatorname{ad}_{\mathsf{A}_t}^* \frac{\delta \mathcal{L}}{\delta \mathsf{A}_t} + L_{\mathsf{S}}^* \frac{\delta \mathcal{L}}{\delta \mathsf{S}} \middle| \mathsf{A}_\xi \right\rangle dt + \left\langle \frac{\delta \mathcal{L}}{\delta \mathsf{A}_t} \middle| \mathsf{A}_\xi \right\rangle \Big|_{t_1}^{t_2}$$
(3.38)

where $\mathrm{ad}_{\mathsf{A}_t}^*$ denotes the coadjoint representation of $\mathfrak{se}(3)$ acting on its dual $\mathfrak{se}^*(3)$, and we have used the fact that $L_{\mathsf{S*}}\mathsf{A}_\xi=\mathsf{SA}_\xi$ for a linear group. We define the coadjoint action on $\frac{\delta\mathscr{L}}{\delta\mathsf{A}_t}\in\mathfrak{se}^*(3)$ by the equation

$$\left\langle \operatorname{ad}_{\mathsf{A}_{t}}^{*} \frac{\delta \mathscr{L}}{\delta \mathsf{A}_{t}} \middle| \mathsf{A}_{\xi} \right\rangle := \left\langle \frac{\delta \mathscr{L}}{\delta \mathsf{A}_{t}} \middle| \operatorname{ad}_{\mathsf{A}_{t}} \mathsf{A}_{\xi} \right\rangle. \tag{3.39}$$

The existence of a Riemannian metric 3.34 allows us to identify $\mathfrak{se}^*(3) \simeq \mathfrak{se}(3)$, or more generally, $T^*\mathrm{SE}(3) \simeq T\mathrm{SE}(3)$. Under this identification, the variational derivative $\frac{\delta \mathscr{L}}{\delta \mathsf{A}_t}$ is equivalent to a gradient in $\mathfrak{se}(3)$,

$$\frac{\delta \mathcal{L}}{\delta \mathsf{A}_t} = \widehat{\nabla_{\omega_t} \mathcal{L}} + \nabla_{\mu_t} \mathcal{L},\tag{3.40}$$

where ∇_{ω_t} and ∇_{μ_t} denote gradients with respect to the angular and linear components of A_t . The quantity $\frac{\delta \mathscr{L}}{\delta S} \in T_S^* SE(3)$ can similarly be expressed as a

vector in $T_{S}SE(3)$,

$$\frac{\delta \mathcal{L}}{\delta S} = \widehat{(\boldsymbol{b}_i \times \nabla_{\boldsymbol{b}_i} \mathcal{L})} R + \nabla_{\boldsymbol{r}} \mathcal{L}, \tag{3.41}$$

and its pullback as an element of $\mathfrak{se}(3)$,

$$L_{\mathsf{S}}^* \frac{\delta \mathscr{L}}{\delta \mathsf{S}} = R^{-1} (\widehat{\boldsymbol{b}_i \times \nabla_{\boldsymbol{b}_i} \mathscr{L}}) R + R^{-1} \nabla_{\boldsymbol{r}} \mathscr{L}, \tag{3.42}$$

where $\mathsf{R} = b_i e^i$, and gradients with respect to the body frame vectors, b_i , and position, r, are denoted ∇_{b_i} and ∇_r , respectively. We can also now express the coadjoint action on elements of $\mathfrak{se}(3)$, rather than $\mathfrak{se}^*(3)$. For any $\mathsf{B} = \hat{\theta} + \nu$ and $\mathsf{B}' = \hat{\theta}' + \nu'$ in $\mathfrak{se}(3)$, we have

$$\mathrm{ad}_{\mathsf{B}}^*\mathsf{B}' = -\widehat{\boldsymbol{\theta} \times \boldsymbol{\theta}'} - \widehat{\boldsymbol{\nu} \times \boldsymbol{\nu}'} - \boldsymbol{\theta} \times \boldsymbol{\nu}'. \tag{3.43}$$

Combining the various expressions above, we find the Euler-Poincaré equations for the body to be

$$(\partial_t + \boldsymbol{\omega}_t \times) \nabla_{\boldsymbol{\omega}_t} \mathcal{L} + \boldsymbol{\mu}_t \times \nabla_{\boldsymbol{\mu}_t} \mathcal{L} - R^{-1} (\boldsymbol{b}_i \times \nabla_{\boldsymbol{b}_i} \mathcal{L}) = 0$$
 (3.44)

$$(\partial_t + \boldsymbol{\omega}_t \times) \nabla_{\boldsymbol{\mu}_t} \mathcal{L} - R^{-1} \nabla_{\boldsymbol{r}} \mathcal{L} = 0, \tag{3.45}$$

where the position and orientation of the body is given by the path-ordered exponential defined by equation (2.48),

$$S(t) = \mathcal{P}\exp \int_{t_0}^t A_t dt$$
 (3.46)

3.3 Moving frames and Cosserat rods

Consider an immersion $r: M \to \mathbb{R}^3$ of a manifold M into \mathbb{R}^3 , and a map,

$$S: M \to SE(3), \tag{3.47}$$

$$S(s) = \begin{pmatrix} R(s) & \mathbf{r}(s) \\ 0 & 1 \end{pmatrix}, \tag{3.48}$$

where the columns, b_i , of the orthogonal matrix, $R = b_i e^i$, are adapted to M in the sense discussed in section 2.3. We say that S is a *moving frame* adapted to M, or a *framing* of M. For a curve, this means $b_1 = T$ is the unit tangent and $b_2 \cdot T = b_3 \cdot T = 0$. If M is a surface, then $b_3 = n$ is the unit normal and (b_1, b_2) span the tangent space of the surface.

The Frenet-Serret frame, (T, N, B), may be viewed in this way by defining,

$$R = Te^1 + Ne^2 + Be^3, (3.49)$$

and the Frenet-Serret equation may be written,

$$\partial_s \mathsf{S} = \mathsf{S} \mathsf{A}_s, \quad \mathsf{A}_s = \begin{pmatrix} \tau \hat{\boldsymbol{e}}_1 + \kappa \hat{\boldsymbol{e}}_3 & \boldsymbol{e}_1 \\ 0 & 0 \end{pmatrix},$$
 (3.50)

where s, κ and τ are the arclength, curvature, and torsion of the curve, respectively. We will call the quantity,

$$\Omega = \Omega_i \mathbf{e}_i = \tau \mathbf{e}_1 + \kappa \mathbf{e}_3, \tag{3.51}$$

the *curvature vector*. Comparing with the analogous rigid body equations, we see that the curvature vector is the spacelike analogue angular velocity. Torsion and curvature represent rotation about the first, $T=\mathsf{R}e_1$, and third, $B=\mathsf{R}e_3$, frame vectors, respectively, but the frame undergoes no rotation about the second vector, $N=\mathsf{R}e_2$. The vanishing of the second component of the curvature vector, $e_2\cdot\Omega=0$, can in fact be taken as the *defining property* of the Frenet-Serret frame.

The Frenet-Serret frame is far from the only frame which can be adapted to the curve. Any other frame which is related to Frenet-Serret frame by

continuously varying rotation about the tangent,

$$\mathsf{R}(s) \mapsto e^{\theta(s)\hat{T}(s)} \mathsf{R}(s) = \mathsf{R}(s)e^{\theta(s)\hat{e}_1},\tag{3.52}$$

is also a perfectly valid choice. Under such a change of frame, the longitudinal $\Omega_{\parallel}=\Omega_1e_1$ and transverse $\Omega_{\perp}=\Omega_2e_2+\Omega_3e_3$ will transform as

$$\Omega_{\parallel} \mapsto \Omega_{\parallel} + \partial_s \theta e_1 \tag{3.53}$$

$$\Omega_{\perp} \mapsto e^{-\theta \hat{e}_1} \Omega_{\perp} = \kappa \sin \theta e_2 + \kappa \cos \theta e_3 \tag{3.54}$$

Given the new frame and the new curvature vector, the quantities (κ, τ, θ) and the Frenet-Serret frame can be recovered using,

$$T = Re_1 \tag{3.55}$$

$$\mathbf{N} = \mathsf{R}\left(\mathbf{\Omega}_{\perp} \times \mathbf{e}_{1}\right) / \kappa \tag{3.56}$$

$$\boldsymbol{B} = \mathsf{R}\boldsymbol{\Omega}_{\perp}/\kappa \tag{3.57}$$

$$\kappa = |\mathbf{\Omega}_{\perp}|,\tag{3.58}$$

$$\tau = \Omega_1 + \frac{e_1 \cdot (\mathbf{\Omega}_{\perp} \times \partial_s \mathbf{\Omega}_{\perp})}{|\mathbf{\Omega}_{\perp}|^2} = \Omega_1 - \partial_s \theta$$
 (3.59)

$$\theta(s) = \theta_0 + \int_0^s \Omega_1 - \tau \, \mathrm{d}s \,. \tag{3.60}$$

An alternative to the Frenet-Serret frame, known as the *Bishop frame* [72], can be constructed by choosing θ such that

$$e_1 \cdot \Omega = \partial_s \theta + \tau = 0. \tag{3.61}$$

The result is a frame which 'rolls' along the curve, without any twisting about the tangent. While the individual components of the curvature vector vary under a change of adapted frame, the magnitude of its transverse part, $|\Omega_{\perp}| = \kappa$, is invariant. Out of all frames adapted to a given curve, the frame with the smallest curvature vector is the Bishop frame, since it's curvature vector only has a transverse part. Due to this fact, the Bishop frame is sometimes referred to as the rotation minimizing frame [73].

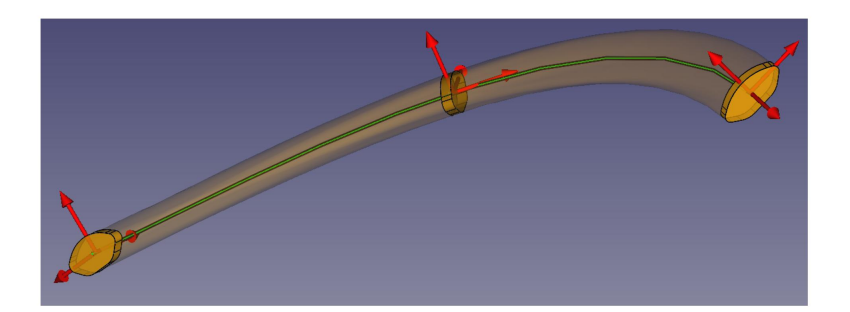


Figure 3.1: Illustration of a framed curve highlighting its centerline (green), cross-sections (orange), and adapted frame (red).

Yet another option is to take the angle θ to represent a genuine geometric

degree of freedom, rather than simply a redundancy in our description of the curve. Physically, we imagine the framed curve as being a thin filament or ribbon, and the frame is interpreted as the material frame of the filament's cross-sections at each point along the curve. Then, the quantity $\theta(s_2) - \theta(s_1)$ measures the total angle through which the material frame rotates, relative to a known reference frame, like the Frenet-Serret or Bishop frame, as it moves moves along the curve from s_1 to s_2 .

If we are to model a physical system, such as a flexible filament, it makes sense to take the material frame as fundamental, rather than defining it relative to something unphysical like the Frenet-Serret frame of the filament's centerline. Components of the curvature vector, which describe physical twisting and bending about the material frame vectors, can then be taken as fundamental dynamical variables. Up until now, we have considered only arclength parameterized curves and *adapted* frames. This is equivalent to requiring the filament satisfy the inextensibility and unshearbility constraints of a Kirchhoff rod [74–76],

$$\partial_s \mathbf{r} = \mathsf{R} \mathbf{e}_1. \tag{3.62}$$

Relaxing this constraint results in a model which is able to account for the

full range of deformations illustrated in Figure 3.2. This more general system is known as a Cosserat rod. As we demonstrate in later sections, it is often useful to treat a system using the full Cosserat model, even when we are only interested in inextensible/unshearable case. This allows us to take advantage of Euler-Poincaré variational methods, and the additional constraints are easily accounted for through the introduction of Lagrange multipliers and constraint forces.

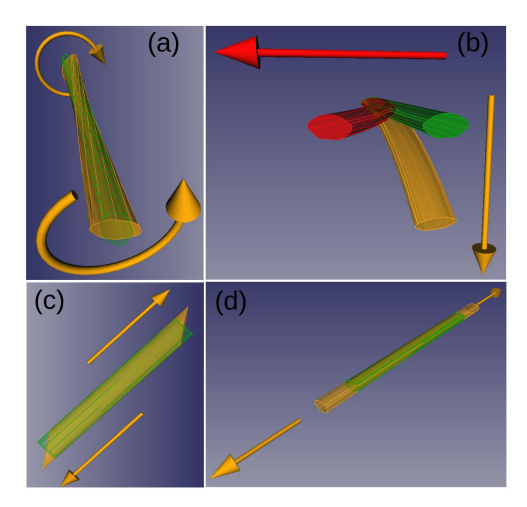


Figure 3.2: The modes of deformation of a Cosserat rod include (a) twisting, (b) bending, (c) shearing, (d) and stretching.

To study the dynamics of the Cosserat rod, we must consider a moving

frame,

$$S(s,t) = \begin{pmatrix} R(s,t) & \mathbf{r}(s,t) \\ 0 & 1 \end{pmatrix}, \tag{3.63}$$

which depends on time t, as well as the material coordinate s. The parameters s and t are each associated with an $\mathfrak{se}(3)$ -valued generator,

$$\partial_s S = SA_s, \quad A_s = \begin{pmatrix} \hat{\omega}_s & \mu_s \\ 0 & 0 \end{pmatrix},$$
 (3.64)

$$\partial_t S = SA_t, \quad A_t = \begin{pmatrix} \hat{\omega}_t & \mu_t \\ 0 & 0 \end{pmatrix}.$$
 (3.65)

When the rod is allowed to be extensible/shearable, the frame may no longer satisfy Eq. (3.62), and the generator A_s now contains information about extensile and shear deformations, $\mu_s = (b_i \cdot \partial_s r)e_i$, in addition to rotational deformation described by ω_s . The timelike generator, A_t , can be physically interpreted just as it was for the rigid body, with ω_t and u_t representing the angular and linear velocity of the material frame.

The generators A_s and A_t can be viewed as components of the $\mathfrak{se}(3)$ -valued

one-form, or gauge potential, defined by,

$$A = S^{-1} dS = A_s ds + A_t dt.$$
 (3.66)

The gauge potential associated with any smooth multi-parameter moving frame must satisfy an integrability condition given by the Maurer-Cartan equation (2.38). The Maurer-Cartan equation on SE(3) is equivalent to a pair of vector equations,

$$\partial_t \omega_s - \partial_s \omega_t + \omega_t \times \omega_s = 0, \tag{3.67}$$

$$\partial_t \mu_s - \partial_s \mu_t + \omega_t \times \mu_s - \omega_s \times \mu_t = 0, \tag{3.68}$$

which are sometimes referred to as Euclidean structure equations. Although here we have interpreted s as a material coordinate and t as time, this integrability condition applies to any pair of parameters which a moving frame may depend on. We have already seen another example of this in our derivation of the Euler-Poincaré equations for the rigid body where we found that variations of the body velocities were similarly constrained by the structure equations.

3.4 Cosserat media

We now turn to the case of a general Cosserat medium. We formulate the problem as a Lagrangian field theory on a base space, $M\subset\mathbb{R}^{n+1}$, parameterized by n spacelike material coordinates and one timelike coordinate, $s=(s^1,\ldots,s^n,s^{n+1}=t)$. The state space of the medium consists of fields over M,

$$S(s) = \begin{pmatrix} R(s) & r(s) \\ 0 & 1 \end{pmatrix}$$
 (3.69)

which take values in the special Euclidean group SE(3). Each field configuration is associated with a gauge potential, $A = A_{\alpha} ds^{\alpha}$, whose components describe local velocity and deformation, and take values in the special Euclidean algebra, $\mathfrak{se}(3)$. A choice of gauge is equivalent to a choice of frame for each $s \in M$ in which to measure velocities and deformations. There are two natural choices when it comes to fixing a gauge which are analogous to the body-fixed frame and space-fixed, or inertial, frame used in classical rigid body dynamics. The body-fixed gauge results in a potential,

$$A^{(B)} = S^{-1} dS, \qquad (3.70)$$

which is equivalent to the pullback of the left-invariant Maurer-Cartan on SE(3) by the field S, while the space-fixed gauge results in a potential,

$$A^{(I)} = dS S^{-1}, (3.71)$$

which is equivalent to the pullback of the right-invariant Maurer-Cartan by S. We will generally work in the body-fixed gauge, $A = S^{-1}\mathrm{d}S$, unless otherwise specified.

The methods which we used in our derivation of the Euler-Poincaré equations for the rigid body can be used with only slight modifications to derive equations governing the general Cosserat medium. Rather than repeating the derivation we simply state the result. The Euler-Poincaré equations for a system with Lagrangian density $\mathcal{L}=\mathcal{L}(\mathsf{S},\mathsf{A})$ are given in the body-fixed gauge by

$$-\partial_{\alpha} \frac{\delta \mathcal{L}}{\delta \mathsf{A}_{\alpha}} + \operatorname{ad}_{\mathsf{A}_{\alpha}}^{*} \frac{\delta \mathcal{L}}{\delta \mathsf{A}_{\alpha}} + L_{\mathsf{S}}^{*} \frac{\delta \mathcal{L}}{\delta \mathsf{S}} = \mathsf{N}, \tag{3.72}$$

$$dA + \frac{1}{2}[A \wedge A] = 0, \tag{3.73}$$

$$S = \mathcal{P} \exp \int A \tag{3.74}$$

where $\mathrm{ad}_{\mathsf{A}_\alpha}^*$ denotes the coadjoint representation of $\mathfrak{se}(3)$, L_S^* denotes pullback

by the left translation operator on SE(3), $[A \wedge A]$ is the bracket for Lie algebravalued differential forms, and N accounts for any non-variational stresses applied to the system. Decomposing external stress as $N=-\hat{m}-f$, separating into of angular and linear parts gives

$$(\partial_{\alpha} + \boldsymbol{\omega}_{\alpha} \times) \nabla_{\boldsymbol{\omega}_{\alpha}} \mathcal{L} + \boldsymbol{\mu}_{\alpha} \times \nabla_{\boldsymbol{\mu}_{\alpha}} \mathcal{L} - R^{-1} (\boldsymbol{b}_{i} \times \nabla_{\boldsymbol{b}_{i}} \mathcal{L}) = \boldsymbol{m}$$
(3.75)

$$(\partial_{\alpha} + \boldsymbol{\omega}_{\alpha} \times) \nabla_{\boldsymbol{\mu}_{\alpha}} \mathcal{L} - R^{-1} \nabla_{\boldsymbol{r}} \mathcal{L} = \boldsymbol{f}$$
(3.76)

$$\partial_{\alpha} \boldsymbol{\omega}_{\beta} - \partial_{\beta} \boldsymbol{\omega}_{\alpha} + \boldsymbol{\omega}_{\alpha} \times \boldsymbol{\omega}_{\beta} = 0 \tag{3.77}$$

$$\partial_{\alpha} \mu_{\beta} - \partial_{\beta} \mu_{\alpha} + \omega_{\alpha} \times \mu_{\beta} - \omega_{\beta} \times \mu_{\alpha} = 0$$
 (3.78)

where equations (3.75), (3.76) are equivalent to equation (3.72) and (3.77), (3.78) are equivalent to equation (3.73). Natural boundary conditions associated with the variational problem are given by

$$(\boldsymbol{\omega}_{\xi} \cdot \nabla_{\boldsymbol{\omega}_{\alpha}} \mathcal{L} + \boldsymbol{\mu}_{\xi} \cdot \nabla_{\boldsymbol{\mu}_{\alpha}} \mathcal{L})|_{\partial S} = 0$$
(3.79)

4.1 Introduction

Motility introduces a number of demands on the mechanical construction of bacterial cells. Such constraints have been studied for motility organelles; slender flagella can buckle below a critical bending stiffness or above a critical motor torque [77, 78], and the same is true of the flexible flagellar hook [79, 80]. The shape and size of bacterial cells is influenced by numerous considerations [81–84], including efficient motility in liquids [85–87]. However, motile bacterial cells are canonically presumed to be rod-shaped, non-deformable structures, and cell stiffness, a feature normally provided by cell wall composition [88–90] and turgor pressure [91], is typically overlooked in studies of motility. Cell wall stiffness regulation alters bacterial cell shape, influences motility, and enables bacteria to adapt and survive [92, 93].

The length of *Proteus mirabilis* (*P. mirabilis*) cells increases by up to 20-40x when they are in a swarming state [94], and deformation in cell shape are visibly clear in a swarm [95, 96]. *P. mirabilis* swarmer cells have reduced cell stiffness compared to normal vegetative cells [96]. Gene deletion has also been used to artificially reduce cell stiffness [97]. But the nature and organization of any motility organelles is also important. A swarmer cell swims by rotating

up to thousands of flagella which are distributed along its surface [98, 99]. The flagellar motion drives active, wavelike surface features more often used to describe ciliated organisms, which themselves are classically modeled as a continuum of active stress [100, 101].

A wild-type *P. mirabilis* cell is stiff and rod-shaped and swims along a straight trajectory, with its flagella oriented with their tips opposite the swimming direction (Fig. 4.1e) [102]. The fluid response to flagellar motion drives the body forward, and induces a rotational velocity along the long axis as dictated by the force- and torque-free nature of swimming in viscous fluids [103]. Elongated swarmer cells, however, can express a wide range of intricate and stunning dynamics. Figure 4.1 shows *P. mirabilis* cells which have buckled under their own activity. The flagellar tips appear to be pointing away from the direction of *local* body motion, suggestive that their orientation depends upon local viscous stresses (Fig. 4.1a-b). Strongly three-dimensional configurations and dynamics are shown in Fig. 4.1c, which includes a spinning motion about the direction of swimming. An even more highly deformed state with multiple self-crossings is shown in Fig. 4.1d.

Such active systems are particularly rich, as even passive slender bodies driven by external forces [104] or flows [105] continue to reveal new buckling behaviors [106–111]. The shapes and dynamics of elongated *P. mirabilis* cells

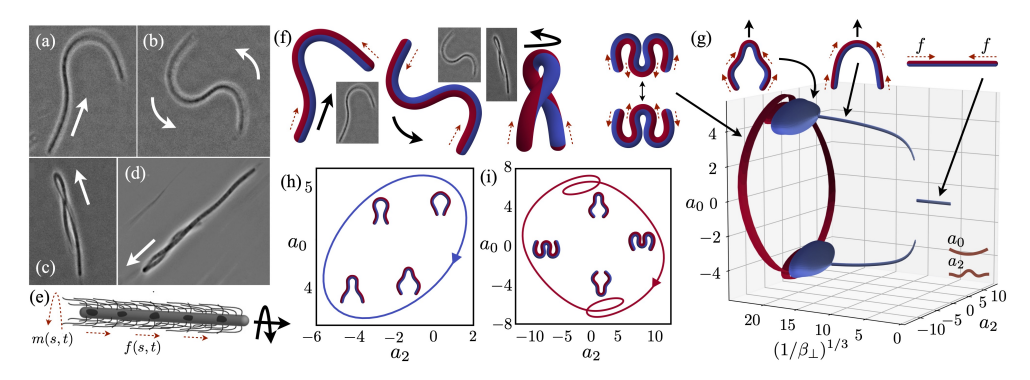


Figure 4.1: (a-d) Swarmer P. mirabilis cells bend, rotate, and twist under their own flagellar activity. Solid arrows indicate the direction of motion. (e) Flagellar stresses are modeled as a continuous force density f(s,t) and proportional moment density m(s,t) which drives and rotates the body through the fluid. (f) An active swimming Kirchhoff rod reproduces U-shaped swimming, S-shaped rotation, and twisted, rotating swimming states found in experiments. Dashed arrows indicate the direction of the local flagellar force and moment densities. (g) Phase diagram illustrating periodic symmetric dynamics in the absence of an active moment m(s,t)=0. The centerline curvature $\kappa(s,t) = \sum_{k=0}^{\infty} a_k(t)\phi_k(s)$ is projected onto the first two even biharmonic modes $(a_0(t), a_2(t))$ and trajectories in a_0 - a_2 space are plotted against $\beta_\perp^{-1/3}$ where $\beta_\perp=B_\perp/(f^*L^3)$ is a dimensionless bending stiffness, with B_\perp the bending modulus, f^* a characteristic active force density, and L the body length. Bifurcations from straight filaments to swimming-U shapes, then to periodic waving-U dynamics, then to periodic flapping-W dynamics are observed as the bending stiffness is reduced. (h) A cross-section of the phase diagram in (g) with $\beta_{\perp}=1.3\times10^{-4}$ (waving-U dynamics). (i) A cross-section of the phase diagram in (g) with $\beta_{\perp} = 7.6 \times 10^{-5}$ (flapping-W dynamics).

share many similarities with active or externally forced filaments which exhibit spontaneous symmetry breaking [112–114]. The U- and S-shaped configurations in Fig. 4.1a-b have been observed numerically in related systems in two dimensions [115], as have spiral-shaped configurations [116]. The response of semi-flexible polymers to molecular-motor-driven stress has seen tremendous interest [117], particularly in the context of cytoskeletal networks and interphase chromatin configurations [118–120]. Flagellar propulsion, however, introduces additional features, for instance a competition between twist/bend elasticity and twist injection [74, 121, 122], and a dynamic rearrangement of flagellar stress. It is plausible that the highly nonlinear twist-bend coupling [123, 124] responsible for the emergence of writhing instabilities [125] and chiral configurations [126] in generic elastic filaments is also responsible for the configurations seen in Fig. 4.1c-d.

In this paper we explore numerically and analytically a Kirchhoff rod model of a long, swimming cell which is driven by active forces and moments associated with flagellar activity. The model reproduces both two- and three-dimensional configurations (Fig. 4.1f) and predicts microorganism buckling and writhing under its own flagellar activity and viscous stress response. Bifurcations in the shapes and dynamics appear as the cell body is made more flexible, including buckling and torsional instabilities commonly observed

in passive elastic systems, and new modes of motion are found upon the introduction of the active moment.

The chapter is organized as follows. In §4.2 we present the active Kirchhoff rod model, in which the deformable body dynamics are described using the Euler-Poincaré formalism [43, 52, 59]. The numerical method used to explore the system, which exploits the geometric structure of the Euclidean group SE(3) and its Lie algebra $\mathfrak{se}(3)$ to seamlessly and accurately incorporate kinematic constraints, is also presented. In §4.3 we consider both analytically and numerically the body configurations and dynamics which emerge from the model equations. The case of a vanishing active moment is first explored, resulting in planar dynamics. The results of a linear stability analysis are shown to compare favorably with full numerical simulations, and associated eigenfunctions provide a baseline from which to explore a sequence of shape bifurcations in the fully nonlinear system. The fully three-dimensional dynamics are then probed, which reveal buckling behaviors analogous to those found in the planar setting, but which also involve a coupling between twisting and bending modes of deformation and stress. A linear stability analysis is revisited, which includes modifications to the predicted unstable wavenumbers and growth rates in the case with no active moment.

Active Kirchhoff rod model 4.2

The cell is assumed to have length L with uniform circular cross-section of diameter a. Aspect ratios a/L of swarmers, typically on the order of 10^{-2} to 5×10^{-2} [96, 102], are sufficiently small that extensile and shear deformations are neglected [75]. Associated with each station of the filament in arclength s and time t is a moving frame (see §3.3)

$$S(s,t) = \begin{pmatrix} R(s,t) & \mathbf{r}(s,t) \\ 0 & 1 \end{pmatrix}$$
(4.1)

representing the Euclidean transformation which maps an inertial frame (e_0,e_1,e_2) located at the origin onto the body's orthonormal material frame $(q_0,q_1,q_2)=(\mathsf{R}\pmb{e}_0,\mathsf{R}\pmb{e}_1,\mathsf{R}\pmb{e}_2)$ located at $\pmb{r}.$ Velocities and deformations may then be represented by the fields which take values in the special Euclidean algebra $\mathfrak{se}(3)$,

$$A_{t} = S^{-1}\partial_{t}S = \begin{pmatrix} \hat{\omega} & \mathbf{u} \\ 0 & 0 \end{pmatrix}, \tag{4.2}$$

$$A_{s} = S^{-1}\partial_{s}S = \begin{pmatrix} \hat{\Omega} & \mathbf{U} \\ 0 & 0 \end{pmatrix}, \tag{4.3}$$

$$\mathsf{A}_s = \mathsf{S}^{-1}\partial_s \mathsf{S} = \begin{pmatrix} \hat{\mathbf{\Omega}} & \mathbf{U} \\ 0 & 0 \end{pmatrix},\tag{4.3}$$

where we have defined the antisymmetric operators $\hat{\omega} := \omega \times$ and $\hat{\Omega} := \Omega \times$. The field A_t describes the body's local linear velocity, $u = R^{-1}\partial_t r$, and local angular velocity, $\hat{\omega} = R^{-1}\partial_t R$, as measured in the material frame, and the field A_s describes the body's local deformation in the form of the twist/curvature operator, $\hat{\Omega} = R^{-1}\partial_s R$, and the centerline tangent vector $U = R^{-1}\partial_s r$. We choose to formulate dynamics of the body directly in terms of the fields $(u, \hat{\omega}, U, \hat{\Omega})$, and apply the method of Euler-Poincaré reduction [39, 59]. Body configurations are written as path-ordered exponentials [127] (see §2.4),

$$S(0,t) = S(0,0) \mathcal{P} \exp \int_0^t A_t(0,\xi) d\xi,$$
 (4.4)

$$S(s,t) = S(0,t) \mathcal{P} \exp \int_0^s A_s(\xi,t) d\xi.$$
 (4.5)

The path-ordered exponential, or product integral, of a matrix-valued curve $X = X(\xi)$ is the limit of an ordered product of matrix exponentials,

$$\mathcal{P}\exp \int_{a}^{b} \mathsf{X}(\xi) \,\mathrm{d}\xi = \lim_{n \to \infty} e^{\mathsf{X}(\xi_{0})\Delta\xi} e^{\mathsf{X}(\xi_{1})\Delta\xi} \dots e^{\mathsf{X}(\xi_{n})\Delta\xi}, \tag{4.6}$$

where $\Delta \xi = (b-a)/n$ and $\xi_k = a + k\Delta \xi$.

Deformation and velocity fields (A_s, A_t) are components of an $\mathfrak{se}(3)$ -valued

one-form,

$$A = A_s ds + A_t dt = S^{-1} dS, \qquad (4.7)$$

where $dS = \partial_s S ds + \partial_t S dt$ is the exterior derivative of S, and (ds, dt) are one-forms dual to the coordinate basis (∂_s, ∂_t) . Integrability of the system dS = SA requires A satisfy the Euclidean structure equation (see §2.4,§2.5),

$$dA + A \wedge A = 0. \tag{4.8}$$

where \wedge is the wedge product for matrix-valued differential forms [71]. This gives the commutation relation,

$$(dA + A \wedge A)(\partial_s, \partial_t) = \partial_s A_t - \partial_t A_s + [A_s, A_t] = 0,$$
(4.9)

where $[A_s, A_t] := A_s A_t - A_t A_s$ is the matrix commutator. Separating its angular and linear components using the fact that $\widehat{a \times b} = \left[\widehat{a}, \widehat{b} \right]$, for any $a, b \in \mathbb{R}^3$,

$$\partial_s \boldsymbol{\omega} - \partial_t \boldsymbol{\Omega} + \boldsymbol{\Omega} \times \boldsymbol{\omega} = \mathbf{0}, \tag{4.10}$$

$$\partial_s \mathbf{u} - \partial_t \mathbf{U} + \mathbf{\Omega} \times \mathbf{u} - \boldsymbol{\omega} \times \mathbf{U} = \mathbf{0}, \tag{4.11}$$

we find the structure equations to be a generalization of the familiar compatibility relations for elastic rods [74, 75].

Viscous stresses, $-\zeta \cdot u$ and $-\zeta_r \omega_{\parallel} = -(U \cdot \omega) U$, are related to the local body velocity through a local resistive force theory, where $\zeta = \zeta_{\parallel} U U^T + \zeta_{\perp} (1 - U U^T)$ with longitudinal ζ_{\parallel} and transverse ζ_{\perp} coefficients, and by a rotational drag coefficient ζ_r [121, 128]. Driving the system away from equilibrium are active stresses arising from a distribution of flagella, modeled here as a continuum providing an effective tangential force density fU and proportional moment density mU := MLfU (Fig. 4.1e). To account for the tendency of flagella to align with local flow, we consider f to evolve according to

$$\tau_f \partial_t f = (f^*/L) \left[1 - (f/f^*)^2 \right] \boldsymbol{U} \cdot \boldsymbol{u} + D_f \partial_s^2 f, \tag{4.12}$$

with $\partial_s f(-L/2) = \partial_s f(L/2) = 0$. The force density tends toward a characteristic magnitude f^* with a relaxation time $\tau_f \zeta_{\parallel} L/f^*$ depending on the dimensionless parameter τ_f , and D_f is a diffusion constant.

The internal energy of the body is given by

$$E = \int_{-L/2}^{L/2} \frac{1}{2} \mathbf{\Omega} \cdot \mathbf{B} \mathbf{\Omega} + \mathbf{\Lambda} \cdot \mathbf{U} \, \mathrm{d}s$$
 (4.13)

where Λ is a Lagrange multiplier which enforces inextensibility and unsheara-

bility,

$$q_0 = \mathsf{R}\boldsymbol{U} \tag{4.14}$$

and $\mathsf{B} = B_{\parallel} \boldsymbol{U} \boldsymbol{U}^T + B_{\perp} (1 - \boldsymbol{U} \boldsymbol{U}^T)$ penalizes twisting and bending with moduli B_{\parallel} and B_{\perp} , respectively [75]. To obtain Euler-Poincaré equations for the reduced system, we equate the structure preserving variation of E with the virtual work done by active and viscous stresses (see §3.4),

$$W = -\int_{-L/2}^{L/2} \langle \mathsf{N}, \mathsf{A}_{\xi} \rangle \, \mathrm{d}s \,, \quad \mathsf{N} = \begin{pmatrix} -\zeta_r \hat{\boldsymbol{\omega}}_{\parallel} & -\boldsymbol{\zeta} \cdot \boldsymbol{u} + f\boldsymbol{U} \\ 0 & 0 \end{pmatrix}$$
(4.15)

where $oldsymbol{\omega}_{\parallel} = (oldsymbol{U} \cdot oldsymbol{\omega}) \, oldsymbol{U}.$ This results in the following equations,

$$\partial_s \mathbf{\Lambda} + \mathbf{\Omega} \times \mathbf{\Lambda} = \boldsymbol{\zeta} \cdot \boldsymbol{u} - f \boldsymbol{U}, \tag{4.16}$$

$$\partial_s (\mathsf{B}\Omega) + \Omega \times \mathsf{B}\Omega + U \times \Lambda = \zeta_r \omega_{\parallel} - mU,$$
 (4.17)

describing local force and moment balance along the body, subject to boundary conditions,

$$\Lambda = 0, \quad \Omega = 0 \tag{4.18}$$

at either end of the body. The kinematic relations (4.4), (4.5), (4.10), (4.11), (4.14), the flagellar evolution law (4.12), and the balance equations (4.16), (4.17) form a closed system describing dynamics of the body and its flagellar distribution.

Evolution equations for the twist $\Omega_{\parallel}=(U\cdot\Omega)U$, curvatures $\Omega_{\perp}=\left(1-UU^{T}\right)\Omega$, and tension $\lambda=U\cdot\Lambda$ are obtained by first solving (4.14),(4.16),(4.17) and the transverse part of (4.11) for $\Lambda_{\perp}=(1-UU^{T})\Lambda$ and the velocities (ω,u) :

$$\mathbf{\Lambda}_{\perp} = \mathbf{U} \times \partial_s \left(B_{\perp} \mathbf{\Omega}_{\perp} \right) + \left(B_{\parallel} - B_{\perp} \right) \left(\mathbf{U} \cdot \mathbf{\Omega}_{\parallel} \right) \mathbf{\Omega}_{\perp}, \tag{4.19}$$

$$\boldsymbol{u} = \zeta^{-1} \left(\partial_s \boldsymbol{\Lambda} + \boldsymbol{\Omega} \times \boldsymbol{\Lambda} + f \boldsymbol{U} \right), \tag{4.20}$$

$$\boldsymbol{\omega} = \frac{1}{\zeta_r} \left(\partial_s \left(B_{\parallel} \boldsymbol{\Omega}_{\parallel} \right) + m \boldsymbol{U} \right) + \boldsymbol{U} \times \left(\partial_s \boldsymbol{u} + \boldsymbol{\Omega} \times \boldsymbol{u} \right). \tag{4.21}$$

Equations (4.19), (4.20), and (4.21) are then substituted into Eq. (4.10) and the longitudinal component of (4.11). The resulting shape evolution equations take the form

$$\partial_t \mathbf{\Omega}_{\parallel} + \left[\frac{B_{\perp} - B_{\parallel}}{\zeta_{\perp}} \kappa^2 - \frac{B_{\parallel}}{\zeta_r} \right] \partial_s^2 \mathbf{\Omega}_{\parallel} = \mathbf{G}_{\parallel}, \tag{4.22}$$

$$\partial_t \mathbf{\Omega}_{\perp} + \frac{B_{\perp}}{\zeta_{\perp}} \partial_s^4 \mathbf{\Omega}_{\perp} = \mathbf{G}_{\perp}, \tag{4.23}$$

$$\begin{split} \partial_{s}^{2}\lambda - \frac{\zeta_{\parallel}}{\zeta_{\perp}}\kappa^{2}\lambda + \frac{B_{\perp}}{2}\partial_{s}^{2}\kappa^{2} + \partial_{s}f \\ + \frac{\zeta_{\parallel}B_{\perp}}{\zeta_{\perp}}\left(\mathbf{\Omega}_{\perp}\cdot\partial_{s}^{2}\mathbf{\Omega}_{\perp} - \kappa^{2}|\mathbf{\Omega}_{\parallel}|^{2} - 2\mathbf{\Omega}_{\parallel}\cdot[\mathbf{\Omega}_{\perp}\times\partial_{s}\mathbf{\Omega}_{\perp}]\right) \\ + \frac{\zeta_{\parallel}B_{\parallel}}{\zeta_{\perp}}\left(\kappa^{2}|\mathbf{\Omega}_{\parallel}|^{2} + \mathbf{\Omega}_{\parallel}\cdot[\mathbf{\Omega}_{\perp}\times\partial_{s}\mathbf{\Omega}_{\perp}]\right) = 0, \quad (4.24) \end{split}$$

where we have defined $\kappa^2=|\Omega_\perp|^2$, and the vector-valued functions G_\parallel and G_\perp depend nonlinearly on spatial derivatives of Ω , λ , and f. Natural boundary conditions require that $\Omega_\parallel,\Omega_\perp,\partial_s\Omega_\perp$, and λ all vanish at both ends of the body.

Upon scaling by the length L, force density f^* , and stiffness B_\perp , the system is found to depend on six dimensionless groups: a relative bending modulus $\beta_\perp = B_\perp/(f^*L^3)$, twist modulus $\beta_\parallel = B_\parallel/(f^*L^3)$, translational drag ratio $\eta = \zeta_\perp/\zeta_\parallel$, rotational drag $\eta_r = \zeta_r/(\zeta_\parallel L^2)$, dimensionless active moment M, and a dimensionless diffusion constant $D = \zeta_\parallel D_f/(f^*L)$. Henceforth all variables are understood to be dimensionless.

To estimate the scale of the active moment, M, we note that a helical flagellum with pitch $P\approx 2\mu$ m, circumference $C\approx 1.5\mu$ m, length $\ell=10\mu$ m, and diameter $d\approx 20$ nm, upon rotation with speed ω generates a force on an affixed body $F_{\nu}\approx 2\mu C^2\ell\omega/Pc$, where μ is the viscosity of water and $c=\ln(\ell^2/d^2)-1$ [129]. Due to its chirality it also generates a torque $L_{\nu}\approx 2\mu C^2\ell\omega/\pi^2c$. Using a body length $L\approx 10^{-5}-10^{-4}$ m gives a range of biologically relevant active moments $M = L_{\nu}/LF_{\nu} \approx 10^{-3} - 10^{-2}$.

A principal advantage of this approach is that it naturally leads to numerical schemes which circumvent violations of inextensibility, unshearability, and frame orthonormality, and do not require soft penalties or explicit parameterization of rotations by Euler angles or quaternions [51, 130–133]. This is accomplished through the use of a structure-preserving numerical method [134] which performs timestepping and spatial integration of S,

$$S(s,t) \mapsto S(s,t+\Delta t), \quad S(s,t) \mapsto S(s+\Delta s,t),$$
 (4.25)

entirely in terms of the $\mathrm{SE}(3)$ composition composition law. First, we note that equation (4.4) is equivalent to

$$S(0, t + \xi) = S(0, t) \mathcal{P} \exp \int_0^{\xi} Z(\xi') d\xi', \qquad (4.26)$$

with $Z(\xi) := A_t(0, t + \xi)$. The ordered exponential can be expressed as $\mathcal{P}\exp\int_0^{\xi} Z(\xi') d\xi' = e^{X(\xi)}$, in terms of a new $\mathfrak{se}(3)$ -valued field, X, related to Z by the Magnus expansion [135]

$$X(\xi) = \int_0^{\xi} Z(\xi) d\xi - \frac{1}{2} \int_0^{\xi} \int_0^{\xi'} [Z(\xi''), Z(\xi')] d\xi'' d\xi' + \dots$$
 (4.27)

Then, writing

$$X(\xi) = \xi \frac{Z(\xi) + Z(0)}{2} + O(\xi^3), \tag{4.28}$$

we have

$$S(0, t + \Delta t) = S(0, t) \exp(\Delta t \frac{A_t(0, t + \Delta t) + A_t(0, t)}{2}) + O(\Delta t^3).$$
 (4.29)

By a similar argument involving A_s rather than A_t , we find

$$S(s + \Delta s, t) = S(s, t) \exp(\Delta s \frac{A_s(s + \Delta s, t) + A_s(s, t)}{2}) + O(\Delta s^3).$$
 (4.30)

Matrix exponentials in (4.29) and (4.30) are computed using the closed form expression for the exponential map on SE(3) (see B for details). Given vectors α and β , we have

$$\exp\begin{pmatrix} \hat{\boldsymbol{\alpha}} & \boldsymbol{\beta} \\ 0 & 0 \end{pmatrix} = \begin{pmatrix} e^{\hat{\boldsymbol{\alpha}}} & V\boldsymbol{\beta} \\ 0 & 1 \end{pmatrix}, \tag{4.31}$$

where
$$e^{\hat{\boldsymbol{\alpha}}} = 1 + \frac{\sin \alpha}{\alpha} \hat{\boldsymbol{\alpha}} + \frac{1 - \cos \alpha}{\alpha^2} \hat{\boldsymbol{\alpha}}^2$$
, $V = 1 + \frac{1 - \cos \alpha}{\alpha^2} \hat{\boldsymbol{\alpha}} + \frac{\alpha - \sin \alpha}{\alpha^3} \hat{\boldsymbol{\alpha}}^2$, and $\alpha = |\boldsymbol{\alpha}|$.

Equations (4.12), (4.22),(4.23), and (4.24) are discretized in space uni-

formly using second-order accurate central difference approximations, and advanced in time using a second-order implicit backward-differentiation scheme with a hybrid nonlinear solver applied at each timestep. Equations (4.4) and (4.5) are solved using the explicit second-order accurate Magnus integrators discussed above. Other approaches to this stiff numerical problem with different treatments of the hydrodynamics have recently been developed [136–145]. The parameters $(\eta, D, \tau_f) = (2, 10^{-3}, 10^{-2})$, timestep size $\Delta t = 10^{-3}$, and spatial gridspacing $\Delta s = 1/64$ are fixed for the duration unless otherwise stated.

4.3 Body configurations and dynamics

No active moment: planar dynamics

In the case of no active moment, M=0, the body configuration is fully characterized by a single rotational strain, the (signed) centerline curvature $\kappa=\pm|\Omega_{\perp}|$. Restricting the shape evolution equations to two dimensions, the

curvature, active force, and tension satisfy

$$\partial_t \kappa = -\frac{\beta_{\perp}}{n} \partial_s^4 \kappa + \frac{1}{n} \partial_s^2 (\kappa \lambda) + \partial_s (\kappa \left[\partial_s \lambda + f \right]) + \frac{\beta_{\perp}}{3} \partial_s^2 (\kappa^3), \qquad (4.32)$$

$$\partial_t f = D\partial_s^2 f + \left(1 - f^2\right) \left(\beta_\perp \kappa \partial_s \kappa + \partial_s \lambda + f\right), \tag{4.33}$$

$$\partial_s^2 \lambda - \frac{\kappa^2}{\eta} \lambda = -\partial_s f - \frac{\beta_\perp}{2} \partial_s^2 \left(\kappa^2 \right) - \frac{\beta_\perp}{\eta} \kappa \partial_s^2 \kappa. \tag{4.34}$$

We note that the tension equation can also be reformulated as an integral equation (see Appendix C.1).

To begin we consider shapes which are symmetric about the body midpoint s=0 (and active forces which are odd). To describe the geometry it is convenient to use the eigenfunctions of ∂_s^4 satisfying force- and moment-free boundary conditions [146] (the first three of which are shown in Fig. 4.2c as dashed red curves). The curvature is decomposed as a sum $\kappa(s,t)=\sum_{k=0}^\infty a_k(t)\phi_k(s)$. Figure 4.1g shows a phase portrait for the dynamics of the first two even biharmonic modes, (a_0,a_2) , for a range of bending stiffness β_\perp with M=0. Values are plotted against $\beta_\perp^{-1/3}$, which is proportional to the body length L.

Phases in Fig. 4.1g are identified by examining the long time behaviour of filaments initialized with a compressive active force density $f(s,0)=-\tanh(10s)$. For $\beta_{\perp}>9.1\times10^{-3}$, the stiff filament relaxes to a straight configu-

ration, with the active stress eventually decaying due to diffusion via Eq. (4.12). At approximately $\beta_{\perp}=9\times 10^{-3}$ there is a bifurcation to steady state U-shaped swimmers with a nonzero a_0 which dominates all other modes. Further decreases in stiffness lead to curvature oscillations (this cross-section of the phase diagram is shown in Fig. 4.1h) and excitation of progressively higher modes. At approximately $\beta_{\perp}=6.8\times 10^{-5}$, another bifurcation is observed to unsteady, periodic flapping dynamics which involve even larger excursions in the phase plane (Fig. 4.1i), and periodic changes in the swimming direction.

Susceptibility to buckling can be understood by exploring the stability of a nearly straight body to generic (planar) perturbations. Upon defining the mean active force density $\overline{f}:=\int_{-1/2}^{1/2}f\,\mathrm{d}s$, we find to first order in κ (assumed small) that

$$\lambda = -\int_{-1/2}^{s} (f - \overline{f}) \,\mathrm{d}s \,, \tag{4.35}$$

$$\partial_t \kappa = -\frac{\beta_{\perp}}{\eta} \partial_s^4 \kappa + \frac{1}{\eta} \partial_s^2 (\lambda \kappa) + \overline{f} \partial_s \kappa. \tag{4.36}$$

Assuming a symmetric compressive force, $\overline{f}=0$, this yields an eigenvalue

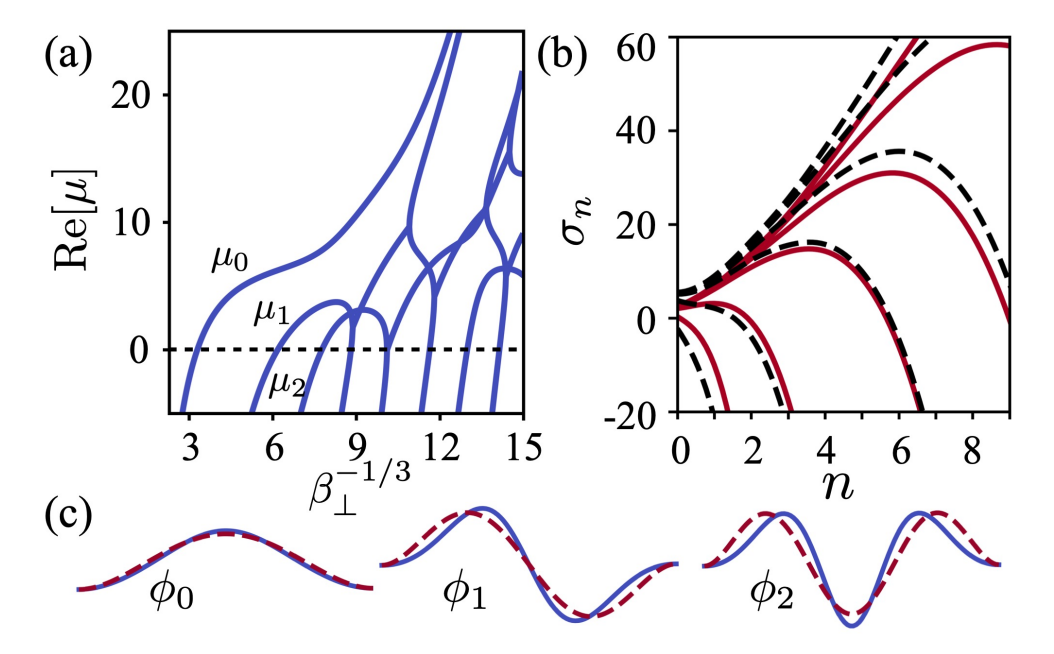


Figure 4.2: (a) Dominant eigenvalues μ_n of the linearized curvature dynamics with no active moment and a piecewise constant force density show the emergence of multiple unstable modes at critical bending stiffnesses; the first at $\beta_{\perp} \approx 1.0 \times 10^{-2}$, or $\beta_{\perp}^{-1/3} \approx 4.6$.

(b) Growth rates of biharmonic eigenfunctions, $\phi_n(s)$, in the fully nonlinear system with M=0 (solid lines) and M=0.01 (dashed). (c) First three unstable modes of the linearized system (solid), and biharmonic eigenfunctions (dashed).

problem,

$$\mathcal{L}[\kappa] = -\frac{\beta_{\perp}}{\eta} \partial_s^2 \left(\partial_s^2 \kappa - \frac{1}{\beta_{\perp}} \lambda \kappa \right),$$

$$\mathcal{L}[\kappa] = \mu \kappa.$$
(4.37)

Figure 4.2a shows the (real part) of dominant eigenvalues μ_n of Eq. (4.37) for a range of stiffness β_{\perp} . The unstable modes of the linear system are illus-

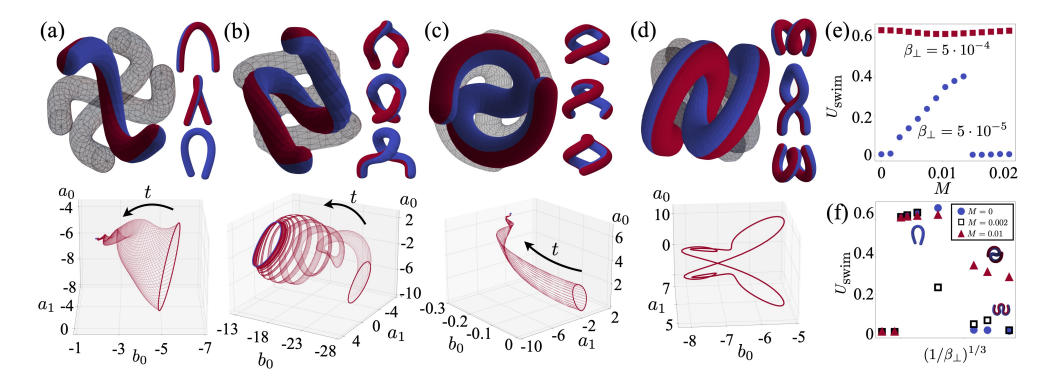


Figure 4.3: (a-d) New attractors emerge upon the addition of an active moment (with body symmetry assumed). Top - snapshots of body configurations over a half-period, bottom - trajectories of the first two bending (a_0,a_1) and the first twisting (b_0) mode coefficients suggests convergence to a fixed shape. (a) $(\beta_{\parallel},\beta_{\perp},M)=(1\times 10^{-4},2.5\times 10^{-4},6\times 10^{-3})$: a U-shaped swimmer with a twist. (b) $(\beta_{\parallel},\beta_{\perp},M)=(1\times 10^{-5},8\times 10^{-5},1.35\times 10^{-2})$: reduced stiffness and increased active moment introduces a limit cycle corresponding to waving while twisting. (c) $(\beta_{\parallel},\beta_{\perp},M)=(1\times 10^{-3},5.45\times 10^{-5},1\times 10^{-2})$: convergence to a new twisted-S shape. (d) $(\beta_{\parallel},\beta_{\perp},M)=(1\times 10^{-3},1.25\times 10^{-4},2\times 10^{-2})$: periodic flapping appears with further increases in M. (e) Swimming speed across a range of active moments for $\beta_{\parallel}=2.5\times 10^{-4}$, for a stiffer $(\beta_{\perp}=5\times 10^{-4},$ squares) and softer $(\beta_{\perp}=5\times 10^{-5},$ circles) body. (f) Swimming speed across a range of bending stiffness for $\beta_{\parallel}=2.5\times 10^{-4}$ and active moments M=0 (circles), M=0.002 (squares), and M=0.01 (triangles).

trated in Fig. 4.2c by solid blue curves, along with the biharmonic eigenfunctions for comparison. Growth rates $\sigma_n = \partial_t a_n(t)|_{t=0}/a_n(0)$, computed using the fully nonlinear system, Eqs. (4.32),(4.33), and (4.34), with $a_n(0) = 10^{-3}$ are shown in Fig. 4.2b.

Critical values of $\beta:=\beta_{\perp}$ at which different spatial modes become unstable are associated with the emergence of nontrivial solutions to (4.37) with $\mu=0$. With the piecewise constant active force, f(s)=1-2H(s), with H(s) the

Heaviside step function, the tension is given by

$$\lambda(s) = 2sH(s) - (s+1/2) = \begin{cases} -(s+1/2) & -1/2 < s < 0, \\ s - 1/2 & 0 < s < 1/2. \end{cases}$$
(4.38)

After integrating (4.37) twice we find

$$\partial_s^2 \kappa - \frac{1}{\beta} \lambda \kappa = c^- s + c^+, \tag{4.39}$$

for constants c^- and c^+ . When $\lambda(s)=\lambda(-s)$, Eq. (4.37) is invariant under $\kappa(s)\mapsto\kappa(-s)$, so, we may assume eigenfunctions have definite parity. When $\kappa(-s)=\kappa(s)$, we find $c^-=0$, and when $\kappa(-s)=-\kappa(s)$ we find $c^+=0$. Restricting to the half interval, -1/2 < s < 0 and introducing $\xi=\beta^{-1/3}\lambda=-(1+2s)/\left(2\beta^{1/3}\right)$, we find κ satisfies a nonhomogeneous Airy equation on $-1/\left(2\beta^{1/3}\right)<\xi<0$,

$$\partial_{\xi}^{2}\kappa - \xi\kappa = a\xi + b, \tag{4.40}$$

$$\kappa|_{\xi=0} \,,\, \partial_{\xi} \kappa|_{\xi=0} = 0, \tag{4.41}$$

where $(a,b)=(-\beta^{1/3}c^-,c^+-c^-/2)$. The solution to (4.40) and (4.41) is given

by

$$\kappa(\xi) = -\pi \operatorname{Ai}(\xi) \int_0^{\xi} (ax+b) \operatorname{Bi}(x) dx + \pi \operatorname{Bi}(\xi) \int_0^{\xi} (ax+b) \operatorname{Ai}(x) dx$$
$$= \pi a \left[\operatorname{Bi}'(0) \operatorname{Ai}(\xi) - \operatorname{Ai}'(0) \operatorname{Bi}(\xi) - 1/\pi \right]$$
$$+ \pi b \left[\operatorname{Bi}(\xi) \int_0^{\xi} \operatorname{Ai}(x) dx - \operatorname{Ai}(\xi) \int_0^{\xi} \operatorname{Bi}(x) dx \right],$$

where

$$Ai(\xi) = \frac{1}{\pi} \int_0^\infty \cos(\frac{x^3}{3} + \xi x) dx, \qquad (4.42)$$

$$Bi(\xi) = \frac{1}{\pi} \int_0^\infty \sin(\frac{x^3}{3} + \xi x) + e^{-x^3/3 + \xi x} dx$$
 (4.43)

are Airy functions, and primes denote derivatives. Writing $\xi^*=-\beta^{-1/3}/2$, parity conditions require $(a,\,\partial_\xi\kappa|_{\xi^*})=(0,0)$, giving

$$\kappa(\xi) = \operatorname{Bi}(\xi) \int_0^{\xi} \operatorname{Ai}(x) \, \mathrm{d}x - \operatorname{Ai}(\xi) \int_0^{\xi} \operatorname{Bi}(x) \, \mathrm{d}x, \qquad (4.44)$$

$$Bi'(\xi^*) \int_0^{\xi^*} Ai(x) dx - Ai'(\xi^*) \int_0^{\xi^*} Bi(x) dx = 0, \tag{4.45}$$

and $(b/a, \kappa|_{\xi^*}) = (-\xi^*, 0)$, giving

$$\kappa(\xi) = \operatorname{Bi}'(0)\operatorname{Ai}(\xi) - \operatorname{Ai}'(0)\operatorname{Bi}(\xi) - 1/\pi$$
$$-\xi^* \left(\operatorname{Bi}(\xi) \int_0^\xi \operatorname{Ai}(x) dx - \operatorname{Ai}(\xi) \int_0^\xi \operatorname{Bi}(x) dx\right), \quad (4.46)$$

$$Bi'(0)Ai(\xi^*) - Ai'(0)Bi(\xi^*) - 1/\pi$$
$$-\xi^* \left(Bi(\xi^*) \int_0^{\xi^*} Ai(x) dx - Ai(\xi^*) \int_0^{\xi^*} Bi(x) dx \right) = 0, \quad (4.47)$$

for even and odd eigenfunctions, respectively.

When compared to the first ten critical stiffnesses in the fully nonlinear dynamics with regularized active force density, predictions of Eqs. (4.45) and (4.47) were found to differ by 0.5%-15%. The first bending stiffness below which the filament becomes unstable from the full system is $\beta_{\perp}=1.0\times 10^{-2}$, whereas the linearized dynamics predict $\beta_{\perp}=1.1\times 10^{-2}$.

Inclusion of an active moment: three-dimensional dynamics

We turn now to the fully three-dimensional system, including the active moment contribution due to flagellar chirality $(M \neq 0)$. Numerous dynamical regimes appear as the result of rotational forcing, with transitions between

newly emergent phases brought about by variations in any one of the twisting stiffness, β_{\parallel} , bending stiffness, β_{\perp} , or active moment, M.

As with the 2D system, we seek a reduced order phase space in which to study these bifurcations. To this end, we consider systems initialized with the twist Ω_0 and curvature Ω_2 even about the midpoint, and the curvature Ω_1 odd. We show in §C.4 that this is equivalent to the system possessing a conserved π -rotational symmetry, and, provided the initial active stress distributions are odd functions of s about the midpoint, this symmetry is conserved. Taking advantage of their conserved parity, the twist and curvatures may be decomposed into sums of harmonic γ_{2k} and biharmonic $\{\phi_{2k}, \phi_{2k+1}\}$ functions satisfying appropriate parity and boundary and conditions:

$$\Omega_0(s,t) = \sum_k b_{2k}(t)\gamma_{2k}(s), \tag{4.48}$$

$$\Omega_1(s,t) = \sum_{k} a_{2k+1}^{(1)}(t)\phi_{2k+1}(s), \tag{4.49}$$

$$\Omega_2(s,t) = \sum_k a_{2k}^{(2)}(t)\phi_{2k}(s). \tag{4.50}$$

Figure 4.3a-d shows characteristic shapes of four observed phases (top), as well as corresponding phase space trajectories of $(b_0,a_1,a_0):=(b_0,a_1^{(1)},a_0^{(2)})$ appearing in the decomposition of twist/curvatures for a range of initial conditions (bottom). For $\beta_{\parallel}<2.5\times10^{-4}$, $\beta_{\perp}>7.5\times10^{-4}$, and $M>1.4\times10^{-2}$

the body adopts a straight configuration. A bifurcation to a twisted-U shape appears upon increasing β_{\parallel} , decreasing β_{\perp} , or decreasing M (Fig. 4.3a). With $M<1.8\times 10^{-2}$, the twisted-U phase persists as β_{\perp} is decreased until approximately $\beta_{\perp}=2\times 10^{-4}$, at which point the system develops periodic oscillations (Fig. 4.3b). Again with $M<1.8\times 10^{-2}$, new S-shaped equilibria emerge for $\beta_{\perp}<1\times 10^{-4}$ (Fig. 4.3c). A fourth phase appears for $M>1.8\times 10^{-2}$ and $\beta_{\perp}<2.5\times 10^{-4}$ with twist-curvature oscillations accompanied by periodic changes in swimming direction (Fig. 4.3d).

Transitions between phases can lead to wide variations in swimming trajectories, and in the swimming speed, defined as the magnitude of the average velocity of the body's midpoint in the lab frame, $U_{swim}(T) = \left| \int_0^T \mathsf{R}(0,t) u(0,t) \, \mathrm{d}t \, \right| / T.$ The complicated relationship between bend and twist is further illustrated by the nonmonotonic, and discontinuous, changes in swimming speed that arise due to variations in bending stiffness β_\perp and active moment M. Figure 4.3e shows the swimming speed as a function of the active moment for two different bending stiffnesses. For the stiffer body the active moment induces waving (from Fig. 4.3a to Fig. 4.3b) but the swimming speed remains roughly unchanged. For the softer body, however, which at M=0 is in the dramatic flapping-W state in two dimensions (Fig. 4.1i), the introduction of the active moment can stabilize the shape in three dimensions and result in a ballistic

trajectory (Fig. 4.3c). Further increases in M, however, then trigger another phase transition to the three-dimensional flapping dynamics of Fig. 4.3d, resulting in average speeds (but not instantaneous speeds) tending to zero. A different view is offered by Fig. 4.3f, which shows the swimming speed across a range of bending stiffnesses for three different active moments. A sufficiently large active moment can delay the onset of flapping dynamics, and thereby stabilize swimming trajectories over a larger range of stiffnesses.

At the lower bending stiffness typical of swarmer cells, rotational forcing introduces a dynamical twist-bend instability. As shown in Fig. 4.2b as dashed lines for M=0.01, the presence of an active moment can decrease the force required to excite higher unstable modes. As described in relation to Fig. 4.3e above, this allows the system to access new energetically favorable out-of-plane equilibria similar to the 'locked curvature' configurations observed in model cilia [113, 118].

Though not explored in detail here, both of the low stiffness configurations shown in Fig. 4.3c,d are generically unstable with respect to asymmetric perturbations, which lead to non-periodic dynamics and trajectories which depend sensitively upon the bending stiffness. The self-contact evident in Fig. 4.1d, and self intersections observed at low bending stiffness in the model, suggest that steric interactions or nonlocal hydrodynamic effects are important

for stabilizing body configurations of longer swarmer cells. Confinement by neighboring cells in bacterial swarms may play a similar role.

5.1 Introduction

Geometrically constrained filaments can be found throughout the natural world. In this chapter we examine the constrained dynamics of surface-bound flexible filaments. Our primary motivation is the interaction between biomembranes and the biopolymers that polymerize on their surfaces. These interactions are known to produce changes in the membrane curvature and topology through a number of mechanical, chemical, and entropic mechanisms [147]. However, many questions about how exactly the polymer-membrane interactions drive membrane remodeling remain open. We will focus on two classes of polymer-membrane interactions: the purely mechanical coupling of semi-flexible polymers to the membrane, and second, the dynamics of curvature sensing proteins bound to the membrane.

Modeling interactions of the sort considered in this chapter typically involves atomistic simulation and related techniques [1, 148, 149]. While insight gained from these simulations has proven to be invaluable to our current understanding of polymer-membrane interactions, computational complexity limits their ability to probe all but the shortest of length- and time-scales. Computationally tractable continuum models provide an attractive alternative for

modeling phenomena occurring at these longer length- and time-scales. We investigate these systems from a continuum mechanics perspective, modeling the proteins and biofilaments as Cosserat rods which are confined both in position and orientation to the membrane surface. We introduce a model for generic surface-bound filaments and derive constrained Euler-Poincaré equations for the system. Analytic and numerical results are presented for special cases, and a number of applications are discussed.

5.2 Filament kinematics and surface geometry

The state of the filament is identified with with a map $S:Q\to SE(3)$ from a 2-dimensional domain $Q\subset\mathbb{R}^2$, parameterized by material coordinate s and time t, into the Special Euclidean group. The matrix,

$$S(s,t) = \begin{pmatrix} R(s,t) & \mathbf{r}(s,t) \\ 0 & 1 \end{pmatrix}, \tag{5.1}$$

represents the Euclidean transformation which maps an inertial frame,

$$\boldsymbol{e}_{1}, \boldsymbol{e}_{2}, \boldsymbol{e}_{3} = \begin{pmatrix} 1 \\ 0 \\ 0 \end{pmatrix}, \begin{pmatrix} 0 \\ 1 \\ 0 \end{pmatrix}, \begin{pmatrix} 0 \\ 0 \\ 1 \end{pmatrix}, \tag{5.2}$$

located at the origin onto the body's orthonormal material frame $q_i(s,t) = R(s,t)e_i$ located at r(s,t). The infinitesimal generators associated with s- and t-translations in coordinate space,

$$S^{-1}\partial_{s}S = \begin{pmatrix} R^{-1}\partial_{s}R & R^{-1}\partial_{s}\mathbf{r} \\ 0 & 0 \end{pmatrix} = \begin{pmatrix} \hat{\mathbf{\Omega}} & \mathbf{U} \\ 0 & 0 \end{pmatrix}, \tag{5.3}$$

$$S^{-1}\partial_t S = \begin{pmatrix} R^{-1}\partial_t R & R^{-1}\partial_t \mathbf{r} \\ 0 & 0 \end{pmatrix} = \begin{pmatrix} \hat{\boldsymbol{\omega}} & \mathbf{u} \\ 0 & 0 \end{pmatrix}, \tag{5.4}$$

are given in terms of the twist-curvature $\hat{\Omega} = \Omega \times$, linear strain U, angular velocity $\hat{\omega} = \omega \times$, and linear velocity u, each measured with respect to the material frame. All together, these quantities define the components of an $\mathfrak{se}(3)$ -valued one-form, or gauge potential [127],

$$A = A_s ds + A_t dt \tag{5.5}$$

$$\mathsf{A}_{s} = \begin{pmatrix} \hat{\mathbf{\Omega}} & \mathbf{U} \\ 0 & 0 \end{pmatrix}, \quad \mathsf{A}_{t} = \begin{pmatrix} \hat{\boldsymbol{\omega}} & \mathbf{u} \\ 0 & 0 \end{pmatrix}, \tag{5.6}$$

which describes how cross-sections of the filament vary with respect to coordinate translations in the base space Q.

Given a path, $\gamma(\xi)=(s(\xi),t(\xi))$, connecting points $\gamma(\xi_1)=(s_1,t_1)$ and

 $\gamma(\xi_2)=(s_2,t_2)$ in Q, we can construct an operator by computing the ordered exponential [150] (see (2.48)) of A along γ ,

$$U(s_1, t_1; s_2, t_2) = \mathcal{P} \exp \int_{\gamma} A = \mathcal{P} \exp \int_{\xi_1}^{\xi_2} \left(A_s \frac{\mathrm{d}s}{\mathrm{d}\xi} + A_t \frac{\mathrm{d}t}{\mathrm{d}\xi} \right) \mathrm{d}\xi . \tag{5.7}$$

Operators of this form will generally depend on the choice of path [151], however, requiring the gauge potential satisfy,

$$\partial_t \mathsf{A}_s - \partial_s \mathsf{A}_t + [\mathsf{A}_t, \mathsf{A}_s] = 0, \tag{5.8}$$

will ensure U is independent of γ . The angular and linear components of (5.8),

$$\partial_t \mathbf{\Omega} - \partial_s \boldsymbol{\omega} + \boldsymbol{\omega} \times \mathbf{\Omega} = 0 \tag{5.9}$$

$$\partial_t \mathbf{U} - \partial_s \mathbf{u} + \boldsymbol{\omega} \times \mathbf{U} - \boldsymbol{\Omega} \times \mathbf{u} = 0 \tag{5.10}$$

are often referred to as the *Euclidean structure equations* [28, 71]. With path independence of U guaranteed by the structure equations, the instantaneous states of microstructure with coordinates (s,t) and (s',t') are related by,

$$S(s',t') = S(s,t)U(s,t;s',t').$$
(5.11)

Approximation of U by Magnus expansion [130] forms the basis of the structurepreserving numerical methods which we apply throughout this dissertation.

Unshearability/inextensibility constraints are satisfied by identifying the tangent vector, $\partial_s r$, with one of the orthonormal frame vectors, q_1 , or equivalently, by requiring $U=e_1$. The remaining strain measures correspond to twisting about the tangent, $\Omega_1=e_1\cdot\Omega$, and bending, $(\Omega_2,\Omega_3)=(e_2\cdot\Omega,e_3\cdot\Omega)$, about q_2 and q_3 , respectively. Under these assumptions, the structure equations become,

$$\partial_t \mathbf{\Omega} = \partial_s \mathbf{\omega} + \mathbf{\Omega} \times \mathbf{\omega} \tag{5.12}$$

$$\partial_s \mathbf{u} + \mathbf{\Omega} \times \mathbf{u} = \boldsymbol{\omega} \times \mathbf{e}_1. \tag{5.13}$$

We define the membrane, $M=\phi^{-1}(0)$, as the zero-level set of $\phi:\mathbb{R}^3\to\mathbb{R}$, with $\phi(\boldsymbol{x})<0$ inside the membrane and $\phi(\boldsymbol{x})>0$ outside the membrane. We denote the outward-pointing unit normal vector by, $\boldsymbol{n}=\nabla\phi/|\nabla\phi|$. We will assume the filament is confined to the surface in the sense that $\phi(\boldsymbol{r})=0$ and $q_3=\boldsymbol{n}(\boldsymbol{r})$. When taken in combination with previously discussed kinematic constraints placed on the filament, these four scalar equations can be reduced

to just two,

$$\phi(\mathbf{r}) = 0, \quad \mathbf{q}_2 \cdot \mathbf{n}(\mathbf{r}) = 0. \tag{5.14}$$

Membrane geometry is described by the first and second fundamental forms [66], which can be written, respectively, as

$$I = 1 - \boldsymbol{n}\boldsymbol{n}^T, \tag{5.15}$$

$$\mathbf{I} = -\mathbf{I} \cdot \nabla \boldsymbol{n} = -\frac{\mathbf{I} \cdot \nabla \nabla \phi \cdot \mathbf{I}}{|\nabla \phi|}.$$
 (5.16)

The first fundamental form I is an orthogonal projection onto the tangent bundle TM, and the second fundamental form II describes curvature of M. Principal curvatures of the surface are given by the (nonzero) eigenvalues of II. We denote the components of II in the basis (q_1, q_2) by K_{ij} . The relation between dynamical quantities and surface curvature can be summarized by

the following,

$$\Omega_1 = -\boldsymbol{q}_1 \cdot \nabla \boldsymbol{n} \cdot \boldsymbol{q}_2 = K_{12}, \tag{5.17}$$

$$\Omega_2 = \mathbf{q}_1 \cdot \nabla \mathbf{n} \cdot \mathbf{q}_1 = -K_{11}, \tag{5.18}$$

$$\omega_1 = -\partial_t \mathbf{r} \cdot \nabla \mathbf{n} \cdot \mathbf{q}_2 = K_{12} u_1 + K_{22} u_2, \tag{5.19}$$

$$\omega_2 = \partial_t \mathbf{r} \cdot \nabla \mathbf{n} \cdot \mathbf{q}_1 = -K_{11} u_1 - K_{12} u_2, \tag{5.20}$$

$$K_{22} = -(\mathcal{K} + \Omega_1^2)/\Omega_2 = \Omega_2 + 2\mathcal{H}$$
 (5.21)

$$\mathcal{H} = -\nabla \cdot \boldsymbol{n}/2,\tag{5.22}$$

$$\mathcal{K} = -\text{tr}(\hat{\boldsymbol{n}} \cdot \nabla \boldsymbol{n} \cdot \hat{\boldsymbol{n}} \cdot \nabla \boldsymbol{n})/2, \tag{5.23}$$

where K and H are the Gaussian and mean curvatures at r. These equations, together with the structure equations require,

$$\partial_s u_1 - \Omega_3 u_2 = 0 \tag{5.24}$$

$$\partial_s u_2 + \Omega_3 u_1 = \omega_3 \tag{5.25}$$

$$\partial_t \Omega_3 = \partial_s \omega_3 + \mathcal{K} u_2. \tag{5.26}$$

We emphasize that equations (5.24), (5.25), and (5.26) are purely a consequence of kinematics and geometry. With the exception of the forces of constraint, they are independent of any applied stresses. A derivation and addi-

tional discussion of these equations can be found in appendix D.1.

5.3 Stress balance

Inextensibility and unshearbility will be incorporated into our variational framework by introducing a vector-valued Lagrange multiplier, $\lambda = \lambda_i e_i$, and surface constraints will be accounted for with scalar Lagrange multipliers ν and χ . We will assume steric effects are characterized by a pairwise interaction energy [53],

$$\mathcal{U} = \frac{1}{2} \int \int G(\mathbf{r}(s), \mathbf{r}(s')) ds' ds, \qquad (5.27)$$

expressed in terms of a symmetric kernel, G(x, y) = G(y, x). The internal energy of the filament be given by

$$E = \int \mathcal{E} \, \mathrm{d}s + \mathcal{U} \tag{5.28}$$

$$\mathcal{E} = \frac{1}{2} (\mathbf{\Omega} - \boldsymbol{\sigma})^T \mathsf{B} (\mathbf{\Omega} - \boldsymbol{\sigma}) + \boldsymbol{\lambda} \cdot \boldsymbol{U} + \nu \phi / |\nabla \phi| + \chi \boldsymbol{q}_2 \cdot \boldsymbol{n}$$
 (5.29)

$$B = B_1 e_1 e_1^T + B_2 e_2 e_2^T + B_3 e_3 e_3^T, (5.30)$$

where B is the stiffness tensor that penalizes deviation from the filament's preferred shape, which we characterize by the intrinsic twist-curvature vector

 $\sigma = \sigma_i e_i$. We will consider a viscous moment density, $\zeta_r \omega_{\parallel}$, and force density, $\zeta_{\parallel} u_{\parallel} + \zeta_{\perp} u_{\perp}$, characterized by separate drag coefficients for rotational, ζ_r , longitudinal, ζ_{\parallel} , and transverse ζ_{\perp} motion. The the full system of Euler-Poincaré equations (3.75) and (3.76), the structure equations, and surface constraints are given by the following,

$$\partial_s m + \Omega \times m + e_1 \times \lambda - \chi e_1 = \zeta_r \omega_1 e_1 \tag{5.31}$$

$$\partial_s \boldsymbol{\lambda} + \boldsymbol{\Omega} \times \boldsymbol{\lambda} - \nu \boldsymbol{e}_3 - \chi \mathsf{R}^T \nabla \boldsymbol{n} \mathsf{R} \boldsymbol{e}_2 + \boldsymbol{f} = \zeta \boldsymbol{u}$$
 (5.32)

$$\partial_t \mathbf{\Omega} = \partial_s \boldsymbol{\omega} + \mathbf{\Omega} \times \boldsymbol{\omega} \tag{5.33}$$

$$\partial_s \mathbf{u} + \mathbf{\Omega} \times \mathbf{u} = \boldsymbol{\omega} \times \mathbf{e}_1 \tag{5.34}$$

$$\partial_s R = R\hat{\Omega}, \tag{5.35}$$

$$\partial_s \mathbf{r} = \mathsf{R} \mathbf{e}_1,\tag{5.36}$$

$$\phi(\mathbf{r}) = 0 \tag{5.37}$$

$$\mathbf{q}_2 \cdot \mathbf{n}(\mathbf{r}) = 0 \tag{5.38}$$

where the steric force is denoted ${m f}=f_i{m e}_i$

$$f(s) = -\int R^{T}(s) \frac{\partial G}{\partial r(s)}(r(s), r(s')) ds'$$

$$= f_{i} e_{i},$$
(5.39)

and internal moment density by, $m=\mathrm{B}\,(\Omega-\sigma)$. After eliminating the Lagrange multipliers (see D.2) ν , χ , and $\lambda_{\perp}=\lambda_2e_2+\lambda_3e_3$, we find that force balance can be expressed,

$$\boldsymbol{u} = \mathsf{M}\boldsymbol{F} \tag{5.40}$$

in terms of an in-surface force density $\mathbf{F} = (F_1 \quad F_2)^T$ with components

$$F_1 = \partial_s \lambda + \mathbf{\Omega} \cdot \partial_s \mathbf{m} + f_1 \tag{5.41}$$

$$F_{2} = -\partial_{s}^{2} m_{3} + (\lambda - K_{12}m_{1} - K_{22}m_{2}) \Omega_{3} - \mathcal{K}m_{3}$$

$$-\partial_{s} (K_{11}m_{1} + K_{12}m_{2}) - \Omega_{1}\partial_{s}m_{2} + K_{22}\partial_{s}m_{1} + f_{2},$$
(5.42)

and effective mobility tensor

$$M = \frac{1}{\zeta_1 \zeta_2 + \zeta_1 \zeta_r K_{22}^2 + \zeta_2 \zeta_r K_{12}^2} \begin{pmatrix} \zeta_2 + \zeta_r K_{22}^2 & -\zeta_r K_{12} K_{22} \\ -\zeta_r K_{12} K_{22} & \zeta_1 + \zeta_r K_{12}^2 \end{pmatrix}.$$
 (5.43)

5.4 Shape equations

The system (5.24), (5.25), (5.26), and (5.40) can be reduced to a set of shape equations governing the centerline position r, unit tangent $q := q_1$, geodesic

curvature $\Omega := \Omega_3$, and tension $\lambda := e_1 \cdot \lambda$,

$$\partial_t \Omega + g(\boldsymbol{q}, \boldsymbol{r}) \partial_s^4 \Omega = h(\boldsymbol{q}, \boldsymbol{r}, \lambda, \partial_s \lambda, \partial_s^2 \lambda, \Omega, \dots, \partial_s^3 \Omega),$$
 (5.44)

$$\partial_s [a(\mathbf{q}, \mathbf{r})\partial_s \lambda] - b(\mathbf{q}, \mathbf{r}, \Omega, \partial_s \Omega)\lambda = c(\mathbf{q}, \mathbf{r}, \Omega, \dots, \partial_s^3 \Omega),$$
 (5.45)

$$\partial_s q = \Omega n \times q + (q \cdot \nabla n \cdot q) n, \quad \partial_s r = q$$
 (5.46)

where (a, b, g) are given by

$$a = \frac{\zeta_2 + \zeta_r K_{22}^2}{\zeta_1 \zeta_2 + \zeta_1 \zeta_r K_{22}^2 + \zeta_2 \zeta_r K_{12}^2},\tag{5.47}$$

$$b = \frac{\left(\zeta_1 + \zeta_r K_{12}^2\right) \Omega^2}{\zeta_1 \zeta_2 + \zeta_1 \zeta_r K_{22}^2 + \zeta_2 \zeta_r K_{12}^2} + \partial_s \left(\frac{\zeta_r K_{12} K_{22} \Omega}{\zeta_1 \zeta_2 + \zeta_1 \zeta_r K_{22}^2 + \zeta_2 \zeta_r K_{12}^2}\right), \quad (5.48)$$

$$g = \frac{B_3 \left(\zeta_1 + \zeta_r K_{12}^2\right)}{\zeta_1 \zeta_2 + \zeta_1 \zeta_r K_{22}^2 + \zeta_2 \zeta_r K_{12}^2},\tag{5.49}$$

and (c,h) are nonlinear functions of the indicated variables. Boundary conditions for a free are given by

$$m_3 = 0,$$

$$\partial_s m_3 + 2K_{12}m_2 + (K_{11} - K_{22}) m_1 = 0$$

$$\lambda + K_{12}m_1 - K_{11}m_2 = 0,$$
(5.50)

while the conditions for a clamped end are

$$F_1 = 0,$$

$$F_2 = 0,$$
 (5.51)
$$M_{12}\partial_s F_1 + M_{22}\partial_s F_2 = 0,$$

where F_1 and F_2 are given by (5.41) and (5.42). Explicit expressions for (c, h), as well as discussion of boundary conditions and numerical methods can be found in appendix D.

5.5 Applications

The endosomal sorting complex required for transport (ESCRT) mediates both scission and sealing of membranes in a wide range of cellular processes [152]. Components of ESCRT form spiral protein structures on the surface of mem-

branes which are believed to play a role in reshaping membranes by applying mechanical stresses [153]. While membrane-bound filaments resemble spirals, atomistic simulations have shown that they will adopt a helical configuration, illustrated in Fig. 5.1, when free of the membrane. The mismatch between the surface curvature and the filament's preferred shape should give rise to a complex interplay between the geometries of the membrane and the filament. A number of models for interactions mediated by similar semi-flexible polymers have been developed [154–162].



Figure 5.1: Equilibrated molecular dynamics simulation of an ESCRT filament illustrating spontaneous curvature and twist reproduced from [1]. (a) Top view and (b) side view show preferred curvatures. (c) Close-up view illustrates intrinsic twist.

As the filament continues to grow, global characteristics of the membrane become significant, and the Gaussian curvature dependence of the membrane energy [163] presents a unique modeling challenge. Because the total Gaussian curvature of a surface is entirely determined by its Euler characteristic [66], changes in topology can involve rapid energy perturbations. It has been proposed that these topological transitions are due to the sudden release of elastic

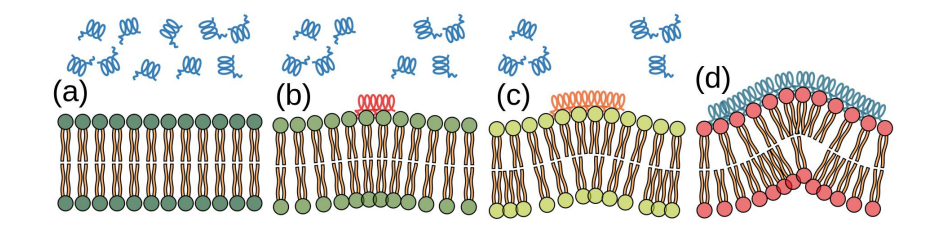


Figure 5.2: Growth of a biofilament on the surface of a lipid bilayer. (a) When proteins are not bound to the membrane, both the membrane and proteins attain their preferred curvatures and store no elastic energy. (b-c) The energy required to bind each subunit of the filament to the membrane includes elastic contributions from both the filament and the membrane. (d) A biofilament composed of sufficiently stiff proteins forms a scaffold which is able to support larger and larger membrane deformations as the filament continues to grow.

energy stored in surface-bound filaments [164, 165].

We model the ESCRT filament as a surface-bound filament with elastic moduli, (B_1, B_2, B_3) , and spontaneous twist/curvature, $(\sigma_1, \sigma_2, \sigma_3)$, determined by atomistic simulations [1]. Steric forces are computed using a regularized Yukawa potential (see Appendix D.6). Each ESCRT filament seems to grow from a single, stationary nucleation site [166], which we model as a clamped end satisfying the boundary conditions (5.51). Equations (5.44), (5.45), and (5.46) are discretized in space using 2nd order central differences, and the system is evolved in time using a 2nd order semi-implicit time stepping scheme which performs the spatial integration of (q, r) using a 2nd order geometric integrator (see Appendix D.5).

As our simulated filament grows from its nucleation site, we observe sudden sudden, rapid conformational changes at certain critical lengths which were highly dependent on membrane geometry. During these buckling events the localization of curvature and twist, illustrated in Figure 5.3, results in highly localized forces and moments being exerted on the membrane.

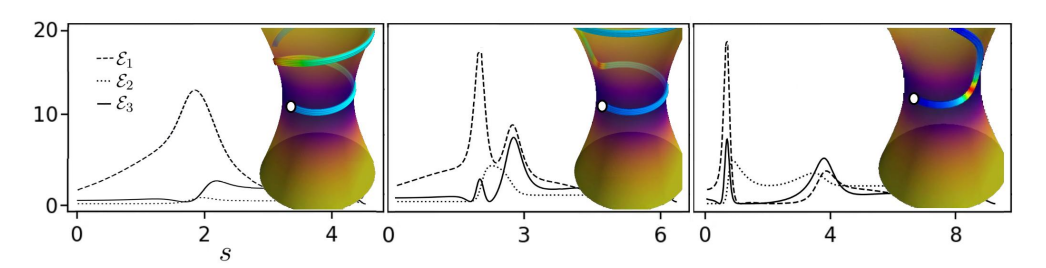


Figure 5.3: With time increasing from left to right, a membrane-bound filament (colored by total energy density) grows from its nucleation site (white circle) around the intercellular bridge connecting two daughter cells. As it reaches the critical length required for buckling, the localization of twist $\mathcal{E}_1 = \frac{1}{2}B_1\Omega_1^2$ and curvature $(\mathcal{E}_2,\mathcal{E}_3) = (\frac{1}{2}B_2\Omega_2^2,\frac{1}{2}B_3\Omega_3^2)$ energy results in large stresses being applied to the membrane.

Next, we will consider the role of proteins as curvature sensors [167–169]. Curvature sensing proteins preferentially bind to membrane regions matching their own equilibrium curvature. As the density of proteins increases their role shifts from curvature sensor to curvature generator, and they begin to produce the initial membrane curvature required for larger scale deformations by other mechanisms [170]. Our focus will be the effect of intrinsic twist and chirality on a protein's ability to navigate the complex energy landscape of a

surface with variable curvature.

We model each protein as a short surface-bound filament with nonzero preferred curvature, $\sigma_2 \neq 0$, which would correspond out-of-plane bending for an un-bound filament. In-plane preferred curvature is taken to be zero, $\sigma_3 = 0$. We assume both ends of the filament are free, with boundary conditions described by (5.50). While equations (5.44), (5.45), and (5.46) are sufficient to determine the evolution of a filament with one clamped and one free end, this is no longer true when both ends are free. In this case, we must track the position and orientation of a single distinguished cross-section, which we take to be at s=0. Using equations (5.40), (5.20), and (5.25) to compute the linear and angular velocity at s=0, we solve

$$\partial_t \mathbf{q}|_{s=0} = \omega_3 \mathbf{n} \times \mathbf{q} - \omega_2 \mathbf{n}|_{s=0}, \qquad (5.52)$$

$$\partial_t \boldsymbol{r}|_{s=0} = u_1 \boldsymbol{q} + u_2 \boldsymbol{n} \times \boldsymbol{q}|_{s=0},$$
 (5.53)

using the 1st order geometric integrator discussed in D.5.

To demonstrate the role of chirality, we performed pairs of simulations initialized with 100 randomly located and oriented filaments, one simulation with intrinsic twist $\sigma_1 \neq 0$ and one without $\sigma_1 = 0$. In each pair of simulations the filaments were chosen to be either positive curvature sensing, $\sigma_2 > 0$, or

negative curvature sensing, $\sigma_2 < 0$. The results of these simulations are shown in Figures 5.4 and 5.5.

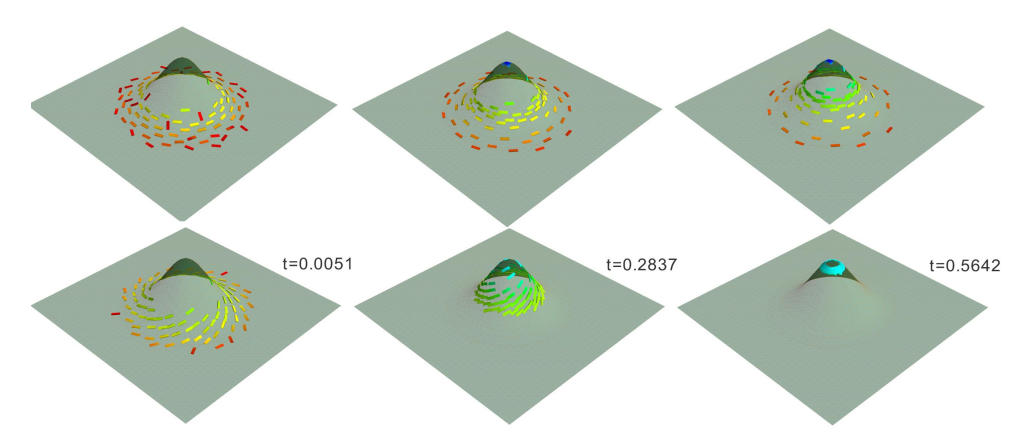


Figure 5.4: Curvature sensing proteins, colored by elastic energy density, with positive preferred curvature $\sigma_2 > 0$ begin to congregate near regions of positive Gaussian curvature. Chiral proteins (bottom) quickly reach equilibria, while achiral proteins (top) approach equilibria much more slowly.

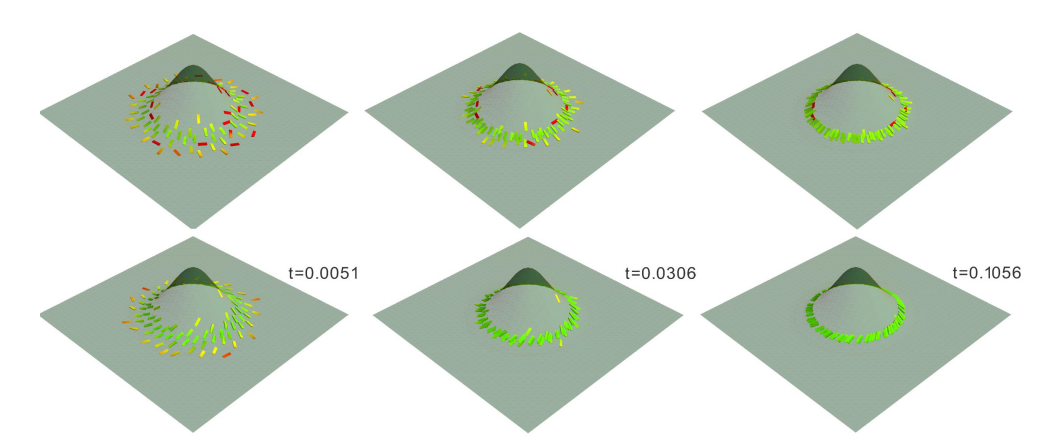


Figure 5.5: Curvature sensing proteins, colored by elastic energy density, with negative preferred curvature $\sigma_2 < 0$ congregate near regions of negative Gaussian curvature.

6 CONCLUDING REMARKS

In this dissertation we developed theoretical and computational tools for modeling Cosserat media within the Euler-Poincaré variational framework. We derived generalized Euler-Poincaré equations governing a Cosserat medium and investigated a number biophysics-inspired systems. A recurring theme is the fundamental role played by geometric structures and symmetries. Throughout this work, we have demonstrated the practical benefits of structure-preserving computational methods, particularly in the case of constrained systems. For example, the numerically problematic inextensibility/unshearability constraints of the Kirchhoff rod can be trivially satisfied in this framework, without the need for ad hoc penalty methods or singularity-prone parametrization of rotations which are common to alternative numerical schemes.

Our study of P. mirabilis swarmer cells in § 4 demonstrates the utility of Euler-Poincaré reduction in the modeling of flexible bodies at low Reynolds number. We have shown that numerous behaviors of individual swimming P. mirabilis swarmer cells are qualitatively captured by an active Kirchhoff rod model. The relative bending stiffness $\beta_{\perp} = B_{\perp}/f^*L^3$, relating the flagellar stress to the cell's material and geometric properties, is seen to play an outsized role. Our analysis reveals a minimal value, approximately $\beta_{\perp} = 1.01 \times 10^{-2}$, required of a cell below which its motility is severely hampered by self-buckling.

For P. mirabilis swarmer cells, this corresponds to a critical bending stiffness of $B_{\perp}=2.6\times 10^{-23} {\rm Nm}^2$ (see C.2), approximately one order of magnitude lower than the experimentally determined stiffness of typical cells [96]. We propose that this offers some evidence that cells may develop and maintain mechanical properties to prevent excessive buckling during motility. That the difference is not tighter may speak either to the approximations made in modeling the highly complex surface array of flagella, and/or related to the larger stresses that the organisms may experience inside of a swarm. This observation may offer insight relevant to the evolutionary development of motility, bacterial adaptation and survival, and potential mechanically-motivated medical interventions.

Bifurcations in body shape produce significant changes in swimming trajectories, as we have begun to explore, but are also expected to affect the ways
in which such bodies interact with one another. This likely has substantial
consequences for the collective motion of bacterial swarms. We have only
begun to scratch the surface of the high dimensional parameter space available
to a generic active Kirchhoff rod. Characterization of critical parameter values
which trigger bifurcations may provide novel experimental methods for quantifying mechanical properties of active, flexible bodies. Such methods may
require a more detailed treatment of the hugely complex, flagellated surface,

or a more elastic energy than we have assumed here. Our model is readily generalizable to account for these additional complexities using (3.75) and (3.76), which do not assume a particular form for the elastic energy, activity, or viscous stress.

In § 5, we developed a theoretical model for a elastic filament confined in both position and orientation to an arbitrary implicitly defined surface. We then applied this model to describe the dynamics of membrane-bound proteins and biopolymers. When the filament length length is comparable to the characteristic length set by the membrane curvature, our simulations suggest that membrane-bound biofilaments will undergo growth-induced buckling. During this buckling process, the filament can apply highly localized forces and moments to membrane. This lends support to the conjecture that buckling of surface-bound polymers plays a role in overcoming energy barriers which resist topological transitions during cell division and vesicle formation. Next, we examined the curvature sensing abilities of chiral proteins, which we modeled as short surface-bound filaments with a preferred curvature and twist. We found that in some cases chirality can increase the robustness of curvature sensing proteins, allowing them to more efficiently locate points on the membrane which match their preferred curvature. The obvious extension of the surface-bound filament model is to include membrane dynamics. The coupling of filament and membrane dynamics poses a formidable computational challenge, but will likely be required to gain a comprehensive understanding of these polymer-membrane interactions.

A APPENDIX: THE ORTHOGONAL GROUP

This appendix summarizes of results related to orthogonal group which are discussed in various sections throughout the main text. The *orthogonal group* O(3) is the group of linear transformations of three-dimensional space which preserve the Euclidean norm |x|. We will identify the orthogonal group with its faithful matrix representation on \mathbb{R}^3 ,

$$O(3) = \left\{ \mathsf{R} \in \mathbb{R}^{3 \times 3} \middle| \mathsf{R}^T \mathsf{R} = 1 \right\}. \tag{A.1}$$

The orthogonal group consists of two disconnected components, the special orthogonal group,

$$SO(3) = \left\{ \mathsf{R} \in \mathbb{R}^{3 \times 3} \middle| \mathsf{R}^T \mathsf{R} = 1, \quad \det(\mathsf{R}) = +1 \right\},$$
 (A.2)

and its complement which consists of orientation reversing transformations. We will focus on the special orthogonal group.

The Lie algebra of SO(3) consists of antisymmetric matrices:

$$\mathfrak{so}(3) = \left\{ \hat{\boldsymbol{\omega}} \in \mathbb{R}^{3 \times 3} \middle| \hat{\boldsymbol{\omega}}^T = -\hat{\boldsymbol{\omega}} \right\}.$$
 (A.3)

There are two possible $\mathfrak{so}(3)$ -valued matrices which can be associated with

each trajectory, R(t), through SO(3)

$$\left(\mathsf{R}^T\dot{\mathsf{R}}\right)^T = -\mathsf{R}^T\dot{\mathsf{R}},\tag{A.4}$$

$$\left(\dot{\mathsf{R}}\mathsf{R}^T\right)^T = -\dot{\mathsf{R}}\mathsf{R}^T,\tag{A.5}$$

which means there are two separate characterizations of the tangent space,

$$T_{\mathsf{R}}SO(3) = \mathsf{R}\mathfrak{so}(3) = \{ \, \mathsf{R}\hat{\boldsymbol{\omega}} | \, \hat{\boldsymbol{\omega}} \in \mathfrak{so}(3) \} \,,$$
 (A.6)

$$T_{\mathsf{R}}SO(3) = \mathfrak{so}(3)\mathsf{R} = \{\hat{\boldsymbol{\omega}}\mathsf{R}|\,\hat{\boldsymbol{\omega}} \in \mathfrak{so}(3)\}.$$
 (A.7)

Elements of $\mathfrak{so}(3)$ obtained by left translation, $\hat{\boldsymbol{\omega}}^{(B)} = \mathsf{R}^T \dot{\mathsf{R}}$, and right translation, $\hat{\boldsymbol{\omega}}^{(I)} = \dot{\mathsf{R}} \mathsf{R}^T$, represent angular velocities measured in the body frame and the ambient inertial frame, respectively. The body and inertial velocities are related by the adjoint action of $\mathrm{SO}(3)$,

$$\hat{\boldsymbol{\omega}}^{(I)} = \mathrm{Ad}_{\mathsf{R}} \hat{\boldsymbol{\omega}}^{(B)} = \mathsf{R} \hat{\boldsymbol{\omega}}^{(B)} \mathsf{R}^{T}. \tag{A.8}$$

We can define a Riemannian metric on SO(3) by,

$$\langle \boldsymbol{a} | \boldsymbol{b} \rangle = \frac{1}{2} \operatorname{tr}(\boldsymbol{a}^T \boldsymbol{b}),$$
 (A.9)

for $a, b \in T_RSO(3)$. This metric is both left-, and right-invariant:

$$\langle a|b\rangle = \langle Ra|Rb\rangle = \langle aR|bR\rangle,$$
 (A.10)

for any R \in SO(3). So, we can always push vectors a, b to the identity, $R^T a$, $R^T b \in \mathfrak{so}(3)$ and take their inner product in the Lie algebra.

In the canonical basis for $\mathfrak{so}(3)$,

$$\hat{\boldsymbol{e}}_{1}, \hat{\boldsymbol{e}}_{2}, \hat{\boldsymbol{e}}_{3} = \begin{pmatrix} 0 & 0 & 0 \\ 0 & 0 & -1 \\ 0 & 1 & 0 \end{pmatrix}, \begin{pmatrix} 0 & 0 & 1 \\ 0 & 0 & 0 \\ -1 & 0 & 0 \end{pmatrix}, \begin{pmatrix} 0 & -1 & 0 \\ 1 & 0 & 0 \\ 0 & 0 & 0 \end{pmatrix}. \tag{A.11}$$

the metric components of (A.9) and the structure constants are given, respectively, by

$$\langle \hat{\boldsymbol{e}}_i | \hat{\boldsymbol{e}}_j \rangle = \delta_{ij} = \begin{cases} 1, & \text{if } i = j \\ & , \\ 0, & \text{if } i \neq j \end{cases}$$
 (A.12)

$$\langle \hat{\boldsymbol{e}}_{i} | [\hat{\boldsymbol{e}}_{j}, \hat{\boldsymbol{e}}_{k}] \rangle = \varepsilon_{ijk}. = \begin{cases} +1, & \text{if } (i, j, k) = (1, 2, 3), (2, 3, 1), (3, 1, 2) \\ \\ -1, & \text{if } (i, j, k) = (2, 1, 3), (3, 2, 1), (1, 3, 2) \end{cases}$$

$$(A.13)$$

$$0, & \text{otherwise}$$

The hat map is a linear transformation,

$$\hat{\cdot}: \mathbb{R}^3 \to \mathfrak{so}(3) \tag{A.14}$$

$$e_i \mapsto \hat{e}_i,$$
 (A.15)

which maps the canonical basis for \mathbb{R}^3 to the canonical basis for $\mathfrak{so}(3)$. Under this association, $\mathfrak{so}(3)$ with bracket,

$$\left[\hat{a},\hat{b}\right]_{\mathfrak{so}(3)} = \hat{a}\hat{b} - \hat{b}\hat{a} \tag{A.16}$$

and inner product (A.9), is isomorphic, as both a Lie algebra and inner product space, to \mathbb{R}^3 with bracket,

$$[\boldsymbol{a},\boldsymbol{b}]_{\mathbb{R}^3} := \boldsymbol{a} \times \boldsymbol{b},\tag{A.17}$$

and the standard dot product. The adjoint representation,

$$Ad: SO(3) \to GL(\mathfrak{so}(3))$$
 (A.18)

$$\mathrm{Ad}_{\mathsf{R}}\hat{\boldsymbol{\omega}} = \mathsf{R}\hat{\boldsymbol{\omega}}\mathsf{R}^T,\tag{A.19}$$

is another faithful representation of SO(3). With the action of SO(3) on $\mathfrak{so}(3)$

and \mathbb{R}^3 given by the adjoint action and matrix multiplication, respectively. The adjoint representation of $\mathfrak{so}(3)$ is given by,

$$\operatorname{ad}_{\hat{\boldsymbol{a}}}\hat{\boldsymbol{b}} = \left[\hat{\boldsymbol{a}}, \hat{\boldsymbol{b}}\right],$$
 (A.20)

and the coadjoint action is defined by

$$\left\langle \hat{\boldsymbol{c}} | \operatorname{ad}_{\hat{\boldsymbol{a}}}^* \hat{\boldsymbol{b}} \right\rangle = \left\langle \operatorname{ad}_{\hat{\boldsymbol{a}}} \hat{\boldsymbol{c}} | \hat{\boldsymbol{b}} \right\rangle.$$
 (A.21)

By the fact that,

$$\langle \operatorname{ad}_{\hat{a}}\hat{c}|\hat{b}\rangle = (a \times c) \cdot b = -c \cdot (a \times b),$$
 (A.22)

the coadjoint is given by

$$\mathrm{ad}_{\hat{\boldsymbol{a}}}^* = -\mathrm{ad}_{\hat{\boldsymbol{a}}}.\tag{A.23}$$

In summary, for all $R \in SO(3)$ and any $a, b, c \in \mathbb{R}^3$ we have

$$\hat{a}b = a \times b \tag{A.24}$$

$$\frac{1}{2}\operatorname{tr}(\hat{\boldsymbol{a}}^T\hat{\boldsymbol{b}}) = \boldsymbol{a} \cdot \boldsymbol{b} \tag{A.25}$$

$$R\hat{\boldsymbol{a}}R^T \Leftrightarrow R\boldsymbol{a} \tag{A.26}$$

$$\hat{c} = \hat{a}\hat{b} - \hat{b}\hat{a} \Leftrightarrow c = a \times b$$
 (A.27)

A.1 The exponential map

The exponential of $\hat{\theta} \in \mathfrak{so}(3)$,

$$e^{\hat{\boldsymbol{\theta}}} = 1 + A\hat{\boldsymbol{\theta}} + B\hat{\boldsymbol{\theta}}^2, \tag{A.28}$$

$$A = \frac{\sin \theta}{\theta}, \quad B = \frac{1 - \cos \theta}{\theta^2},$$
 (A.29)

describes a rotation a rotation about an axis parallel to $\theta \in \mathbb{R}^3$ by $\theta = |\theta|$ radians. If \hat{e}_i is a basis for $\mathfrak{so}(3)$ and $\hat{\theta} = \theta_i \hat{e}_i$, then the map $\mathsf{R}(\theta) = e^{\hat{\theta}}$ defines a local coordinate chart in some neighborhood of the identity $1 \in \mathrm{SO}(3)$. Given a rotation matrix $\mathsf{R} \in \mathrm{SO}(3)$, the axis of rotation can be obtained by applying the inverse hat map to the antisymmetric matrix $\mathsf{R} - \mathsf{R}^T$ and the angle can be

obtained using

$$tr(R) = 2\cos(\theta) + 1. \tag{A.30}$$

Rotations about coordinate axes are given by

$$e^{\theta \hat{e}_1} = \begin{pmatrix} 1 & 0 & 0 \\ 0 & \cos(\theta) & -\sin(\theta) \\ 0 & \sin(\theta) & \cos(\theta) \end{pmatrix}$$
(A.31)

$$e^{\theta \hat{e}_2} = \begin{pmatrix} \cos(\theta) & 0 & \sin(\theta) \\ 0 & 1 & 0 \\ -\sin(\theta) & 0 & \cos(\theta) \end{pmatrix}$$
 (A.32)

$$e^{\theta \hat{e}_3} = \begin{pmatrix} \cos(\theta) & -\sin(\theta) & 0 \\ \sin(\theta) & \cos(\theta) & 0 \\ 0 & 0 & 1 \end{pmatrix}$$
 (A.33)

The logarithm of a rotation matrix is given by

$$\log(\mathsf{R}) = \frac{\theta}{2\sin\theta} \left(\mathsf{R} - \mathsf{R}^T \right),\tag{A.34}$$

$$\theta = \arccos(\frac{\operatorname{tr}(\mathsf{R}) - 1}{2}). \tag{A.35}$$

A.2 Euler angles

If $\hat{a}, \hat{b}, \hat{c} \in \mathfrak{so}(3)$ are nonzero antisymmetric 3-by-three matrices with $[\hat{a}, \hat{b}] \neq 0$ and $[\hat{b}, \hat{c}] \neq 0$, then the function

$$\mathsf{R}(\alpha,\beta,\gamma) = e^{\alpha \hat{\boldsymbol{a}}} e^{\beta \hat{\boldsymbol{b}}} e^{\gamma \hat{\boldsymbol{c}}} \tag{A.36}$$

defines a local coordinate chart on some subset of SO(3). If \hat{a} , \hat{b} , and \hat{c} are linearly independent, then the chart is defined in some neighborhood of the identity $1 \in SO(3)$. The Euler angle parametrization [34] is an example of this type of chart. In this parametrization, the orientation of a rigid body is described by a sequence of three rotations about body-fixed axes, or, equivalently, by rotating about the corresponding space-fixed axes in the opposite order. We assume the initial body-fixed frame is chosen to coincide with the the space-fixed frame, e_i , and denote the body-fixed frame vectors after the first and second rotation by $e_{i'}$ and $e_{i''}$, respectively. The three rotation operators

are given by

$$R_z(\alpha) = e^{\alpha \hat{\boldsymbol{e}}_z},\tag{A.37}$$

$$\mathbf{e}_{i'} = \mathsf{R}_z(\alpha)\mathbf{e}_i,\tag{A.38}$$

$$\mathsf{R}_{x'}(\beta) = e^{\beta \hat{\mathbf{e}}_{x'}} = e^{\alpha \hat{\mathbf{e}}_z} e^{\beta \hat{\mathbf{e}}_x} e^{-\alpha \hat{\mathbf{e}}_z},\tag{A.39}$$

$$\mathbf{e}_{i''} = \mathsf{R}_{x'}(\beta)\mathbf{e}_{i'},\tag{A.40}$$

$$R_{z''}(\gamma) = e^{\gamma \hat{\mathbf{e}}_{z''}} = e^{\alpha \hat{\mathbf{e}}_z} e^{\beta \hat{\mathbf{e}}_x} e^{\gamma \hat{\mathbf{e}}_z} e^{-\beta \hat{\mathbf{e}}_x} e^{-\alpha \hat{\mathbf{e}}_z}. \tag{A.41}$$

Then, their composition can be expressed in terms of body-fixed and spacefixed frames as

$$\begin{split} \mathsf{R}(\alpha,\beta,\gamma) &= \mathsf{R}_{z''}(\gamma) \mathsf{R}_{x'}(\beta) \mathsf{R}_z(\alpha) \\ &= e^{\gamma \hat{\mathbf{e}}_{z''}} e^{\beta \hat{\mathbf{e}}_{x'}} e^{\alpha \hat{\mathbf{e}}_z} \\ &= e^{\alpha \hat{\mathbf{e}}_z} e^{\beta \hat{\mathbf{e}}_x} e^{\gamma \hat{\mathbf{e}}_z} \\ &= \mathsf{R}_z(\alpha) \mathsf{R}_x(\beta) \mathsf{R}_z(\gamma) \end{split} \tag{A.42}$$

Gimbal lock occurs at values of (α, β, γ) for which the derivative of R does not have full rank,

$$rank(dR) < 3, \tag{A.43}$$

as a map $dR : \mathbb{R}^3 \to T_RSO(3)$. If we define the $\mathfrak{so}(3)$ -valued one-form,

$$\hat{\boldsymbol{\omega}} := \mathsf{R}^{-1} d\mathsf{R}
= d\alpha \, e^{-\gamma \hat{\boldsymbol{e}}_z} e^{-\beta \hat{\boldsymbol{e}}_x} \hat{\boldsymbol{e}}_z e^{\beta \hat{\boldsymbol{e}}_x} e^{\gamma \hat{\boldsymbol{e}}_z} + d\beta \, e^{-\gamma \hat{\boldsymbol{e}}_z} \hat{\boldsymbol{e}}_x e^{\gamma \hat{\boldsymbol{e}}_z} + d\gamma \, \hat{\boldsymbol{e}}_z
(A.44)$$

then the associated \mathbb{R}^3 -valued form is given by

$$\boldsymbol{\omega} = d\alpha \, e^{-\gamma \hat{\boldsymbol{e}}_z} e^{-\beta \hat{\boldsymbol{e}}_x} \boldsymbol{e}_z + d\beta \, e^{-\gamma \hat{\boldsymbol{e}}_z} \boldsymbol{e}_x + d\gamma \, \boldsymbol{e}_z$$

$$= \left(e^{-\gamma \hat{\boldsymbol{e}}_z} e^{-\beta \hat{\boldsymbol{e}}_x} \boldsymbol{e}_z \, \middle| \, e^{-\gamma \hat{\boldsymbol{e}}_z} \boldsymbol{e}_x \, \middle| \, \boldsymbol{e}_z \right) \begin{pmatrix} d\alpha \\ d\beta \\ d\gamma \end{pmatrix}. \tag{A.45}$$

It follows that (A.43) is equivalent to

$$0 = \det \left(e^{-\gamma \hat{\mathbf{e}}_z} e^{-\beta \hat{\mathbf{e}}_x} \mathbf{e}_z \mid e^{-\gamma \hat{\mathbf{e}}_z} \mathbf{e}_x \mid \mathbf{e}_z \right)$$

$$= \det \left(e^{-\beta \hat{\mathbf{e}}_x} \mathbf{e}_z \mid \mathbf{e}_x \mid \mathbf{e}_z \right)$$

$$= -\sin(\beta)$$
(A.46)

More generally, with $\mathsf{R}(\alpha,\beta,\gamma)=e^{\alpha\hat{\pmb{a}}}e^{\beta\hat{\pmb{b}}}e^{\gamma\hat{\pmb{c}}}$, the condition (A.43) is equivalent to,

$$0 = \det \left(e^{-\gamma \hat{c}} e^{-\beta \hat{b}} \mathbf{a} \mid e^{-\gamma \hat{c}} \mathbf{b} \mid \mathbf{c} \right)$$

$$= \det \left(e^{-\beta \hat{b}} \mathbf{a} \mid \mathbf{b} \mid \mathbf{c} \right)$$

$$= \left(e^{-\beta \hat{b}} \mathbf{a} \right) \cdot (\mathbf{b} \times \mathbf{c})$$
(A.47)

A.3 Diagonalization

Choosing a coordinate system with $e_z=\pmb{\theta}/\theta$ the eigenvectors of $\mathsf{R}=e^{\hat{\pmb{\theta}}}$ are given by

$$e_0 = e_z, \tag{A.48}$$

$$\boldsymbol{e}_{+} = -\frac{1}{\sqrt{2}} \left(\boldsymbol{e}_{x} - i \boldsymbol{e}_{y} \right), \tag{A.49}$$

$$e_{-} = \frac{1}{\sqrt{2}} \left(e_x + i e_y \right), \tag{A.50}$$

with corresponding eigenvalues given by

$$Re_p = e^{ip\theta}e_p. \tag{A.51}$$

The orthogonal transformation can them be written as

$$R = e^{i\theta} \mathbf{e}_{+} \mathbf{e}_{+}^{\dagger} + e^{-i\theta} \mathbf{e}_{-} \mathbf{e}_{-}^{\dagger} + \mathbf{e}_{0} \mathbf{e}_{0}^{\dagger}$$
(A.52)

These eigenvectors are orthonormal with respect to the standard inner product in \mathbb{C}^3 , and the sign convention is chosen to be consistent with the Condon–Shortley phase convention for spherical harmonics,

$$r = \sum_{m=-1}^{1} 2\sqrt{\frac{\pi}{3}} r Y_{1m} e_m.$$
 (A.53)

This appendix summarizes of results related to Euclidean group which are discussed in various sections throughout the main text. The *Special Euclidean* $group \operatorname{SE}(3)$ is the semi-direct product $SO(3) \ltimes \mathbb{R}^3$ of the three-dimensional $Special \ Orthogonal \ group \ SO(3)$ with the three-dimensional $translation \ group \ \mathbb{R}^3$. The composition law is given by $(\mathsf{R}, \boldsymbol{x})(\mathsf{R}', \boldsymbol{x}') = (\mathsf{RR}', \mathsf{R}\boldsymbol{x}' + \boldsymbol{x})$, and inverses by $(\mathsf{R}, \boldsymbol{x})^{-1} = (\mathsf{R}^{-1}, -\mathsf{R}^{-1}\boldsymbol{x})$.

The special Euclidean group, and its Lie algebra, $\mathfrak{se}(3)$, have faithful matrix representations given by

$$SE(3) = \left\{ \begin{pmatrix} R & \boldsymbol{x} \\ 0 & 1 \end{pmatrix} \middle| R \in SO(3), \boldsymbol{x} \in \mathbb{R}^3 \right\}, \tag{B.1}$$

$$\mathfrak{se}(3) = \left\{ \begin{pmatrix} \hat{\boldsymbol{\omega}} & \boldsymbol{\mu} \\ 0 & 0 \end{pmatrix} \middle| \hat{\boldsymbol{\omega}} \in \mathfrak{so}(3), \boldsymbol{\mu} \in \mathbb{R}^3 \right\}$$
(B.2)

Each tangent vector in $T_SSE(3)$,

$$\boldsymbol{a} = \begin{pmatrix} \dot{\mathsf{R}} & \dot{\boldsymbol{x}} \\ 0 & 0 \end{pmatrix} \tag{B.3}$$

is naturally associated with two elements of $\mathfrak{se}(3)$, one given by left translation,

$$\mathsf{S}^{-1}\boldsymbol{a} = \begin{pmatrix} \mathsf{R}^{-1}\dot{\mathsf{R}} & \mathsf{R}^{-1}\dot{\boldsymbol{x}} \\ 0 & 0 \end{pmatrix} \tag{B.4}$$

and another by right translation,

$$a\mathsf{S}^{-1} = \begin{pmatrix} \dot{\mathsf{R}}\mathsf{R}^{-1} & \dot{\boldsymbol{x}} - \dot{\mathsf{R}}\mathsf{R}^{-1}\boldsymbol{x} \\ 0 & 0 \end{pmatrix}. \tag{B.5}$$

We can endow SE(3) with a Riemannian metric which is only left-invariant as follows. Given tangent vectors in $T_SSE(3)$,

$$\boldsymbol{a} = \begin{pmatrix} \dot{\mathsf{R}} & \dot{\boldsymbol{x}} \\ 0 & 0 \end{pmatrix},\tag{B.6}$$

$$\boldsymbol{b} = \begin{pmatrix} \dot{P} & \dot{\boldsymbol{z}} \\ 0 & 0 \end{pmatrix}, \tag{B.7}$$

we define their inner product to be,

$$\langle \boldsymbol{a} | \boldsymbol{b} \rangle_{\text{SE}(3)} = \langle \dot{\mathsf{R}} | \dot{P} \rangle_{\text{SO}(3)} + \langle \dot{\boldsymbol{x}} | \dot{\boldsymbol{z}} \rangle_{\mathbb{R}^3} = \frac{1}{2} \text{tr}(\dot{\mathsf{R}}^T \dot{P}) + \dot{\boldsymbol{x}}^T \dot{\boldsymbol{z}}$$
 (B.8)

The Lie algebra, $\mathfrak{se}(3)$, is spanned by the six generators,

$$\begin{pmatrix}
\hat{\boldsymbol{e}}_{1} & 0 \\
0 & 0
\end{pmatrix}, \begin{pmatrix}
\hat{\boldsymbol{e}}_{2} & 0 \\
0 & 0
\end{pmatrix}, \begin{pmatrix}
\hat{\boldsymbol{e}}_{3} & 0 \\
0 & 0
\end{pmatrix}$$

$$\begin{pmatrix}
0 & \boldsymbol{e}_{1} \\
0 & 0
\end{pmatrix}, \begin{pmatrix}
0 & \boldsymbol{e}_{2} \\
0 & 0
\end{pmatrix}, \begin{pmatrix}
0 & \boldsymbol{e}_{3} \\
0 & 0
\end{pmatrix}, (B.9)$$

which, by a slight abuse of notation, we will often simply write as \hat{e}_i and e_i . The structure constants are defined by the following commutation relations:

$$[\hat{\boldsymbol{e}}_a, \hat{\boldsymbol{e}}_b] = \varepsilon_{abc} \hat{\boldsymbol{e}}_c \tag{B.10}$$

$$[\hat{\boldsymbol{e}}_a, \boldsymbol{e}_b] = \varepsilon_{abc} \boldsymbol{e}_c \tag{B.11}$$

$$[\boldsymbol{e}_a, \boldsymbol{e}_b] = 0. \tag{B.12}$$

With $\theta = |\theta|$, the exponential map can be expressed as

$$\exp\begin{pmatrix} \hat{\boldsymbol{\theta}} & \boldsymbol{\mu} \\ 0 & 0 \end{pmatrix} = \begin{pmatrix} e^{\hat{\boldsymbol{\theta}}} & V\boldsymbol{\mu} \\ 0 & 1 \end{pmatrix}, \tag{B.13}$$

$$e^{\hat{\boldsymbol{\theta}}} = 1 + A\hat{\boldsymbol{\theta}} + B\hat{\boldsymbol{\theta}}^2, \quad V = 1 + B\hat{\boldsymbol{\theta}} + C\hat{\boldsymbol{\theta}}^2$$
 (B.14)

$$A = \sin(\theta)/\theta, \quad B = \frac{1 - \cos(\theta)}{\theta^2},$$
 (B.15)

$$C = (1 - A)/\theta^2 = (\theta - \sin(\theta))/\theta^3.$$
 (B.16)

The logarithm is given by

$$\log \begin{pmatrix} \mathsf{R} & \boldsymbol{x} \\ 0 & 1 \end{pmatrix} = \begin{pmatrix} \log \mathsf{R} & V^{-1} \boldsymbol{x} \\ 0 & 0 \end{pmatrix} \tag{B.17}$$

$$\theta = \arccos(\frac{\operatorname{tr}(\mathsf{R}) - 1}{2}),\tag{B.18}$$

$$\hat{\theta} = \log R = \frac{\theta}{2\sin\theta} (R - R^T)$$
 (B.19)

$$V^{-1} = 1 - \frac{1}{2}\hat{\boldsymbol{\theta}} + \frac{1}{\theta^2} \left(1 - \frac{A}{2B} \right) \hat{\boldsymbol{\theta}}^2$$
 (B.20)

where A and B are defined as above. Expanding in powers of θ , we find,

$$\frac{\theta}{2\sin\theta} = 1/2 + \theta^2/12 + 7\theta^4/720 + 31\theta^6/30240 + O(\theta^8)$$
 (B.21)

$$A = \sum_{j=0}^{\infty} \frac{(-1)^j}{(2j+1)!} \theta^{2j}$$
 (B.22)

$$=1-\theta^2/3!+\theta^4/5!-\theta^6/7!+O(\theta^8)$$
 (B.23)

$$= 1 - \theta^2/6 + \theta^4/120 - \theta^6/540 + O(\theta^8)$$
 (B.24)

$$B = \sum_{j=0}^{\infty} \frac{(-1)^j}{(2j+2)!} \theta^{2j}$$
 (B.25)

$$= 1/2! - \theta^2/4! + \theta^4/6! - \theta^6/8! + O(\theta^8)$$
 (B.26)

$$= 1/2 - \theta^2/24 + \theta^4/720 - \theta^6/40320 + O(\theta^8)$$
 (B.27)

$$C = \sum_{j=0}^{\infty} \frac{(-1)^j}{(2j+3)!} \theta^{2j}$$
 (B.28)

$$= 1/3! - \theta^2/5! + \theta^4/7! - \theta^6/9! + O(\theta^8)$$
(B.29)

$$= 1/6 - \theta^2/120 + \theta^4/5040 - \theta^6/362880 + O(\theta^8)$$
 (B.30)

$$\frac{1}{\theta^2} \left(1 - \frac{A}{2B} \right) = 1/12 + \theta^2/720 + \theta^4/30240 + \theta^6/1209600 + O(\theta^8)$$
 (B.31)

Given two elements of $\mathfrak{se}(3)$,

$$\psi = \begin{pmatrix} \hat{\boldsymbol{\theta}} & \boldsymbol{\mu} \\ 0 & 0 \end{pmatrix}, \quad \gamma = \begin{pmatrix} \hat{\boldsymbol{\phi}} & \boldsymbol{\nu} \\ 0 & 0 \end{pmatrix}, \tag{B.32}$$

the adjoint and coadjoint action on $\mathfrak{se}(3)$ can be expressed as

$$ad_{\psi} \gamma = \begin{pmatrix} \left[\hat{\boldsymbol{\theta}}, \hat{\boldsymbol{\phi}} \right] & \hat{\boldsymbol{\theta}} \boldsymbol{\nu} - \hat{\boldsymbol{\phi}} \boldsymbol{\mu} \\ 0 & 0 \end{pmatrix} = \widehat{\boldsymbol{\theta} \times \boldsymbol{\phi}} + \boldsymbol{\theta} \times \boldsymbol{\nu} - \boldsymbol{\phi} \times \boldsymbol{\mu}$$
 (B.33)

$$\operatorname{ad}_{\boldsymbol{\psi}}^* \boldsymbol{\gamma} = - \begin{pmatrix} \left[\hat{\boldsymbol{\theta}}, \hat{\boldsymbol{\phi}} \right] + \widehat{\boldsymbol{\mu} \times \boldsymbol{\nu}} & \hat{\boldsymbol{\theta}} \boldsymbol{\nu} \\ 0 & 0 \end{pmatrix} = -\widehat{\boldsymbol{\theta} \times \boldsymbol{\phi}} - \widehat{\boldsymbol{\mu} \times \boldsymbol{\nu}} - \boldsymbol{\theta} \times \boldsymbol{\nu}$$
 (B.34)

With $\alpha = \hat{\chi} + \eta$, $\psi = \hat{\theta} + \mu$, $\gamma = \hat{\phi} + \nu$, we have

$$\langle \alpha | ad_{\psi}^* \gamma \rangle = -\chi \cdot (\theta \times \phi + \mu \times \nu) - \eta \cdot (\theta \times \nu)$$
 (B.35)

$$= (\boldsymbol{\theta} \times \boldsymbol{\chi}) \cdot \boldsymbol{\phi} + (\boldsymbol{\theta} \times \boldsymbol{\nu} - \boldsymbol{\chi} \times \boldsymbol{\mu}) \cdot \boldsymbol{\nu}$$
 (B.36)

$$= \langle \operatorname{ad}_{\psi} \alpha | \gamma \rangle \tag{B.37}$$

This appendix contains additional details, calculations, and derivations for § 4.

C.1 Integral equation for tension

The tension differential equation (4.24) can be formulated as a Fredholm integral equation. This section derives a perturbative series for the two dimensional case. Equation (4.34) for the 2d active filament is equivalent to the integral equation

$$\lambda(s) = -\frac{\beta}{2}\kappa^{2}(s) - \int_{-1/2}^{1/2} G(s, s') \partial_{s'} f(s') ds' - \frac{\beta}{2\eta} \kappa^{2}(s)$$

$$+ \frac{\beta}{\eta} \int_{-1/2}^{1/2} G(s, s') [\partial_{s'} \kappa(s')]^{2} ds' + \frac{1}{\eta} \int_{-1/2}^{1/2} G(s, s') \kappa^{2}(s') \lambda(s') ds'$$
(C.1)

where G is the Dirichlet Green function for the Laplace equation on the interval [1/2,1/2] with homogeneous boundary conditions,

$$G(s,s') = \begin{cases} (s'-1/2)(s+1/2), & \text{for } s < s' \\ (s'+1/2)(s-1/2), & \text{for } s > s' \end{cases}$$
 (C.2)

$$= (s' - 1/2)(s + 1/2)\Theta(s' - s) + (s' + 1/2)(s - 1/2)\Theta(s - s').$$
 (C.3)

To simplify notation, define the following:

$$\varepsilon = \frac{1}{n} \tag{C.4}$$

$$\langle s|g_0\rangle = g_0(s) = -\frac{\beta}{2}\kappa^2(s) - \int_{-1/2}^{1/2} G(s,s')\partial_{s'}f(s')ds'$$
 (C.5)

$$\langle s|g_1\rangle = g_1(s) = -\frac{\beta}{2}\kappa^2(s) + \beta \int_{-1/2}^{1/2} G(s,s') [\partial_{s'}\kappa(s')]^2 ds'$$
 (C.6)

$$K = \int_{-1/2}^{1/2} \int_{-1/2}^{1/2} G(s, s') \kappa^{2}(s') |s\rangle \langle s'| ds ds'.$$
 (C.7)

Equation (C.1) can then be written as

$$|\lambda\rangle = |g_0\rangle + \varepsilon |g_1\rangle + \varepsilon K |\lambda\rangle,$$
 (C.8)

which has the solution

$$|\lambda\rangle = |g_0\rangle + \sum_{j=1} \varepsilon^j \mathsf{K}^{j-1} \left[\mathsf{K} |g_0\rangle + |g_1\rangle \right]. \tag{C.9}$$

The first two terms in $\lambda=\lambda_0+arepsilon\lambda_1+arepsilon^2\lambda_2+\ldots$ are given by

$$\lambda_0(s) = -\frac{\beta}{2}\kappa^2(s) - \int_{-1/2}^{1/2} G(s, s') \partial_{s'} f(s') \, \mathrm{d}s'$$
 (C.10)

$$\lambda_{1}(s) = -\frac{\beta}{2}\kappa^{2}(s) + \beta \int_{-1/2}^{1/2} G(s, s') [\partial_{s'}\kappa(s')]^{2} ds'$$

$$-\frac{\beta}{2} \int_{-1/2}^{1/2} G(s, s') \kappa^{4}(s') ds' - \int_{-1/2}^{1/2} \int_{-1/2}^{1/2} G(s, s'') \kappa^{2}(s'') G(s'', s') \partial_{s'} f(s') ds' ds''$$
(C.11)

C.2 Estimate of critical dimensional bending stiffness

Swarmers with lengths in the range $L=10-100\,\mu\mathrm{m}$ were found to swim with an average velocity $u^*=13\,\mu\mathrm{m/s}$ when placed in a motility buffer with viscosity $\mu=.001\,\mathrm{Pa\cdot s}$ [99]. Using the critical dimensionless bending stiffness $\beta_{\perp}^*=.0101$, a body diameter of $a=1\,\mu\mathrm{m}$, a longitudinal drag coefficient $\zeta_{\parallel}=2\pi\mu/\ln(L/a)$, and characteristic force density $f^*=\zeta_{\parallel}u^*$, we predict the critical dimensional bending stiffness for swarmer cells to be in the range $B_{\perp}\approx 3.6\times 10^{-25}-1.8\times 10^{-22}\,\mathrm{Nm}^2$. Experimental measurements have suggested an average swarmer cell bending stiffness of $5.5\times 10^{-22}\,\mathrm{Nm}^2$ [96]. Taking a characteristic body length of $L=50\,\mu\mathrm{m}$ results in a critical value of $B_{\perp}\approx 2.6\times 10^{-23}\,\mathrm{Nm}^2$.

C.3 Evolution equations in an inertial frame

With primes denoting s-derivatives and dots denoting t-derivatives, we can write $u=\mathsf{R}^{-1}\dot{r},\,e_0=\mathsf{R}^{-1}r',\,\Omega_\perp=\mathsf{R}^{-1}(r'\times r''),\,\omega_\perp=\mathsf{R}^{-1}(r'\times\dot{r}').$ The

structure equations and inextensibility/unshearability imply

$$\dot{\Omega}_0 = \omega_0' + \mathbf{r}' \cdot (\mathbf{r}'' \times \dot{\mathbf{r}}'), \qquad (C.12)$$

$$\mathbf{r}' \cdot \dot{\mathbf{r}}' = 0, \tag{C.13}$$

and the stress balance equations can be written in an inertial frame as

$$\left(B_{\parallel}\Omega_{0}\mathbf{r}' + B_{\perp}\mathbf{r}' \times \mathbf{r}''\right)' + \mathbf{r}' \times \mathbf{\Lambda} + m\mathbf{r}' - \zeta_{r}\omega_{0}\mathbf{r}' = 0, \tag{C.14}$$

$$\mathbf{\Lambda}' + f\mathbf{r}' - \zeta \dot{\mathbf{r}} = 0, \tag{C.15}$$

where $\zeta = \zeta_{\parallel} \boldsymbol{r}' \boldsymbol{r}'^T + \zeta_{\perp} (1 - \boldsymbol{r}' \boldsymbol{r}'^T)$. Eliminating ω_0 and $\boldsymbol{\Lambda}_{\perp} = (1 - \boldsymbol{r} \boldsymbol{r}'^T) \boldsymbol{\Lambda}$, we find

$$\omega_0 = \frac{B_{\parallel}}{\zeta_r} \Omega_0' + \frac{1}{\zeta_r} m' \tag{C.16}$$

$$\mathbf{\Lambda}_{\perp} = \mathbf{r}' \times \left(B_{\parallel} \Omega_0 \mathbf{r}' + B_{\perp} \mathbf{r}' \times \mathbf{r}'' \right)' \tag{C.17}$$

$$\dot{\Omega}_0 = \frac{B_{\parallel}}{\zeta_r} \Omega_0'' + \frac{1}{\zeta_r} m'' + \mathbf{r}' \cdot (\mathbf{r}'' \times \dot{\mathbf{r}}')$$
 (C.18)

$$\lambda'' - \frac{\zeta_{\parallel}}{\zeta_{\perp}} \kappa^2 \lambda + f' + \frac{1}{2} B_{\perp}(\kappa^2)'' + \frac{\zeta_{\parallel}}{\zeta_{\perp}} \kappa^2 \tau \left(B_{\parallel} \Omega_0 - B_{\perp} \tau \right) + \frac{\zeta_{\parallel} B_{\perp}}{\zeta_{\perp}} \kappa \kappa'' = 0$$
(C.19)

where $\lambda = r' \cdot \Lambda$. Torsion can be eliminated using

$$\Omega_0 \kappa^2 \tau = \kappa^2 \Omega_0^2 + \Omega_0 \mathbf{e}_0 \cdot (\mathbf{\Omega}_\perp \times \mathbf{\Omega}_\perp') \tag{C.20}$$

$$\kappa \kappa'' - \kappa^2 \tau^2 = \mathbf{\Omega}_{\perp} \cdot \mathbf{\Omega}_{\perp}'' - \kappa^2 \Omega_0^2 - 2\Omega_0 \mathbf{e}_0 \cdot (\mathbf{\Omega}_{\perp} \times \mathbf{\Omega}_{\perp}')$$
 (C.21)

to recover the tension equation given in the main manuscript.

C.4 Symmetries

This section contains a collection of results related to symmetries and conserved quantities for the active filament model.

Curvature/torsion parity and rotational symmetry

Consider an arclength parameterized curve r(s) with Frenet-Serret frame (T, N, B), curvature κ , and torsion τ . Suppose the midpoint is at s=0, and define the following:

$$S = \begin{pmatrix} R & \mathbf{r} \\ 0 & 1 \end{pmatrix} = \begin{pmatrix} \mathbf{T} \mathbf{e}_0^T + \mathbf{N} \mathbf{e}_1^T + \mathbf{B} \mathbf{e}_2^T & \mathbf{r} \\ 0 & 1 \end{pmatrix}$$
(C.22)

$$A = \begin{pmatrix} \hat{\Omega} & e_0 \\ 0 & 0 \end{pmatrix} = \begin{pmatrix} \tau \hat{e}_0 + \kappa \hat{e}_2 & e_0 \\ 0 & 0 \end{pmatrix}$$
 (C.23)

Curvature and torsion are even functions of s if and only if the (Frenet-Serret) framed curve is invariant under rotation by π about an axis which intersects the curve at $\mathbf{r}(0)$ and which is perpendicular to $\mathbf{T}(0)$. If the curvature is nonvanishing at s=0, then the axis of rotation is parallel to $\mathbf{n}=\mathbf{N}(0)$. This is equivalent to saying that the equation

$$A(-s) = A(s) \tag{C.24}$$

holds if and only if

$$S(-s) = S_0 G S_0^{-1} S(s) G^{-1}$$

$$= \begin{pmatrix} e^{\pi \hat{N}(0)} R(s) e^{\pi \hat{e}_1} & \mathbf{r}(0) + e^{\pi \hat{N}(0)} (\mathbf{r}(s) - \mathbf{r}(0)) \\ 0 & 1 \end{pmatrix}$$
(C.25)

where $S_0 := S(0)$ and G is given by

$$\mathsf{G} = \begin{pmatrix} e^{\pi \hat{\mathbf{e}}_1} & 0 \\ 0 & 1 \end{pmatrix} = \begin{pmatrix} -\mathbf{e}_0 \mathbf{e}_0^T + \mathbf{e}_1 \mathbf{e}_1^T - \mathbf{e}_2 \mathbf{e}_2^T & 0 \\ 0 & 1 \end{pmatrix} \tag{C.26}$$

Proof. We begin by proving the $S_0 = 1$ case. If $S_0 = 1$ then $T(0) = e_0$,

$$N(0) = e_1, B(0) = e_2, r(0) = 0,$$

$$S(s) = \prod_{\xi=0}^{\xi=s} e^{A(\xi) d\xi} = \mathcal{P} \exp \int_0^s A(\xi) d\xi, \qquad (C.27)$$

and Eq. (C.25) reduces to

$$S(-s) = GS(s)G^{-1}$$

$$= \begin{pmatrix} e^{\pi \hat{\mathbf{e}}_1} R(s) e^{\pi \hat{\mathbf{e}}_1} & e^{\pi \hat{\mathbf{e}}_1} \mathbf{r}(s) \\ 0 & 1 \end{pmatrix}$$
(C.28)

First, we suppose A(-s) = A(s) and show (C.24) \Rightarrow (C.28). We find that S transforms under $s \mapsto -s$ as

$$S(-s) = \prod_{\xi=0}^{\xi=-s} e^{A(\xi) d\xi} = \prod_{\xi=0}^{\xi=s} e^{-A(-\xi) d\xi} = \prod_{\xi=0}^{\xi=s} e^{-A(\xi) d\xi}, \qquad (C.29)$$

where the last equality uses A(-s) = A(s). Since A satisfies

$$\mathsf{GAG}^{-1} = \begin{pmatrix} e^{\pi \hat{e}_1} \left(\tau \hat{e}_0 + \kappa \hat{e}_2 \right) e^{-\pi \hat{e}_1} & e^{\pi \hat{e}_1} e_0 \\ 0 & 0 \end{pmatrix}$$
 (C.30)

$$= \begin{pmatrix} -\tau \hat{\boldsymbol{e}}_0 - \kappa \hat{\boldsymbol{e}}_2 & -\boldsymbol{e}_0 \\ 0 & 0 \end{pmatrix} \tag{C.31}$$

$$= -A, (C.32)$$

we have

$$S(-s) = \prod_{\xi=0}^{\xi=s} e^{GA(\xi)G^{-1}d\xi}$$
 (C.33)

$$= G \left(\prod_{\xi=0}^{\xi=s} e^{A(\xi) d\xi} \right) G^{-1}$$
 (C.34)

$$= \mathsf{GS}(s)\mathsf{G}^{-1} \tag{C.35}$$

which proves $(C.24) \Rightarrow (C.28)$.

Now we assume (C.28) and show (C.28) \Rightarrow (C.24). Taking a derivative

of (C.28) and using $GAG^{-1} = -A$, we find

$$-S(-s)A(-s) = GS(s)A(s)G^{-1}$$

$$= GS(s)G^{-1}GA(s)G^{-1}$$

$$= S(-s)GA(s)G^{-1}$$

$$= -S(-s)A(s)$$
(C.36)

which proves $(C.28) \Rightarrow (C.24)$. To prove the general case, $(C.25) \Leftrightarrow (C.24)$, just apply the above argument to $\tilde{S} := S_0^{-1} S$.

Filaments with a circular cross-section

When representing a filament with circular cross-section by a framed curve,

$$S = \begin{pmatrix} R & r \\ 0 & 1 \end{pmatrix}, A = S^{-1} dS$$
 (C.37)

$$A = \begin{pmatrix} \hat{\Omega} & U \\ 0 & 0 \end{pmatrix} ds + \begin{pmatrix} \hat{\omega} & u \\ 0 & 0 \end{pmatrix} dt, \qquad (C.38)$$

$$U = e_0 \tag{C.39}$$

the initial direction for the transverse frame vectors $q_1 = Re_1$, $q_2 = Re_2$ at s = 0 is arbitrary. The gauge group U(1) acts by rotating the frame at each point along

the curve by a constant angle about the curve tangent $q_0={\sf R}e_0=\partial_s r$. Gauge invariants include the centerline r and all associated geometric quantities (e.g. curvature, torsion, and Frenet-Serret frame), as well as the twist $\Omega_0=e_0\cdot\Omega$. Gauge transformations can be represented by SE(3)-valued matrices

$$\mathsf{G} = \begin{pmatrix} e^{\theta \hat{\mathbf{e}}_0} & 0\\ 0 & 1 \end{pmatrix} \tag{C.40}$$

whose action on S is defined by

$$S \mapsto SG^{-1} = \begin{pmatrix} Re^{-\theta \hat{e}_0} & \mathbf{r} \\ 0 & 1 \end{pmatrix}$$

$$= \begin{pmatrix} e^{-\theta \hat{q}_0}R & \mathbf{r} \\ 0 & 1 \end{pmatrix}$$

$$(C.41)$$

Under a change of gauge, A transforms as

$$A \mapsto \mathsf{G}\mathsf{A}\mathsf{G}^{-1}. \tag{C.42}$$

Or, in terms of its components

$$\mathbf{\Omega} \mapsto \Omega_0 \mathbf{e}_0 + e^{\theta \hat{\mathbf{e}}_0} \mathbf{\Omega}_{\perp} \tag{C.43}$$

$$U \mapsto U$$
 (C.44)

$$\boldsymbol{\omega} \mapsto \omega_0 \boldsymbol{e}_0 + e^{\theta \hat{\boldsymbol{e}}_0} \boldsymbol{\omega}_{\perp} \tag{C.45}$$

$$\boldsymbol{u} \mapsto u_0 \boldsymbol{e}_0 + e^{\theta \hat{\boldsymbol{e}}_0} \boldsymbol{u}_{\perp} \tag{C.46}$$

Symmetries of the shape equations

The evolution equations of § 4 are invariant under C.41,C.42. As a result, solutions which differ only by a constant phase at t=0

$$\tilde{\mathsf{A}}(s,0) = \mathsf{G}\mathsf{A}(s,0)\mathsf{G}^{-1} \tag{C.47}$$

will have the same relative phase at future times

$$\tilde{\mathsf{A}}(s,t) = \mathsf{G}\mathsf{A}(s,t)\mathsf{G}^{-1}.\tag{C.48}$$

Invariance of the evolution equations given in $\S 4$ can be seen as a consequence of the fact that the energy, inextensibility/unshearability constraints, dissipation function, and active stresses for the model, as well as the structure

equations, are invariant under C.41,C.42. These invariance properties can also be verified by direct examination of the structure and stress balance equations (see §3.3 and §C.3).

In statics problems, the phase difference between the Frenet-Serret and material frames at s=0 can always be eliminated through a proper choice of gauge, however, this is generally not possible for dynamics problems. Exceptions can be found when certain symmetry conditions are met. When twist Ω_0 is an even function, the conditions listed below are equivalent

- (1) Curvature κ and torsion τ are even functions of s
- (2) The centerline r(s) is invariant under rotation by π about an axis which intersects the curve at s=0
- (3) There exists a gauge in which Ω_1 and Ω_2 have definite and opposite parity

If, in addition, the active stresses f, m are odd, then these symmetries, as well as the phase difference between the Material and Frenet-Serret frames at s=0,

are conserved. That is, if Ω_0 , Ω_2 are even, and Ω_1 , f, m are odd at t = 0,

$$\Omega_{0}(-s,0) = \Omega_{0}(s,0)$$

$$\Omega_{1}(-s,0) = -\Omega_{1}(s,0)$$

$$\Omega_{2}(-s,0) = \Omega_{2}(s,0)$$

$$f(-s,0) = -f(s,0)$$

$$m(-s,0) = -m(s,0)$$
(C.49)

then the parity of Ω_0 , Ω_1 , Ω_2 , f, m, and λ are conserved for all t > 0,

$$\Omega_0(-s,t) = \Omega_0(s,t)$$

$$\Omega_1(-s,t) = -\Omega_1(s,t)$$

$$\Omega_2(-s,t) = \Omega_2(s,t)$$

$$f(-s,t) = -f(s,t)$$

$$m(-s,t) = -m(s,t)$$

$$\lambda(-s,t) = \lambda(s,t)$$
(C.50)

 $q_1(0,t)$ is constant in time

$$q_1(0,t) = q_1(0,0),$$
 (C.51)

the centerline remains invariant under rotation by π about an axis parallel to ${\bf q}_1(0,t)={\bf q}_1(0,0)$ which intersects the centerline at ${\bf r}(0,0)$

$$r(-s,t) = r(0,0) + e^{\pi \hat{q}_1(0,0)} (r(s,t) - r(0,0)),$$
 (C.52)

and both the linear and angular velocities are directed along the symmetry axis at $s=0\,$

$$u(0,t) = u_1(0,t)e_1$$
 (C.53)

$$\boldsymbol{\omega}(0,t) = \omega_1(0,t)\boldsymbol{e}_1 \tag{C.54}$$

Under the above symmetry assumptions, enforcing free boundary conditions at $s=\pm L/2$ is equivalent to

$$\Omega_0'|_{s=0} = 0$$
 (C.55)

$$\Omega_1|_{s=0} = 0, \, \Omega_1''|_{s=0} = 0$$
 (C.56)

$$\Omega_2'|_{s=0} = 0, \, \Omega_2'''|_{s=0} = 0$$
 (C.57)

$$\lambda'|_{s=0} = 0 \tag{C.58}$$

$$\Omega_0|_{s=L/2} = 0$$
 (C.59)

$$\Omega_1|_{s=L/2} = 0, \, \Omega_1'|_{s=L/2} = 0$$
 (C.60)

$$\Omega_2|_{s=L/2} = 0, \, \Omega_2'|_{s=L/2} = 0$$
 (C.61)

$$\lambda|_{s=L/2} = 0. \tag{C.62}$$

Example of physically equivalent, but out of phase solutions are given by the following. The system with initial conditions given by

$$\Omega_0(s,0) = \frac{M}{B_{\parallel}} \log(\frac{\cosh(10s)}{\cosh(5)}) \tag{C.63}$$

$$\Omega_1(s,0) = -6\phi_0(s)\sin(2\pi s)$$
 (C.64)

$$\Omega_2(s,0) = 6\phi_0(s)\cos(2\pi s)$$
 (C.65)

$$f(s,0) = -\tanh(10s)$$
 (C.66)

$$m(s,0) = -M \tanh(10s) \tag{C.67}$$

$$S(0,0) = 1, (C.68)$$

where ϕ_0 is the first even eigenfunction of ∂_s^4 , satisfies the symmetry conditions outlined in the above, so, the parity of Ω_0 , Ω_1 , Ω_2 , f, m, and λ are conserved.

Consider systems with initial conditions

$$\Omega_0^{(j)}(s,0) = \Omega_0(s,0) \tag{C.69}$$

$$f^{(j)}(s,0) = f(s,0) \tag{C.70}$$

$$m^{(j)}(s,0) = m(s,0)$$
 (C.71)

$$\begin{pmatrix} \Omega_1^{(j)}(s,0) \\ \Omega_2^{(j)}(s,0) \end{pmatrix} = \begin{pmatrix} \cos(2j\pi/3) & -\sin(2j\pi/3) \\ \cos(2j\pi/3) & \sin(2j\pi/3) \end{pmatrix} \begin{pmatrix} -6\phi_0(s)\sin(2\pi s) \\ 6\phi_0(s)\cos(2\pi s) \end{pmatrix}$$
(C.72)

$$S^{(j)}(0,0) = \begin{pmatrix} 1 & 0 & 0 & 0 \\ 0 & \cos(2j\pi/3) & \sin(2j\pi/3) & 0 \\ 0 & -\sin(2j\pi/3) & \cos(2j\pi/3) & 0 \\ 0 & 0 & 0 & 1 \end{pmatrix}$$
 (C.73)

for j=0,1,2. Gauge independence of the equations of motion implies the relative phase of these systems systems is independent of time:

$$\Omega_0^{(j)}(s,t) = \Omega_0(s,t)$$
(C.74)

$$f^{(j)}(s,t) = f(s,t)$$
 (C.75)

$$m^{(j)}(s,t) = m(s,t)$$
 (C.76)

$$\begin{pmatrix}
\Omega_{1}^{(j)}(s,t) \\
\Omega_{2}^{(j)}(s,t)
\end{pmatrix} = \begin{pmatrix}
\cos(2j\pi/3) & -\sin(2j\pi/3) \\
\cos(2j\pi/3) & \sin(2j\pi/3)
\end{pmatrix} \begin{pmatrix}
\Omega_{1}(s,t) \\
\Omega_{2}(s,t)
\end{pmatrix}$$

$$= \begin{pmatrix}
\cos(2j\pi/3)\Omega_{1}(s,t) - \sin(2j\pi/3)\Omega_{2}(s,t) \\
\sin(2j\pi/3)\Omega_{1}(s,t) + \cos(2j\pi/3)\Omega_{2}(s,t)
\end{pmatrix}$$
(C.77)

$$\mathsf{S}^{(j)}(s,t) = \mathsf{S}(s,t) \begin{pmatrix} 1 & 0 & 0 & 0 \\ 0 & \cos(2j\pi/3) & \sin(2j\pi/3) & 0 \\ 0 & -\sin(2j\pi/3) & \cos(2j\pi/3) & 0 \\ 0 & 0 & 0 & 1 \end{pmatrix} \tag{C.78}$$

D APPENDIX: SURFACE-BOUND BIOPOLYMERS

This appendix derives and discusses computational methods for solving the equations governing tension $\lambda=e_1\cdot \lambda$, geodesic curvature $\Omega:=e_3\cdot \Omega$, unit tangent $q:=q_1$, and centerline r of the surface-bound filament model introduced in § 5 from the Euler-Poincaré equations, structure equations, and surface constraints,

$$\partial_s \mathbf{m} + \mathbf{\Omega} \times \mathbf{m} + \mathbf{U} \times \mathbf{\lambda} - \chi \mathbf{e}_1 = \zeta_r \omega_1 \mathbf{e}_1 \tag{D.1}$$

$$\partial_s \lambda + \Omega \times \lambda - \nu e_3 - \chi \mathsf{R}^T \nabla n \mathsf{R} e_2 + f = \zeta u$$
 (D.2)

$$\partial_t \mathbf{\Omega} = \partial_s \boldsymbol{\omega} + \mathbf{\Omega} \times \boldsymbol{\omega} \tag{D.3}$$

$$\partial_s \mathbf{u} + \mathbf{\Omega} \times \mathbf{u} = \partial_t \mathbf{U} + \mathbf{\omega} \times \mathbf{U} \tag{D.4}$$

$$\partial_s \mathbf{r} = \mathsf{R} \mathbf{e}_1 \tag{D.5}$$

$$\phi(\mathbf{r}) = 0 \tag{D.6}$$

$$\mathbf{q}_2 \cdot \mathbf{n}(\mathbf{r}) = 0. \tag{D.7}$$

The following relations between the framed curve and surface geometries will be used at various points throughout this appendix.

$$I = 1 - \boldsymbol{n}\boldsymbol{n}^T = \boldsymbol{q}_1 \boldsymbol{q}_1^T + \boldsymbol{q}_2 \boldsymbol{q}_2^T$$
 (D.8)

$$K_{ij} := -\mathbf{q}_i \cdot \nabla \mathbf{n} \cdot \mathbf{q}_j \tag{D.9}$$

$$K = \begin{pmatrix} K_{11} & K_{12} \\ K_{12} & K_{22} \end{pmatrix} = \begin{pmatrix} -\Omega_2 & \Omega_1 \\ \Omega_1 & K_{22} \end{pmatrix}$$
 (D.10)

$$\nabla \boldsymbol{n} \cdot \boldsymbol{n} = 0 \tag{D.11}$$

$$\partial_s \mathbf{r} \cdot \nabla \mathbf{n} = \mathsf{R} \left(\mathbf{\Omega} \times \mathbf{e}_3 \right)$$
 (D.12)

$$\boldsymbol{n} \cdot \partial_t \boldsymbol{r} = \boldsymbol{e}_3 \cdot \boldsymbol{u} = 0 \tag{D.13}$$

$$\Omega_1 = -\boldsymbol{q}_1 \cdot \nabla \boldsymbol{n} \cdot \boldsymbol{q}_2 = K_{12} \tag{D.14}$$

$$\Omega_2 = \mathbf{q}_1 \cdot \nabla \mathbf{n} \cdot \mathbf{q}_1 = -K_{11} \tag{D.15}$$

$$\omega_1 = -\partial_t \mathbf{r} \cdot \nabla \mathbf{n} \cdot \mathbf{q}_2 = K_{12} u_1 + K_{22} u_2 \tag{D.16}$$

$$\omega_2 = \partial_t \mathbf{r} \cdot \nabla \mathbf{n} \cdot \mathbf{q}_1 = -K_{11}u_1 - K_{12}u_2 \tag{D.17}$$

Gaussian curvature K

$$\mathcal{K} = \det(\mathsf{K}) = -\frac{1}{2} \operatorname{tr}(\hat{\boldsymbol{n}} \cdot \nabla \boldsymbol{n} \cdot \hat{\boldsymbol{n}} \cdot \nabla \boldsymbol{n})$$
 (D.18)

$$\nabla \boldsymbol{n}^T \cdot \hat{\boldsymbol{n}} \cdot \nabla \boldsymbol{n} = \mathcal{K} \hat{\boldsymbol{n}} \tag{D.19}$$

Mean curvature \mathcal{H}

$$\nabla \cdot \boldsymbol{n} = \operatorname{tr}(\nabla \boldsymbol{n}) = -2\mathcal{H} \tag{D.20}$$

D.1 Surface geometry and constraints

The following calculations are based purely on kinematic constraints associated with of inextensibility/unshearbility $\boldsymbol{U}=\boldsymbol{e}_1$, surface confinement, $\phi(\boldsymbol{r})=0$ and $\boldsymbol{q}_3=\boldsymbol{n}$, the structure equations $\mathrm{d}\mathsf{A}+\mathsf{A}\land\mathsf{A}=0$, and the equation $\mathrm{d}\mathsf{S}=\mathsf{S}\mathsf{A}$. By inextensibility/unshearability, the structure equations reduce to

$$\partial_t \mathbf{\Omega} = \partial_s \boldsymbol{\omega} + \mathbf{\Omega} \times \boldsymbol{\omega} \tag{D.21}$$

$$\partial_s \boldsymbol{u} + \boldsymbol{\Omega} \times \boldsymbol{u} = \boldsymbol{\omega} \times \boldsymbol{e}_1.$$
 (D.22)

Using the fact that

$$u_3 = \boldsymbol{e}_3 \cdot \boldsymbol{u} = \boldsymbol{n} \cdot \partial_t \boldsymbol{r} = 0, \tag{D.23}$$

we find just three independent scalar equations,

$$\partial_s u_1 - \Omega_3 u_2 = 0 \tag{D.24}$$

$$\partial_s u_2 + \Omega_3 u_1 = \omega_3 \tag{D.25}$$

$$\partial_t \Omega_3 = \partial_s \omega_3 + \Omega_1 \omega_2 - \Omega_2 \omega_1$$

$$= \partial_s \omega_3 + \mathcal{K} u_2,$$
(D.26)

where \mathcal{K} is the Gaussian curvature of the surface. The first will give an equation for the tension, and the second and third combine to give an evolution equation for the geodesic curvature

$$\partial_t \Omega_3 = \partial_s \omega_3 + \Omega_1 \omega_2 - \Omega_2 \omega_1$$

$$= \partial_s \omega_3 + \mathcal{K} u_2$$

$$= \partial_s^2 u_2 + \partial_s \Omega_3 u_1 + \Omega_3 \partial_s u_1 + \mathcal{K} u_2$$

$$= \partial_s^2 u_2 + \left(\Omega_3^2 + \mathcal{K}\right) u_2 + \partial_s \Omega_3 u_1$$
(D.27)

D.2 The mobility tensor

Here we will derive the effective in-surface mobility tensor. First we eliminate the Lagrange multipliers ν , χ , and λ_{\perp} . Crossing moment balance (D.1) with e_1 and defining $\lambda:=e_1\cdot \lambda$ gives

$$\lambda = \lambda e_1 + e_1 \times (\partial_s m + \Omega \times m)$$
 (D.28)

$$\lambda_2 = -\partial_s m_3 - \Omega_1 m_2 + \Omega_2 m_1 \tag{D.29}$$

$$= -\partial_s m_3 - K_{11} m_1 - K_{12} m_2 \tag{D.30}$$

$$\lambda_3 = \partial_s m_2 + \Omega_3 m_1 - \Omega_1 m_3 \tag{D.31}$$

$$= \partial_s m_2 + \Omega_3 m_1 - K_{12} m_3 \tag{D.32}$$

The remaining e_1 component of moment balance gives

$$\chi = \mathbf{e}_1 \cdot (\partial_s \mathbf{m} + \mathbf{\Omega} \times \mathbf{m}) - \zeta_r \omega_1 \tag{D.33}$$

$$= e_1 \cdot (\partial_s \mathbf{m} + \mathbf{\Omega} \times \mathbf{m}) - \zeta_r K_{12} u_1 - \zeta_r K_{22} u_2$$
 (D.34)

Then a miracle happens [171] and you get

$$\begin{pmatrix} \partial_{s}\lambda + \mathbf{\Omega} \cdot \partial_{s}\mathbf{m} + f_{1} \\ \mathbf{e}_{2} \cdot (\partial_{s}\lambda + \mathbf{\Omega} \times \lambda) + K_{22}\mathbf{e}_{1} \cdot (\partial_{s}\mathbf{m} + \mathbf{\Omega} \times \mathbf{m}) + f_{2} \end{pmatrix} = \begin{pmatrix} \zeta_{1} + \zeta_{r}K_{12}^{2} & \zeta_{r}K_{12}K_{22} \\ \zeta_{r}K_{12}K_{22} & \zeta_{2} + \zeta_{r}K_{22}^{2} \end{pmatrix} \begin{pmatrix} u_{1} \\ u_{2} \end{pmatrix}$$
(D.35)

where components of the steric force are given by

$$f_1(s) = -\mathbf{q}_1(s) \cdot \int \frac{\partial G}{\partial \mathbf{r}(s)} (\mathbf{r}(s), \mathbf{r}(s')) ds' = -\partial_s \int G(\mathbf{r}(s), \mathbf{r}(s')) ds' \quad (D.36)$$

$$f_2(s) = -\mathbf{q}_2(s) \cdot \int \frac{\partial G}{\partial \mathbf{r}(s)} (\mathbf{r}(s), \mathbf{r}(s')) ds' \quad (D.37)$$

Define the effective mobility tensor

$$M = \frac{1}{\zeta_{1}\zeta_{2} + \zeta_{1}\zeta_{r}K_{22}^{2} + \zeta_{2}\zeta_{r}K_{12}^{2}} \begin{pmatrix} \zeta_{2} + \zeta_{r}K_{22}^{2} & -\zeta_{r}K_{12}K_{22} \\ -\zeta_{r}K_{12}K_{22} & \zeta_{1} + \zeta_{r}K_{12}^{2} \end{pmatrix}$$
(D.38)
$$= \sum_{i,j=1}^{2} M_{ij}e_{i}e_{j}^{T}$$
(D.39)

and force density

$$F = F_{1}e_{1} + F_{2}e_{2}$$

$$= \begin{pmatrix} \partial_{s}\lambda + \Omega \cdot \partial_{s}m + f_{1} \\ e_{2} \cdot (\partial_{s}\lambda + \Omega \times \lambda) + K_{22}e_{1} \cdot (\partial_{s}m + \Omega \times m) + f_{2} \end{pmatrix}$$

$$= \begin{pmatrix} \partial_{s}\lambda + \Omega \cdot \partial_{s}m + f_{1} \\ \Omega\lambda + e_{2} \cdot (\partial_{s}\lambda_{\perp} + \Omega \times \lambda_{\perp}) + K_{22}e_{1} \cdot (\partial_{s}m + \Omega \times m) + f_{2} \end{pmatrix}$$

$$= \begin{pmatrix} \partial_{s}\lambda + \Omega \cdot \partial_{s}m + f_{1} \\ \partial_{s}\lambda + \Omega \cdot \partial_{s}m + f_{1} \\ \Omega_{3}\lambda + \partial_{s}\lambda_{2} - \Omega_{1}\lambda_{3} + K_{22}\partial_{s}m_{1} - K_{22}K_{11}m_{3} - K_{22}\Omega_{3}m_{2} + f_{2} \end{pmatrix}$$
(D.40)

where,

$$F_2 = -\partial_s^2 m_3 + (\lambda - K_{12}m_1 - K_{22}m_2)\Omega_3 - \mathcal{K}m_3$$
 (D.41)

$$-\partial_s (K_{11}m_1 + K_{12}m_2) - \Omega_1 \partial_s m_2 + K_{22} \partial_s m_1 + f_2$$
 (D.42)

Multiplying (D.35) by M, we find

$$\boldsymbol{u} = \mathsf{M}\boldsymbol{F}.\tag{D.43}$$

D.3 Shape equations

Defining X and Y by,

$$\mathsf{M}\boldsymbol{F} = \mathsf{M} \begin{pmatrix} \partial_s \lambda \\ \Omega \lambda \end{pmatrix} + \mathsf{M}Y \tag{D.44}$$

$$= M \begin{pmatrix} \partial_s \lambda \\ \Omega \lambda \end{pmatrix} + X, \tag{D.45}$$

we find that

$$u_1 = M_{11}\partial_s \lambda + M_{12}\Omega \lambda + X_1, \tag{D.46}$$

$$u_2 = M_{12}\partial_s \lambda + M_{22}\Omega\lambda + X_2. \tag{D.47}$$

When substituted into (D.24), we find

$$\partial_{s}u_{1} - \Omega u_{2} = M_{11}\partial_{s}^{2}\lambda + \partial_{s}M_{11}\partial_{s}\lambda + M_{12}\Omega\partial_{s}\lambda + \partial_{s}\left(M_{12}\Omega\right)\lambda$$

$$+ \partial_{s}X_{1} - M_{12}\Omega\partial_{s}\lambda - M_{22}\Omega^{2}\lambda - \Omega X_{2}$$

$$= M_{11}\partial_{s}^{2}\lambda + \partial_{s}M_{11}\partial_{s}\lambda + \left(\partial_{s}\left(M_{12}\Omega\right) - M_{22}\Omega^{2}\right)\lambda$$

$$+ \partial_{s}X_{1} - \Omega X_{2}$$

$$(D.48)$$

or, equivalently

$$\partial_s^2 \lambda + \frac{\partial_s M_{11}}{M_{11}} \partial_s \lambda + \frac{\partial_s (M_{12}\Omega) - M_{22}\Omega^2}{M_{11}} \lambda = \frac{-\partial_s (M_{1j}Y_j) + \Omega M_{j2}Y_j}{M_{11}} \quad (D.49)$$

where
$$M_{11} = \frac{\zeta_2 + \zeta_r K_{22}^2}{\zeta_1 \zeta_2 + \zeta_1 \zeta_r K_{22}^2 + \zeta_2 \zeta_r K_{12}^2}$$
, $M_{12} = \frac{-\zeta_r K_{12} K_{22}}{\zeta_1 \zeta_2 + \zeta_1 \zeta_r K_{22}^2 + \zeta_2 \zeta_r K_{12}^2}$, $M_{22} = \frac{\zeta_1 + \zeta_r K_{12}^2}{\zeta_1 \zeta_2 + \zeta_1 \zeta_r K_{22}^2 + \zeta_2 \zeta_r K_{12}^2}$, $Y_1 = \mathbf{\Omega} \cdot \partial_s \mathbf{m} + f_1$, and $Y_2 = \mathbf{e}_2 \cdot (\partial_s \mathbf{\lambda}_\perp + \mathbf{\Omega} \times \mathbf{\lambda}_\perp) + K_{22} \mathbf{e}_1 \cdot (\partial_s \mathbf{m} + \mathbf{\Omega} \times \mathbf{m}) + f_2$.

The evolution equation for the geodesic curvature is obtained in a similar fashion by substituting the above expressions for (u_1, u_2) into Eq. (D.27).

D.4 Boundary conditions

Free end

The boundary term which appears in the first variation of the energy (5.28), is given by

$$\delta \mathcal{W} = \boldsymbol{m} \cdot \boldsymbol{\theta} + \boldsymbol{\lambda} \cdot \boldsymbol{v}, \tag{D.50}$$

where (θ, v) are components of the generator of the variation (see §3),

$$\delta \mathsf{S} = \mathsf{S} \mathsf{A}_{\xi}, \quad \mathsf{A}_{\xi} = \begin{pmatrix} \hat{\boldsymbol{\theta}} & \boldsymbol{v} \\ 0 & 0 \end{pmatrix} = \begin{pmatrix} \mathsf{R}^{-1} \delta \mathsf{R} & \mathsf{R}^{-1} \delta \boldsymbol{r} \\ 0 & 0 \end{pmatrix}.$$
 (D.51)

For a free end, constraints require,

$$0 = \delta \phi = \delta \mathbf{r} \cdot \nabla \phi = \mathbf{v} \cdot \mathsf{R}^{-1} \nabla \phi \tag{D.52}$$

$$\delta \boldsymbol{n} = R(\boldsymbol{\theta} \times \boldsymbol{e}_3) = \nabla \boldsymbol{n}^T \delta \boldsymbol{r} = \nabla \boldsymbol{n}^T R \boldsymbol{v}$$

$$\Rightarrow \boldsymbol{\theta} = \hat{\boldsymbol{e}}_3 R^T \nabla \boldsymbol{n}^T R \boldsymbol{v}$$
(D.53)

Or, in components,

$$\boldsymbol{v} = v_1 \boldsymbol{e}_1 + v_2 \boldsymbol{e}_2 \tag{D.54}$$

$$\boldsymbol{\theta} = \theta_1 \boldsymbol{e}_1 + \theta_2 \boldsymbol{e}_2 + \theta_3 \boldsymbol{e}_3 \tag{D.55}$$

$$\theta_1 = K_{12}v_1 + K_{22}v_2 \tag{D.56}$$

$$\theta_2 = -K_{11}v_1 - K_{12}v_2. \tag{D.57}$$

Applying D'Alembert's principle,

$$\delta \mathcal{W} = \left[\boldsymbol{\lambda} - \nabla \boldsymbol{n}^T \cdot (\boldsymbol{e}_3 \times \boldsymbol{m}) \right] \cdot \boldsymbol{v} + m_3 \theta_3$$

$$= \left[\lambda \boldsymbol{e}_1 + \boldsymbol{e}_1 \times (\partial_s \boldsymbol{m} + \boldsymbol{\Omega} \times \boldsymbol{m}) - \nabla \boldsymbol{n}^T \cdot (\boldsymbol{e}_3 \times \boldsymbol{m}) \right] \cdot \boldsymbol{v} + m_3 \theta_3$$

$$= \left[\lambda + K_{12} m_1 - K_{11} m_2 \right] v_1 \qquad (D.58)$$

$$- \left[\partial_s m_3 + 2K_{12} m_2 + (K_{11} - K_{22}) m_1 \right] v_2$$

$$+ m_3 \theta_3$$

we find boundary conditions for the free end are given by,

$$m_3 = 0 \tag{D.59}$$

$$\partial_s m_3 + 2K_{12}m_2 + (K_{11} - K_{22})m_1 = 0$$
 (D.60)

$$\lambda + K_{12}m_1 - K_{11}m_2 = 0. (D.61)$$

Clamped end

Linear and angular velocities at the clamped end must be zero: $u_1=u_2=0$ and $\omega_3=0$. Vanishing of u_1,u_2 is equivalent to ${\pmb F}={\sf M}^{-1}{\pmb u}=0$.

$$\mathbf{F} = \begin{pmatrix} \partial_s \lambda + \mathbf{\Omega} \cdot \partial_s \mathbf{m} + f_1 \\ \Omega_3 \lambda + \partial_s \lambda_2 - \Omega_1 \lambda_3 + K_{22} \partial_s m_1 - K_{22} K_{11} m_3 - K_{22} \Omega_3 m_2 + f_2 \end{pmatrix} = 0$$
(D.62)

From the structure equation, we have $\omega_3=\partial_s u_2+\Omega u_1$. Together with $F_1=F_2=0$, this implies the boundary conditions for a clamped end are given by,

$$F_1 = 0 \tag{D.63}$$

$$F_2 = 0 \tag{D.64}$$

$$M_{12}\partial_s F_1 + M_{22}\partial_s F_2 = 0. {(D.65)}$$

D.5 Numerics

This section contains information about numerical methods for the simulation of surface-bound polymers, and formulas used in implementation of geometric

integration schemes on SE(3). Define the following

$$R = qe_1^T + (n \times q)e_2^T + ne_3^T \in SO(3)$$
 (D.66)

$$\boldsymbol{\mu} = \mu_1 \boldsymbol{e}_1 + \mu_2 \boldsymbol{e}_2 \in \mathbb{R}^3 \tag{D.67}$$

$$\boldsymbol{\theta} = \theta_1 \boldsymbol{e}_1 + \theta_2 \boldsymbol{e}_2 + \theta_3 \boldsymbol{e}_3 \in \mathbb{R}^3, \quad \theta = |\boldsymbol{\theta}|$$
 (D.68)

$$A = \sin(\theta)/\theta$$
, $B = \frac{1 - \cos(\theta)}{\theta^2}$, $C = (1 - A)/\theta^2 = (\theta - \sin(\theta))/\theta^3$ (D.69)

$$V = 1 + B\hat{\boldsymbol{\theta}} + C\hat{\boldsymbol{\theta}}^2. \tag{D.70}$$

Then, we have

$$\begin{pmatrix}
\mathsf{R} & \mathbf{r} \\
0 & 1
\end{pmatrix} \exp \begin{pmatrix} \hat{\boldsymbol{\theta}} & \boldsymbol{\mu} \\
0 & 0
\end{pmatrix} = \begin{pmatrix}
\mathsf{R}e^{\hat{\boldsymbol{\theta}}} & \mathbf{r} + \mathsf{RV}\boldsymbol{\mu} \\
0 & 1
\end{pmatrix},
\tag{D.71}$$

$$Re^{\hat{\boldsymbol{\theta}}}\boldsymbol{e}_{1} = R\left(\boldsymbol{e}_{1} + A\boldsymbol{\theta} \times \boldsymbol{e}_{1} + B\boldsymbol{\theta} \times (\boldsymbol{\theta} \times \boldsymbol{e}_{1})\right)$$

$$= \begin{pmatrix} \boldsymbol{q} & \boldsymbol{n} \times \boldsymbol{q} & \boldsymbol{n} \end{pmatrix} \begin{pmatrix} 1 - B(\theta_{2}^{2} + \theta_{3}^{2}) \\ A\theta_{3} + B\theta_{1}\theta_{2} \\ -A\theta_{2} + B\theta_{1}\theta_{3} \end{pmatrix}$$
(D.72)

$$r + \mathsf{RV}\boldsymbol{\mu} = r + \mathsf{R}(\boldsymbol{\mu} + B\boldsymbol{\theta} \times \boldsymbol{\mu} + C\boldsymbol{\theta} \times (\boldsymbol{\theta} \times \boldsymbol{\mu}))$$

$$= r + \left(\boldsymbol{q} \quad \boldsymbol{n} \times \boldsymbol{q} \quad \boldsymbol{n}\right) \begin{pmatrix} [1 - C(\theta_2^2 + \theta_3^2)]\mu_1 + (C\theta_1\theta_2 - B\theta_3)\mu_2 \\ (C\theta_1\theta_2 + B\theta_3)\mu_1 + [1 - C(\theta_3^2 + \theta_1^2)]\mu_2 \\ (C\theta_1\theta_3 - B\theta_2)\mu_1 + (C\theta_2\theta_3 + B\theta_1)\mu_2 \end{pmatrix}$$
(D.73)

To speed up computations, and also avoid computational issues when $\theta \approx 0$, we evaluate (A, B, C) by truncating the power series given in Appendix B.

Explicit 1st order geometric timestep

Taylor expansion shows

$$S(t+h) = S(t)e^{hA_t(t)} + O(h^2).$$
 (D.74)

Since $A_t(t)$ can be computed as a function of the spatial derivatives of (Ω, λ, q, r) at the current time, this gives a first order explicit timestepping method for (q, r). Take $\mu = hu$ and $\theta = h\omega$ in equations (D.72) and (D.73) above. Then,

we have

$$\mathbf{q} \mapsto \mathsf{R}e^{\hat{\boldsymbol{\theta}}} \mathbf{e}_{1}$$

$$= \mathsf{R} \left(\mathbf{e}_{1} + A\boldsymbol{\theta} \times \mathbf{e}_{1} + B\boldsymbol{\theta} \times (\boldsymbol{\theta} \times \mathbf{e}_{1}) \right)$$

$$= \left(\mathbf{q} \cdot \boldsymbol{n} \times \mathbf{q} \cdot \boldsymbol{n} \right) \begin{pmatrix} 1 - B(\theta_{2}^{2} + \theta_{3}^{2}) \\ A\theta_{3} + B\theta_{1}\theta_{2} \\ -A\theta_{2} + B\theta_{1}\theta_{3} \end{pmatrix}$$
(D.75)

$$r \mapsto r + h\mathsf{RV}u$$

$$= r + h\mathsf{R}(u + B\boldsymbol{\theta} \times u + C\boldsymbol{\theta} \times (\boldsymbol{\theta} \times u))$$

$$= r + h\left(q \quad n \times q \quad n\right) \begin{pmatrix} [1 - C(\theta_2^2 + \theta_3^2)]u_1 + (C\theta_1\theta_2 - B\theta_3)u_2 \\ (C\theta_1\theta_2 + B\theta_3)u_1 + [1 - C(\theta_3^2 + \theta_1^2)]u_2 \\ (C\theta_1\theta_3 - B\theta_2)u_1 + (C\theta_2\theta_3 + B\theta_1)u_2 \end{pmatrix}$$
(D.76)

Implicit 2nd order geometric integration

Taylor expansion shows

$$S(s+h) = S(s)e^{\frac{h}{2}(A_s(s+h) + A_s(s))} + O(h^3).$$
 (D.77)

Take μ and θ from equations (D.72) and (D.73) to be the following

$$\mu = he_1, \quad \theta = \frac{h}{2} \left(\Omega(s+h) + \Omega(s) \right).$$
 (D.78)

We end up with a second order implicit method because,

$$\theta = \theta(s, s+h), \quad V = V(s, s+h)$$
 (D.79)

$$A = A(s, s+h), \quad B = B(s, s+h), \quad C = C(s, s+h)$$
 (D.80)

now depend on the spatial derivatives of (Ω, λ, q, r) at both s and s+h. Assuming we know $(\Omega(s+h), \lambda(s+h))$, then (q(s+h), r(s+h)) are fixed points of

$$\mathbf{q}(s+h) \mapsto \mathsf{R}(s)e^{\hat{\boldsymbol{\theta}}(s,s+h)}\mathbf{e}_{1}$$

$$= \mathsf{R}(s)\left(\mathbf{e}_{1} + A\boldsymbol{\theta} \times \mathbf{e}_{1} + B\boldsymbol{\theta} \times (\boldsymbol{\theta} \times \mathbf{e}_{1})\right)$$

$$= \begin{pmatrix} \mathbf{q}(s) & \mathbf{n}(s) \times \mathbf{q}(s) & \mathbf{n}(s) \end{pmatrix} \begin{pmatrix} 1 - B(\theta_{2}^{2} + \theta_{3}^{2}) \\ A\theta_{3} + B\theta_{1}\theta_{2} \\ -A\theta_{2} + B\theta_{1}\theta_{3} \end{pmatrix}$$
(D.81)

$$r(s+h) \mapsto r(s) + h\mathsf{R}(s)\mathsf{V}(s,s+h)\boldsymbol{e}_{1}$$

$$= r(s) + h\mathsf{R}(s) (\boldsymbol{e}_{1} + B\boldsymbol{\theta} \times \boldsymbol{e}_{1} + C\boldsymbol{\theta} \times (\boldsymbol{\theta} \times \boldsymbol{e}_{1}))$$

$$= r(s) + h \left(\boldsymbol{q}(s) \quad \boldsymbol{n}(s) \times \boldsymbol{q}(s) \quad \boldsymbol{n}(s)\right) \begin{pmatrix} 1 - C(\theta_{2}^{2} + \theta_{3}^{2}) \\ (C\theta_{1}\theta_{2} + B\theta_{3}) \\ (C\theta_{1}\theta_{3} - B\theta_{2}) \end{pmatrix}$$
(D.82)

and can be computed by iteration.

D.6 Yukawa potential

The Yukawa potential is the fundamental solution to the screened Poisson equation,

$$\left[\nabla^2 - 1/a^2\right] G(\boldsymbol{x}) = -\delta(\boldsymbol{x}) \tag{D.83}$$

$$G(\boldsymbol{x}) = \frac{1}{4\pi |\boldsymbol{x}|} e^{-|\boldsymbol{x}|/a}$$
 (D.84)

$$= \frac{1}{(2\pi)^3} \int \frac{1}{|\boldsymbol{k}|^2 + 1/a^2} e^{i\boldsymbol{k}\cdot\boldsymbol{x}} dV(\boldsymbol{k})$$
 (D.85)

$$= \frac{1}{2\pi^2 r} \int_0^\infty \frac{k \sin(kr)}{k^2 + 1/a^2} dk$$
 (D.86)

$$-\nabla G(\boldsymbol{x}) = \frac{(r+a)e^{-r/a}}{4\pi a r^3} \boldsymbol{x}$$
 (D.87)

The solution to

$$\left[\nabla^2 - 1/a^2\right]\phi(\boldsymbol{x}) = -\rho(\boldsymbol{x}) \tag{D.88}$$

with $\phi(\infty) = 0$ is

$$\phi(\mathbf{x}) = \int G(\mathbf{x} - \mathbf{x}') \rho(\mathbf{x}') dV(\mathbf{x}')$$
 (D.89)

BIBLIOGRAPHY

- [1] T. Mandal, W. Lough, S. E. Spagnolie, A. Audhya, and Q. Cui, Biophysical Journal 118, 1333 (2020).
- [2] S. Lie, Nachrichten von der Königl. Gesellschaft der Wissenschaften und der Georg-Augusts-Universität zu Göttingen , 529 (1874).
- [3] P. J. Olver, *Applications of Lie Groups to Differential Equations* (Springer Science & Business Media, 1993).
- [4] E. Noether, Nachrichten der Königlichen Gesellschaft der Wissenschaften zu Göttingen , 235 (1918).
- [5] Y. Kosmann-Schwarzbach and B. E. Schwarzbach, *The Noether Theorems* (Springer, 2011).
- [6] H. Poincaré, in *Proc. acad. sci*, Vol. 140 (1905) pp. 1504–1508.
- [7] H. Poincaré, Rendiconti del Circolo matematico di Palermo **21**, 129 (1906).
- [8] A. Einstein, Annalen der physik (1905).
- [9] H. Weyl, The Theory of Groups and Quantum Mechanics (Dover, 1932).
- [10] E. P. Wigner, Ann. Math. **40**, 149 (1939).
- [11] E. P. Wigner, *Group Theory and its Application to the Quantum Mechanics of Atomic Spectra* (Academic Press, 1959).
- [12] B. C. Hall, Quantum Theory for Mathematicians (Springer, 2013).
- [13] N. J. Vilenkin, *Special functions and the theory of group representations*, Vol. 22 (American Mathematical Society, 1968).
- [14] M. D. Schwartz, *Quantum field theory and the standard model* (Cambridge university press, 2013).

- [15] J. M. Selig, in *Computational Noncommutative Algebra and Applications*, edited by J. Byrnes (Springer, Dordrecht, 2004) pp. 101–125.
- [16] C. Rui, I. V. Kolmanovsky, and N. H. McClamroch, IEEE Transactions on Automatic Control **45**, 1455 (2000).
- [17] P. J. Olver, "Moving frames in geometry, algebra, computer vision, and numerical analysis," in *Foundations of Computational Mathematics*, London Mathematical Society Lecture Note Series, edited by R. Devore, A. Iserles, and E. Süli (Cambridge University Press, 2001) p. 267–298.
- [18] P. Diaconis, Lecture Notes-Monograph Series 11, i (1988).
- [19] G. S. Chirikjian, *Stochastic models, information theory, and Lie groups, volume* 2: *Analytic methods and modern applications*, Vol. 2 (Springer Science & Business Media, 2011).
- [20] P. J. Olver, London Mathematical Society Impact150 Stories 1, 14 (2015).
- [21] A. W. Knapp, Lie groups beyond an introduction (Springer, 1996).
- [22] B. O'Neill, Semi-Riemannian Geometry with Applications to Relativity (Academic Press, 1983).
- [23] B. F. Schutz, *Geometrical methods of mathematical physics* (Cambridge University Press, 1980).
- [24] J. Baez and J. P. Muniain, *Gauge Fields, Knots and Gravity* (World Scientific, 1994).
- [25] M. Nakahara, *Geometry, topology and physics* (IOP Publishing, 2003).
- [26] É. Cartan, Exposés de Géométrie (1935).
- [27] É. Cartan, Cahiers Scientifiques **18** (1937).
- [28] S. Sternberg, *Lectures on differential geometry* (American Mathematical Society, 1999).

- [29] V. I. Arnold, *Dynamical Systems III*, Vol. 3 (Springer-Verlag, 1988).
- [30] H. Poincaré, C.R. Acad. Sci. 132, 369 (1901).
- [31] H. Cendra, J. E. Marsden, and T. S. Ratiu, *Lagrangian reduction by stages* (American Mathematical Soc., 2001).
- [32] J. E. Marsden and T. S. Ratiu, *Introduction to mechanics and symmetry: a basic exposition of classical mechanical systems* (Springer Science & Business Media, 2013).
- [33] D. D. Holm, T. Schmah, and C. Stoica, *Geometric mechanics and symmetry:* from finite to infinite dimensions (Oxford University Press, 2009).
- [34] V. I. Arnold, *Mathematical Methods of Classical Mechanics* (Springer-Verlag, 1989).
- [35] V. Arnold, Annales de l'Institut Fourier 16, 319 (1966).
- [36] D. G. Ebin and J. Marsden, Annals of Mathematics, 102 (1970).
- [37] D. D. Holm, J. E. Marsden, T. Ratiu, and A. Weinstein, Physics reports 123, 1 (1985).
- [38] H. Cendra, D. D. Holm, M. J. W. Hoyle, and J. E. Marsden, Journal of Mathematical Physics **39**, 3138 (1998).
- [39] D. D. Holm, J. E. Marsden, and T. S. Ratiu, Advances in Mathematics 137, 1 (1998).
- [40] F. Gay-Balmaz and T. S. Ratiu, Advances in Applied Mathematics **42**, 176 (2009).
- [41] M. Castrillón López, T. S. Ratiu, and S. Shkoller, Proceedings of the American Mathematical Society **128**, 2155 (1999).
- [42] M. Castrillón López and T. S. Ratiu, Communications in mathematical physics **236**, 223 (2003).

- [43] D. C. P. Ellis, F. Gay-Balmaz, D. D. Holm, and T. S. Ratiu, Journal of Geometry and Physics **61**, 2120 (2011).
- [44] M. Á. Berbel and M. Castrillón López, Journal of Geometry and Physics **191**, 104879 (2023).
- [45] D. Bleecker, *Gauge Theory and Variational Principles* (Addison-Wesley Publishing Company, 1981).
- [46] R. Lakes, Nature **361**, 511 (1993).
- [47] A. C. Eringen, *Microcontinuum field theories: I. Foundations and solids* (Springer Science & Business Media, 2001).
- [48] A. C. Eringen, *Microcontinuum field theories: II. Fluent media* (Springer Science & Business Media, 2001).
- [49] E. Cosserat and F. Cosserat, *Théorie des Corps Déformables* (Hermann, Paris, 1909).
- [50] O. M. O'Reilly, Modeling Nonlinear Problems in the Mechanics of Strings and Rods (Springer, 2017).
- [51] G. G. Giusteri and E. Fried, Journal of Elasticity 132, 43 (2018).
- [52] F. Boyer and F. Renda, Journal of Nonlinear Science 27, 1 (2017).
- [53] D. C. P. Ellis, F. Gay-Balmaz, D. D. Holm, V. Putkaradze, and T. S. Ratiu, Archive for rational mechanics and analysis **197**, 811 (2010).
- [54] T. Gould and D. A. Burton, New Journal of Physics 8, 137 (2006).
- [55] P. Rangamani, A. Benjamini, A. Agrawal, B. Smit, D. J. Steigmann, and G. Oster, Biomechanics and modeling in mechanobiology **13**, 697 (2014).
- [56] J. Yang and R. Lakes, Journal of biomechanics 15, 91 (1982).
- [57] P. De Gennes and J. Prost, *The Physics of Liquid Crystals*, 83 (Oxford university press, 1993).

- [58] I. Vardoulakis, Cosserat Continuum Mechanics: With Applications to Granular Media (Springer, 2018).
- [59] F. Gay-Balmaz, D. D. Holm, and T. S. Ratiu, J. Geom. Mech. 1, 417 (2009).
- [60] I. Dzyaloshinskii, in *Modern Trends in the Theory of Condensed Matter: Proceedings of the XVI Karpacz Winter School of Theoretical Physics, February* 19–March 3, 1979 Karpacz, Poland (Springer, 2008) pp. 204–224.
- [61] M. Mézard, G. Parisi, and M. Virasoro, *Spin Glass Theory and Beyond* (World Scientific, 1987).
- [62] T. H. Berlin and M. Kac, Physical Review 86, 821 (1952).
- [63] M. E. Peskin and D. V. Schroeder, *An Introduction to Quantum Field Theory* (Addison-Wesley, 1995).
- [64] M. Kardar, Statistical physics of fields (Cambridge University Press, 2007).
- [65] S. V. Ketov, Quantum non-linear sigma-models: from quantum field theory to supersymmetry, conformal field theory, black holes and strings (Springer, 2000).
- [66] W. M. Boothby, An Introduction to Differentiable Manifolds and Riemannian Geometry (Academic Press, 1986).
- [67] D. H. Sattinger and O. L. Weaver, *Lie groups and algebras with applications to physics, geometry, and mechanics*, Vol. 61 (Springer Science & Business Media, 2013).
- [68] B. C. Hall, Lie Groups, Lie Algebras, and Representations: An Elementary Introduction (Springer, 2003).
- [69] R. Gilmore, *Lie Groups, Physics, and Geometry: An Introduction for Physicists, Engineers and Chemists* (Cambridge University Press, 2008).
- [70] D. Lovelock and H. Rund, *Tensors, Differential Forms, and Variational Principles* (Courier Corporation, 1989).

- [71] R. W. R. Darling, *Differential Forms and Connections* (Cambridge University Press, 1994).
- [72] R. L. Bishop, The American Mathematical Monthly 82, 246 (1975).
- [73] F. Klok, Computer Aided Geometric Design 3, 217 (1986).
- [74] T. R. Powers, Rev. Modern Phys. 82, 1607 (2010).
- [75] S. S. Antman, Nonlinear Problems of Elasticity (Springer, 1995).
- [76] J. Langer and D. A. Singer, SIAM Review 38, 605 (1996).
- [77] R. Vogel and H. Stark, Euro. Phys. J. E **35**, 15 (2012).
- [78] M. K. Jawed, N. K. Khouri, F. Da, E. Grinspun, and P. M. Reis, Phys. Rev. Lett. **115**, 168101 (2015).
- [79] F. T. M. Nguyen and M. D. Graham, Phys. Rev. E 98, 042419 (2018).
- [80] Z. Zou, W. Lough, and S. Spagnolie, Phys. Rev. Fluids 6, 103102 (2021).
- [81] K. D. Young, Microbiol. Mol. Biol. Rev. 70, 660 (2006).
- [82] W. F. Marshall, K. D. Young, M. Swaffer, E. Wood, P. Nurse, A. Kimura, J. Frankel, J. Wallingford, V. Walbot, X. Qu, et al., BMC Biol. 10, 1 (2012).
- [83] L. Willis and K. C. Huang, Nature Rev. Microbiol. **15**, 606 (2017).
- [84] F. Si, G. Le Treut, J. T. Sauls, S. Vadia, P. A. Levin, and S. Jun, Curr. Biol. 29, 1760 (2019).
- [85] J. E. Avron, O. Gat, and O. Kenneth, Phys. Rev. Lett. **93**, 186001 (2004).
- [86] S. E. Spagnolie and E. Lauga, Phys. Fluids **22**, 031901 (2010).
- [87] R. Schuech, T. Hoehfurtner, D. J. Smith, and S. Humphries, Proc. Natl. Acad. Sci. 116, 14440 (2019).

- [88] H. H. Tuson, G. K. Auer, L. D. Renner, M. Hasebe, C. Tropini, M. Salick, W. C. Crone, A. Gopinathan, K. C. Huang, and D. B. Weibel, Mol Microbiol. 84, 874 (2012).
- [89] E. R. Rojas, G. Billings, P. D. Odermatt, G. K. Auer, L. Zhu, A. Miguel, F. Chang, D. B. Weibel, J. A. Theriot, and K. C. Huang, Nature 559, 617 (2018).
- [90] S. Al-Mosleh, A. Gopinathan, C. D. Santangelo, K. C. Huang, and E. R. Rojas, Proc. Natl. Acad. Sci. **119** (2022).
- [91] E. R. Rojas and K. C. Huang, Curr. Op. Microbiol. 42, 62 (2018).
- [92] G. K. Auer, T. K. Lee, M. Rajendram, S. Cesar, A. Miguel, K. C. Huang, and D. B. Weibel, Cell systems 2, 402 (2016).
- [93] G. K. Auer and D. B. Weibel, Biochemistry **56**, 3710 (2017).
- [94] P. N. Rather, Env. Microbiol. 7, 1065 (2005).
- [95] M. F. Copeland and D. B. Weibel, Soft Matter 5, 1174 (2009).
- [96] G. K. Auer, P. M. Oliver, M. Rajendram, T.-Y. Lin, Q. Yao, G. J. Jensen, and D. B. Weibel, Mbio 10, e00210 (2019).
- [97] R. R. Trivedi, J. A. Crooks, G. K. Auer, J. Pendry, I. P. Foik, A. Siryaporn, N. L. Abbott, Z. Gitai, and D. B. Weibel, MBio 9, e01340 (2018).
- [98] D. B. Kearns, Nature Rev. Microbiol. **8**, 634 (2010).
- [99] H. H. Tuson, M. F. Copeland, S. Carey, R. Sacotte, and D. B. Weibel, J. Bacteriol. 195, 368 (2013).
- [100] J. Blake, J. Fluid Mech. 55, 1 (1972).
- [101] C. Brennen and H. Winet, Ann. Rev. Fluid Mech. 9, 339 (1977).
- [102] J. F. M. Hoeniger, Microbiol. **40**, 29 (1965).

- [103] E. Lauga, *The Fluid Dynamics of Cell Motility*, Vol. 62 (Cambridge University Press, 2020).
- [104] O. Du Roure, A. Lindner, E. N. Nazockdast, and M. J. Shelley, Annu. Rev. of Fluid Mech. **51**, 539 (2019).
- [105] A. Lindner and M. Shelley, Fluid-structure interactions in low-Reynolds-number flows **168** (2015).
- [106] L. Li, H. Manikantan, D. Saintillan, and S. E. Spagnolie, J. Fluid Mech. 735, 705 (2013).
- [107] J. T. Pham, A. Morozov, A. J. Crosby, A. Lindner, and O. du Roure, Phys. Rev. E 92, 011004(R) (2015).
- [108] H. Manikantan and D. Saintillan, Phys. Rev. E **92**, 041002(R) (2015).
- [109] Y. Liu, B. Chakrabarti, D. Saintillan, A. Lindner, and O. Du Roure, Proc. Natl. Acad. Sci. 115, 9438 (2018).
- [110] B. Chakrabarti, Y. Liu, J. LaGrone, R. Cortez, L. Fauci, O. du Roure, D. Saintillan, and A. Lindner, Nature Phys. **16**, 689 (2020).
- [111] C. Floyd, H. Ni, R. S. Gunaratne, R. Erban, and G. A. Papoian, J. Chem. Theory and Comput. 18, 4865 (2022).
- [112] G. Jayaraman, S. Ramachandran, S. Ghose, A. Laskar, M. S. Bhamla, P. S. Kumar, and R. Adhikari, Phys. Rev. Lett. **109**, 158302 (2012).
- [113] F. Ling, H. Guo, and E. Kanso, J. Roy. Soc. Interface 15, 20180594 (2018).
- [114] X. Shi, A.-K. Pumm, J. Isensee, W. Zhao, D. Verschueren, A. Martin-Gonzalez, R. Golestanian, H. Dietz, and C. Dekker, Nature Phys. 18, 1105 (2022).
- [115] A. Laskar and R. Adhikari, Soft Matter 11, 9073 (2015).
- [116] R. E. Isele-Holder, J. Elgeti, and G. Gompper, Soft Matter 11, 7181 (2015).

- [117] R. G. Winkler, J. Elgeti, and G. Gompper, Journal of the Physical Society of Japan **86**, 101014 (2017).
- [118] Y. Man and E. Kanso, Soft Matter 15, 5163 (2019).
- [119] A. Ghosh and N. Gov, Biophys. J. **107**, 1065 (2014).
- [120] D. Saintillan, M. J. Shelley, and A. Zidovska, Proc. Natl. Acad. Sci. 115, 11442 (2018).
- [121] C. W. Wolgemuth, T. R. Powers, and R. E. Goldstein, Phys. Rev. Lett. 84, 1623 (2000).
- [122] S. Lim and C. S. Peskin, SIAM J. Sci. Comput. 25, 2066 (2004).
- [123] R. E. Goldstein, T. R. Powers, and C. H. Wiggins, Phys. Rev. Lett. **80**, 5232 (1998).
- [124] A. Goriely and M. Tabor, Physica D **105**, 45 (1997).
- [125] A. Goriely and M. Tabor, Physica D **105**, 20 (1997).
- [126] M. Nizette and A. Goriely, J. Math. Phys. 40, 2830 (1999).
- [127] A. Shapere and F. Wilczek, J. Fluid Mech. 198, 557 (1989).
- [128] H. Wada, Phys. Rev. E **84**, 042901 (2011).
- [129] E. Lauga and T. Powers, Rep. Prog. Phys. **72**, 096601 (2009).
- [130] A. Iserles, H. Z. Munthe-Kaas, S. P. Nørsett, and A. Zanna, Acta Numer. **9**, 215 (2000).
- [131] J. Park and W.-K. Chung, IEEE Transactions on Robotics 21, 850 (2005).
- [132] E. Haier, C. Lubich, and G. Wanner, Geometric Numerical Integration: Structure-Preserving Algorithms for Ordinary Differential Equations (Springer, 2006).
- [133] P. E. Crouch and R. Grossman, Journal of Nonlinear Science 3, 1 (1993).

- [134] A. Iserles and S. P. Nørsett, Philos. Trans. Royal Soc. A 357, 983 (1999).
- [135] S. Blanes, F. Casas, J.-A. Oteo, and J. Ros, Physics reports 470, 151 (2009).
- [136] S. Lim, Phys. Fluids 22, 024104 (2010).
- [137] B. E. Griffith and S. Lim, Comm. Comput. Phys. 12, 433 (2012).
- [138] S. D. Olson, S. Lim, and R. Cortez, J. Comput. Phys. 238, 169 (2013).
- [139] W. Lee, Y. Kim, S. D. Olson, and S. Lim, Phys. Rev. E 90, 033012 (2014).
- [140] L. Koens and E. Lauga, Phys. Fluids 28, 013101 (2016).
- [141] O. Maxian, B. Sprinkle, C. S. Peskin, and A. Donev, Phys. Rev. Fluids 7, 074101 (2022).
- [142] B. J. Walker, K. Ishimoto, and E. A. Gaffney, Phys. Rev. Fluids **8**, 034101 (2023).
- [143] M. Garg and A. Kumar, Math. Mech. Solids 28, 692 (2023).
- [144] Y. L. Lin, N. J. Derr, and C. H. Rycroft, Proc. Natl. Acad. Sci. 119, e2105338118 (2022).
- [145] O. Maxian and A. Donev, J. Fluid Mech. 952, A5 (2022).
- [146] C. H. Wiggins, D. Riveline, A. Ott, and R. E. Goldstein, Biophys. J. 74, 1043 (1998).
- [147] P. Bassereau, R. Jin, T. Baumgart, M. Deserno, R. Dimova, V. A. Frolov, P. V. Bashkirov, H. Grubmüller, R. Jahn, H. J. Risselada, et al., Journal of physics D: Applied physics 51, 343001 (2018).
- [148] T. Mandal, S. E. Spagnolie, A. Audhya, and Q. Cui, Biophysical Journal 120, 3211 (2021).
- [149] S. J. Marrink, V. Corradi, P. C. Souza, H. I. Ingólfsson, D. P. Tieleman, and M. S. Sansom, Chemical Reviews 119, 6184 (2019), pMID: 30623647, https://doi.org/10.1021/acs.chemrev.8b00460.

- [150] R. P. Feynman, Phys. Rev. 84, 108 (1951).
- [151] A. Shapere and F. Wilczek, *Geometric phases in physics*, Vol. 5 (World scientific, 1989).
- [152] A. L. Schuh and A. Audhya, Critical Reviews in Biochemistry and Molecular Biology 49, 242 (2014), https://doi.org/10.3109/10409238.2014.881777.
- [153] L. Harker-Kirschneck and a, Proc. Natl. Acad. Sci. **119**, e2107763119 (2022).
- [154] T. C. Bidone, H. Tang, and D. Vavylonis, Biophysical journal 107, 2618 (2014).
- [155] M. Lenz, D. J. G. Crow, and J.-F. m. c. Joanny, Phys. Rev. Lett. **103**, 038101 (2009).
- [156] A. Roux, K. Uyhazi, A. Frost, and P. De Camilli, Nature 441, 528 (2006).
- [157] C. Shi, G. Zou, Z. Wu, M. Wang, X. Zhang, H. Gao, and X. Yi, Proceedings of the National Academy of Sciences 120, e2300380120 (2023).
- [158] M. S. Peterson, A. Baskaran, and M. F. Hagan, Nature communications 12, 7247 (2021).
- [159] J. Guven and P. Vázquez-Montejo, Physical Review E 85, 026603 (2012).
- [160] P. Vázquez-Montejo, Z. McDargh, M. Deserno, and J. Guven, Physical Review E **91**, 063203 (2015).
- [161] A. J. Spakowitz and Z.-G. Wang, Physical review letters 91, 166102 (2003).
- [162] Z. A. McDargh, P. Vázquez-Montejo, J. Guven, and M. Deserno, Biophysical journal 111, 2470 (2016).
- [163] W. Helfrich, Zeitschrift für Naturforschung c 28, 693 (1973).

- [164] A.-K. Pfitzner, J. M. von Filseck, and A. Roux, Trends in cell biology **31**, 856 (2021).
- [165] N. Chiaruttini, L. Redondo-Morata, A. Colom, F. Humbert, M. Lenz, S. Scheuring, and A. Roux, Cell 163, 866 (2015).
- [166] C. Dimaano, C. B. Jones, A. Hanono, M. Curtiss, and M. Babst, Molecular biology of the cell **19**, 465 (2008).
- [167] I.-H. Lee, H. Kai, L.-A. Carlson, J. T. Groves, and J. H. Hurley, Proceedings of the National Academy of Sciences 112, 15892 (2015).
- [168] A. Bertin, N. De Franceschi, E. de La Mora, S. Maity, M. Alqabandi, N. Miguet, A. Di Cicco, W. H. Roos, S. Mangenot, W. Weissenhorn, *et al.*, Nature communications **11**, 2663 (2020).
- [169] B. Nepal, A. Sepehri, and T. Lazaridis, Protein Science 29, 1473 (2020).
- [170] T. Baumgart, B. R. Capraro, C. Zhu, and S. L. Das, Annual Review of Physical Chemistry **62**, 483 (2011), pMID: 21219150, https://doi.org/10.1146/annurev.physchem.012809.103450.
- [171] S. Harris, American Scientist 74, 542 (1986).